Marks Marinbahs

STUDY OF THE DYNAMICS, STRENGTH AND TECHNICAL CONDITION ASSESSMENT OF TRACTION ELECTROMECHANICAL EQUIPMENT

Doctoral Thesis

RIGA TECHNICAL UNIVERSITY

Faculty of Mechanical Engineering, Transport and Aeronautics
Institute of Aeronautics

Marks Marinbahs

Doctoral Student of the Study Programme "Transport"

STUDY OF THE DYNAMICS, STRENGTH AND TECHNICAL CONDITION ASSESSMENT OF TRACTION ELECTROMECHANICAL EQUIPMENT

Doctoral Thesis

Scientific supervisor:
Professor *Dr. habil. sc. ing.*
VITĀLIJS PAVELKO
Scientific advisor:
Docent *Dr. sc. ing.*
OĻEGS SĻISKIS

Riga 2023

ACKNOWLEDGMENTS

CONTENTS

TOPICALITY OF THE WORK

The actuality of the set task set also determines the constant increase in the operating speeds and loads of modern rolling stock, namely suburban and regional electric trains. In railway equipment, a traction electric drive is widely used, in most cases, the elements of which, after installation, become inaccessible for direct control. There is a trend in the development and mass operation of electric trains with an asynchronous drive to improve performance in the intensification of traffic. In turn, the electric drive is an independent and complex system, since the processes occurring in it have a different physical nature. Therefore, in order to assess the technical condition of the mechanical and electrical elements of electromechanical equipment, as well as to control its technical condition, it is advisable to carry out comprehensive tests when putting the equipment into operation. The foregoing is especially relevant for new products as well as at the stage of acceptance testing of serial products.

Currently, methods for diagnosing the mechanical part of the electric drive based on vibration and acoustic parameters are widely used. Methods for electrical control of motors based on the consumed current are being developed. The main drawback of the existing methods of separate control of mechanical and electromechanical units is that they do not take into account the interconnection and interdependence of the total operation of the drive elements, in particular the motor and gearbox, which are often checked separately.

OBJECTIVE OF THE DOCTORAL THESIS

The aim of the Doctoral Thesis is to study the possibilities of the dynamics, strength and technical condition assessment of traction electromechanical equipment in industrial and continuous production conditions and to improve the completeness and efficiency of pre-operational test trials based on the creation of a methodology for an integrated approach to the control and analysis of the mechanical strength and vibration activity of traction equipment.

To achieve the aim, the following tasks have been solved:
1. Development of a methodology for comprehensive analysis of the design of electromechanical equipment based on its operating conditions.
2. Development and implementation of a methodology for determining the safety margin of the equipment taking into account the mechanical loads of the drive.
3. Analysis of the influence of defects in equipment units on the change in diagnostic parameters and the establishment of links between them.
4. Practical approbation of the technique for monitoring the technical condition of electromechanical equipment based on its vibration activity.

To solve the tasks, an analysis of the work on the creation of methods, techniques and systems for non-destructive testing and diagnostics of electromechanical equipment was carried out.

The study of methods and models of non-destructive testing of mechanical and electromechanical equipment based on vibration analysis is the subject of many research papers. However, in these studies, methods and techniques for monitoring and predicting the service life of units based on mechanical parameters are mainly presented. Little attention has been paid to controlling the vibration of mechanical components in the drive.

SCIENTIFIC NOVELTY OF THE WORK

Scientific novelty of the Thesis:

1. A methodology for assessing the technical condition of electromechanical equipment units has been developed taking into consideration the analysis of mechanical parameters as part of a real traction electric drive. Mechanical diagnostic parameters are the general level of vibration acceleration and vibration velocity.

2. Based on the established connection between diagnostic signs and the type of defect or malfunction, an approach is proposed for its detection.

3. A methodology for estimating the safety margin of electromechanical equipment is proposed, which has the most sensitive diagnostic features with the possibility of estimating the safety margin of the equipment under conditions of changing external loads.

THEORETICAL AND PRACTICAL SIGNIFICANCE OF THE WORK

The theoretical and practical significance of the work lies in the fact that a method for monitoring the technical condition of electromechanical equipment has been developed and tested, which increases its reliability and efficiency. This will make it possible to switch to automated control of the actual state of traction electrical equipment. Based on the results of the study, the methodology and means are proposed for monitoring the technical condition of motor-gear units produced by JSC "Rīgas elektromašīnbūves rūpnīca" used on suburban motor car bogies with a design speed of up to 160 km/h.

RESEARCH METHODS, RELIABILITY AND VALIDITY OF RESULTS

The presented results of the dissertation work are obtained on the basis of theoretical and experimental research. The theoretical study was carried out using digital processing of diagnostic signals, system analysis, and statistical analysis. The experimental study was carried out in laboratory and production conditions and includes approbation of the developed methodology and controls on stands. Processing of experimental data was carried out in a semi-automatic mode using the developed software products in the LabView software. The reliability of the results obtained is confirmed by the correct formulation of the problems, the correspondence of the theoretical results to the experimental data, and the consistency with the results of other authors.

An experiment was used to study the influence of the technical condition of electromechanical equipment on changes in key parameters.

The present research is based on the results of theoretical and experimental developments, which are presented in five chapters.

In Chapter 1, on the basis of research, an overview of existing methods and techniques for monitoring and diagnosing the technical condition of electromechanical equipment is given. The standards for vibration control are also considered.

Chapter 2 analyses the existing methods for processing diagnostic signals, as well as signs of manifestation of defects in the main units. The object of control is also considered: the motor-reducer block of the motor car of the electric train. The main attention is paid to the development of a methodology for the integrated control of electromechanical equipment, including a model and algorithm for the operation of an information-measuring system for monitoring the technical condition, a model and algorithm for estimating the resource of equipment.

Chapter 3 presents the development of a virtual and physical test and measurement system, including a description of the subject of research and a description of the drive control system. A model is presented to determine the critical points of maximum structural stress. The main attention is paid to the development of a methodology for the integrated control of electromechanical equipment, including a model and algorithm for the operation of an information-measuring system for monitoring the technical condition, a model and algorithm for estimating the resource of equipment.

Chapter 4 presents the results of the analysis of the influence of the loading of the object under study on the change in diagnostic parameters based on an experimental study of the methodology and means of monitoring the technical condition of the equipment. The model for predicting the safety margin of the equipment has been experimentally tested.

Chapter 5 describes the practical application of the methodology in the production environment of JSC "Rīgas elektromašīnbūves rūpnīca". The data of the control object (geared motor units of passenger electric trains used on the bogies of motor cars of passenger electric trains) were collected and analysed and the most vulnerable segments of the structure requiring direct monitoring of their condition were identified.

The research is based on:
1) the method for determining mechanical loads and assessing the safety margin of the supporting structures of traction motor-reduced units and the method for evaluating the operation of electromechanical equipment based on the relationship, interaction and subsequent joint analysis of the vibration parameters of the equipment;
2) the structure and hardware-software implementation of bench testing of equipment to identify the technical condition of electromechanical equipment;
3) the results of an experimental study confirming the possibility of increasing the efficiency of the process of conducting acceptance tests and evaluating the safety margin of electromechanical equipment through the integrated use of vibration and energy parameters.

CHAPTER 1. STATUS ANALYSIS AND DIRECTIONS OF RESEARCH

1.1. Determination of the reliability of traction machines and equipment at the stage of industrial testing

The economic efficiency of machines and equipment directly depends on their technical condition. At present, two types of equipment maintenance have become widespread in enterprises: maintenance after failure and maintenance according to the regulations. However, this leads, on the one hand, to a significant underutilization of the resource of the structures of the units and the machine as a whole, and, on the other hand, does not adequately ensure their reliability. In an unforeseen breakdown, the enterprise incurs significant economic costs. In the second case, when maintenance is carried out according to the regulations, this also leads to additional costs. This is due to the fact that any "movement" violates the quality of the kinematic relationships in the mechanism, achieved by the natural running-in of mating components and parts during operation.

Technical diagnostics, based on scientific methods and means of non-destructive testing, makes it possible to objectively determine the state of technical objects, as well as to perceive diagnostic signals at a level inaccessible to perception by the human senses.

In particular, the most important condition for the efficient operation of transport equipment (in particular, railway transport) is the trouble-free operation of its subsystems, the main of which is traction electrical equipment. One of the possible ways to maintain a high level of system reliability is the use of methods, techniques and means of non-destructive testing. The use of complex methods and techniques for assessing the performance of objects and their technical implementation is an urgent task, since its solution will improve the overall efficiency of the equipment [1], [2].

Currently, much attention is paid to the control of transport systems. This is evidenced by a large volume of publications, international conferences, specialized exhibitions. Non-destructive testing is widely used in aerospace, air, rail, road, water and pipeline transport, energy, metallurgy, metalworking, fuel, mining, chemical and paper industries.

As noted in [3], one of the main tasks of modern mechanical engineering is to ensure high quality and reliability of machines at minimal economic cost.

It is obvious that the successful solution of this problem increases the competitiveness of manufactured machines and equipment in the world markets that meet European and international quality standards.

Thus, the urgency of equipment TS control is high and there is a need to design and implement such methods, techniques and tools. However, before monitoring the TS of equipment, it is necessary to identify those components of the machine that are much more exposed to breakage, instability due to sensitivity to the environment and defects.

An electric drive is a system consisting of mechanical and electrical subsystems with a control system. In turn, the mechanical subsystem consists of bearing assemblies, as well as mechanical gears.

The general list of defects in the mechanical part can be divided into three groups [4]–[10].

The first group - bearing mounting defects: misalignment of the bearing rings; non-uniform radial (axial) bearing preload.

The second group - defects in the operation of the bearing: wear of the outer ring; shells, cracks on the outer ring; wear of the inner ring; shells, cracks on the inner ring; wear of rolling elements; shells, chips, cracks on rolling elements; wear (defects) of the separator; aging (deficiency) of lubrication.

The third group - defects of the rotor, couplings and mechanical gears that create dynamic loads on the bearings: running in (shaft breakage); coupling defects; gear teeth defects; gear engagement defects.

Defects in mechanical transmissions, which are most often encountered during equipment operation [11]–[13]:

a) gear defects (tooth wear; tooth breakage; shock gearing; shaft misalignment - fracture and displacement of shafts; bent shaft);

b) belt drive defects (belt wear, loose tension, pulley misalignment, pulley eccentricity, belt resonance, etc.);

c) chain drive defects (chain wear; loose tension; pulley misalignment; pulley eccentricity; chain resonance), etc. Also in mechanical units, defects in drive shafts, couplings, cooling systems, and lubrication can occur.

However, all these malfunctions can first of all occur if there are defects in bearings and mechanical transmissions.

Defects in the electrical subsystem are defects in drive motors. The most common defects of electric motors (asynchronous motor is considered in this PhD work) [14]–[17]: operation of the electric motor in two phases; interturn circuit; overload and overheating of the motor stator; rotor imbalance; breakage or loosening of the fastening of the rods in the squirrel cage; uneven air gap between the stator and rotor; damage to the stator windings or insulation; loosening of the stator windings.

In this dissertation work, an object consisting of an electric motor and a mechanical transmission - a traction geared motor unit (hereinafter referred to as MGU) was investigated, since it is a typical electromechanical equipment.

1.2 Overview of existing methods and techniques for monitoring and diagnosing the technical condition of electromechanical equipment

At present, much attention is paid to the control and diagnostics of complex technical systems. This is evidenced by a large number of publications, and the refinement of international standards ISO / TC 108 "Vibration and shock" (ISO 17359:2003, ISO 13380:2002, ISO 13379:2003, ISO 10816-6:1995, ISO 13373-1:2002, ISO/DIS 13373-2, ISO/DIS 15242-1, ISO 13374-1:2003) [18]–[24].

According to the International Confederation for Measurement Technology and Instrumentation IMECO, only through the introduction of diagnostic tools, for example, for power plants, the labor intensity and repair time are reduced by more than 40%, fuel

consumption is reduced by 4% and the technical utilization of equipment is increased by 12% [25].

Any control and diagnostic system operates on the principle of deviations (the Salisbury principle). The difference between the actual and reference value of the diagnostic parameters is calculated, which is called the diagnostic symptom. The error with which the value of a diagnostic symptom is estimated largely determines the quality and reliability of the diagnosis and prognosis of the controlled object [26].

Monitoring and diagnostics should solve the problem of assessing the actual state of objects in the process of operation and provide information for organizing the repair cycle.

The authors of works [27]–[29] on the basis of vibrodiagnostic methods for monitoring bearing assemblies of wheel-motor blocks of railway transport have identified the most informative combinations of signs of the main failures of bearings and gears, reflected in the frequency and time domains. In the frequency domain, these are sets of harmonic components of the direct spectrum and the spectrum of the vibration signal envelope. In the time domain, these are the rms value and the gain of the vibration acceleration signal. These signs characterize the development of the defect.

Based on the analysis of possible descriptions of signals used to identify faults, the following conclusions were drawn by the author:

1) due to the peculiarities of the vibration signals from the MGU, it is advisable to analyze the vibration signals in the time domain to determine the defects.

2) the frequency Fourier transform should be carried out with averaging over several time samples.

3) statistical processing of diagnostic material allows not only to detect and prevent defects, but also to pursue a technical policy in the field of operation and repair of rolling stock.

The issues of control of rolling stock in general, traction motors and MGU are also widely covered in works [30]–[41].

In these works, the regularities of the occurrence of vibration in the bearing units of electric drives during their operation are theoretically substantiated and it is proved that when the bearing elements of the bearings wear out, their spectral characteristic is determined by the circular frequency of the rotor. Also, the influence of electrical parameters during the abnormal operation of the electric motor on its vibrational characteristic was revealed, and it was proved that the spectral component of vibration is directly related to the current frequency and the circular speed of the rotor of the electric motor.

The long-term forecast of the bearing states is carried out by the method of identifying vibrational models of the development of each defect. These models are based on a limitation on the rate of development of bearing wear defects, which assumes that the minimum possible time for the development of a defect from the moment of inception to the pre-accident state is about 20% of the average bearing life.

The works [42]–[48] present the results of studies showing the possibilities of using the current signal of an induction motor for remote diagnostics of the mechanisms of electric actuators.

The appearance or development in time of a particular defect leads to a redistribution of energy between the components of the spectrum of the resulting oscillatory process. Knowledge of the physical features and regularities of the processes of oscillation initiation in the structures of an electromechanical system allows one to qualitatively identify diagnostic features, the

change of which unambiguously indicates specific faults (the initiation and development of defects in one or another kinematic pair of an electromechanical system) and allows them to be assessed.

Taking into account the obtained theoretical results, the following provisions were formulated [46]:

1) the stator windings of the electric motor are an element of the measuring electrodynamic transducer.

2) the electric drive of the electromechanical system can be considered as a measuring electrodynamic converter of oscillations into a current signal.

The methods of spectral analysis and digital signal processing were used to analyze the current signals of electric fittings. Experimental studies were carried out on full-scale samples using an information-measuring system. As a result [47]:

1) a justification for the use of an asynchronous motor of an electric drive valve as an electromechanical converter generating a signal about the state of the kinematic pairs of the drive by changing the moment of load resistance reduced to the motor shaft has been obtained.

2) it has been established that in certain frequency ranges of the current signal spectrum of an asynchronous motor operating in the motor mode, there are harmonics that reflect the manifestation of defects that occur in the kinematic pairs of mechanical drive units.

3) a method is proposed for detecting defects in the mechanical elements of electric fittings, based on the selection of the corresponding harmonics in the spectrum of the current signal, which manifest themselves in the form of amplitude modulation of the main network harmonic of the supply network.

A number of authors of works [49]–[54] solved the problem of building an intelligent system for diagnosing electromechanical systems used in mining machines. The proposed system implements methods for monitoring and predicting states, optimizing search diagnostic procedures based on the use of neural networks, which provides control of the operation of an electromechanical system according to the actual technical condition.

The authors proposed a number of new technical solutions [55]–[59] that increase the reliability of pattern recognition based on the implementation of the generalizing ability of a multilayer neural network. The results of these scientific works show that vibroacoustic control of various objects, together with the use of artificial intelligence methods, leads to an increase in the efficiency of diagnosis. However, current analysis also allows obtaining sufficiently reliable information about the technical condition of electric drive equipment. Thus, the task is to conduct a comprehensive assessment of equipment using recognition methods based on a neural network.

Much work on the development and application of vibration control methods was carried out by the authors [1], [11], [13], [60]–[66], in particular, on the development of vibration spectral analysis methods.

The simplest monitoring systems are a total vibration (noise) level meter and a device for measuring the crest factor of the vibration signal, i.e. shock pulse recorder. At present, the rapid development of computer technology and the reduction in its prices make it possible to fully use more complex information technologies in practice.

Of the commonly used measuring instruments implemented on the basis of computer technology, one can single out shape analyzers, spectral analyzers and envelope spectrum analyzers.

It should also be noted that there are a number of standards for vibration control. Most of the complexes and equipment control systems are based on these standards:

1) ISO 13373-1-2009 Vibration condition monitoring of machines. This standard describes the basic concepts of vibration control, the types of sensors used, their attachment points [67].

2) GOST R 52545.1-2006 Vibration measurement methods. Determines the vibration discharge of a rolling bearing and establishes the requirements for environmental conditions during measurements (only on a test bench) [68]. The standard also specifies the measurement of vibration parameters in one or more frequency bands from 20 to 10,000 Hz. For different types of bearings, specific frequency ranges are set. When measuring the vibration of ball deep groove and angular contact bearings of a certain size range for low, medium and high frequency bands, the following limits are set respectively: from 50 to 300 Hz, from 300 to 1800 Hz and from 1800 to 10000 Hz.

3) GOST 24346-80 Vibration. Terms and Definitions. This International Standard establishes basic terms and definitions in the field of vibration [69].

4) ISO 10816-3-2002 Vibration. Monitoring the condition of machines based on the results of vibration measurements on non-rotating parts. Part 3. This standard describes criteria for evaluating the degree of vibration activity of machines in the place of their operation by measuring vibration on housings or bearing supports [70].

5) GOST 32106-2013 Monitoring of the condition of equipment in hazardous industries. Vibration of centrifugal pump and compressor units. This standard applies to units with a power of more than 2 kW and establishes guidance for assessing their vibration state during operation and acceptance tests after installation and repair. The standard also establishes vibration levels that characterize the state of drive elements [71].

Thus, in the regulatory and scientific and technical literature on vibration control, there are quite complete data characterizing the state of electromechanical equipment at the time of development of the full service life. The currently known standard regarding equipment diagnostics by current consumption is GOST ISO 20958-2015 (Condition monitoring and diagnostics of machines.

Spectral analysis of electrical signals of a three-phase asynchronous motor). This standard is applicable to three-phase asynchronous motors and establishes guidance on methods for monitoring their technical condition and diagnosing based on the spectral analysis of electrical signals in real time [72], [73].

There are also a number of standards that provide general guidance for interpreting data and diagnosing machines:

1) ISO 13379-1-2015 Condition monitoring and diagnostics of machines. Methods for interpreting data and diagnosing. Part 1. General guidance. The standard describes the tasks of diagnosing machines, and also allows you to establish approaches for diagnosing machines [20].

2) ISO 13379-1-2015 Condition monitoring and diagnostics of machines. Methods for interpreting data and diagnosing. Part 2. Data driven approach. The standard establishes guidance on the application of methods for monitoring the condition and diagnosing based on data [20].

The above normative documents reflect the high level of development of vibration diagnostic methods. The modern level of development of hardware and software allows for high-quality data collection and processing.

1.3. Features of the control of electromechanical equipment with operating processes of various physical nature

The traction electric drive is a technical system used to convert electrical energy into mechanical energy in order to set the working body of the machine in motion. In this case, the electric drive also performs the function of controlling this movement. Thus, the indicated transformation of the two types of energy is interconnected.

The fluctuations of physical parameters arising in the system (changes in power, forces, moments, speeds, accelerations), generated both by external influences and by developing defects in the electromechanical part of the system, are mutually reflected in the mechanical and electrical characteristics. This is also indirectly reflected in the diagnostic signals generated by these phenomena of various physical nature.

These changes are associated with the electromagnetic torque of the motor, which is determined by the value of the current consumed, the voltage of the phases and the state of the material of the rotor, stator, friction conditions in the supports and the amount of slip.

1.3.1. Analysis of vibration control methods

Based on the analysis of literary sources, it was revealed that rolling bearings are the most common and most frequently failing elements of the rotor mechanism. They carry out spatial fixation of rotating rotors and perceive the main part of the static and dynamic forces arising in the mechanism. Therefore, the technical condition of bearings is the most important component that determines the performance of the mechanism as a whole [8], [45], [60], [61].

The remaining defects that occur in rotating equipment can be divided into four groups [16]: defects of the "Bearing" level, defects of the "Mechanism" level, defects of mechanical weakening, defects of gears.

The following methods of digital signal processing are currently widely used in practice to control the TS of equipment in the field of vibration diagnostics: PIC factor, according to the spectrum of the vibration signal, according to the spectrum of the envelope, and the method of shock pulses. The method of vibration control by the spectrum of the vibration signal is usually considered by practical diagnosticians to be the main, the most effective one [16].

As part of the dissertation research, an analysis of the existing methods of vibration control was carried out, presented in Table 1.1.

Table 1.1

Comparative Table of Existing Methods of Vibration Control

No.	Vibration control method	Application	Advantages	Disadvantages
1	**General vibration measurement**	Preliminary assessment of the technical condition of the nodes	1. Ease of information processing; 2. Ease of interpretation of the results.	1. Low sensitivity; 2. Low degree of reliability of vehicle recognition
2	**Peak factor**	Bearing condition monitoring (mainly)	1. Ease of information processing; 2. Ease of interpretation of the results.	1. Low noise immunity; 2. The need for multiple measurements
3	**Trend analysis**	Determination of the main trends in vibration parameters change over time	Ability to predict the remaining resource of the node	1. A large amount of measurement information is required; 2. It is required to determine the boundaries of threshold values
4	**Band analysis**	Assessment of vibration levels in the frequency band	Ability to analyze vibration at specific frequencies	Further analysis of information is needed
5	**Spectral analysis**	Identification of defects and malfunctions of units in the field of low-frequency vibration	1. Allows you to identify a large number of defects; 2.Implemented in all modern diagnostic equipment	1. Analysis of only stationary vibration; 2. Impossibility to identify incipient defects
6	**The spectrum of the envelope**	Identification of incipient defects	High sensitivity to defects at an early stage	Use of specialized expensive equipment
7	**Wavelet analysis**	Local features of the signal	1. Low requirements for computing power; 2. Localization of a defect simultaneously in the frequency and time domains	Difficulty in interpreting results

Table 1.1 shows that each of the considered methods is used to solve a single problem, and it is preferable to use several vibration control methods in combination to control equipment.

1.3.2. Analysis of methods for processing drive motor current signals when monitoring the technical condition of equipment

Current based control can be implemented on most machines by using current transformers that are installed in the inverter. The use of current signals is convenient when controlling a large number of motors. In addition, the type of faults in the current signal is uniform and is not affected by external factors [74].

Thus, the analysis of the consumed current is currently a promising method for assessing the condition of both the electric motor and mechanical equipment.

Studies [74], [75] have shown that each type of fault is associated with a corresponding frequency component in the stator phase current. For example, the frequency components of the stator current of an induction motor can be divided into two separate groups:

1) spectral components: excitation frequencies, supply harmonics; spatial harmonics associated with the spatial arrangement of the winding;

2) abnormal spectral components: as a result of stator malfunctions; incorrect installation; load change.

In the well-known diagnostic complexes, when analyzing the current consumed by the drive motor, the signal is received by the current converter from the stator, and the data is processed by the data acquisition board. Next, get the frequency spectrum using the Fourier transform. Typically, a narrow band filter is used to isolate the fundamental harmonics, and a low pass filter is used to eliminate higher harmonics.

Thus, the theory of the Fourier transform was further developed in wavelet analysis. Wavelet theory is a powerful alternative to the classical methods of signal analysis, as it provides a more flexible signal processing technique [76], [77].

Analysis of the current spectrum based on the Fourier transform can be quite accurate and useful in steady state and transient operation of the MGU.

1.4. Features of the construction of modern systems for monitoring the technical condition of electromechanical equipment

The main features of the control of the electric drive of railway vehicles are:

1) a set of MGU of the same composition (4 MGU per section);

2) change in the external load of the MGU due to the heterogeneity of the track (including movement up and down), as well as uneven loading (in terms of the number of passengers, etc.);

3) checking the status of the most critical nodes is carried out periodically in the depot according to a certain regulation.

The use of methods and techniques of vibration control for an electric drive of a railway vehicle (MGU) moving along rails is associated with the need to isolate a useful diagnostic signal from a variety of interference caused, for example, by the imposition of impacts on bearing supports from rail irregularities and other sources.

In works [78]–[86], the following main goals of technical condition control are formulated, which determine its effectiveness:

1) detection of malfunctions or defects at the initial stage of their development; identification of specific defective units or parts; identification and elimination of the causes of the defect or malfunction;

2) assessment of the admissibility and expediency of further operation of the equipment, taking into account forecasting in case of identified defects or malfunctions; optimization of operating modes, allowing the safe operation of the unit with identified defects or malfunctions.

The main task of acceptance testing is to issue a warning about the occurrence of a defect or malfunction before their development poses a danger to the reliability of the equipment being monitored.

Control methods are also classified according to the type of physical processes occurring in the object: mechanical, electrical, vibration, ultrasonic, shock-pulse, thermal, magnetic, etc.

1.5. Main results and conclusions of Chapter 1

1. Various methods, techniques, models and algorithms are used to control equipment. Vibration control systems are the most common.
2. In turn, the electric drive is an independent and complex system, since the processes occurring in it have a different physical nature. Therefore, to assess the technical condition of the mechanical and electrical elements of electromechanical equipment, it is advisable to use complex monitoring tools.
3. A review of existing diagnostic methods, techniques and complexes and standards created on their basis shows a high level of development of vibration diagnostics.
4. To create a more effective technique for controlling, it is necessary to identify a set of controlled parameters of different physical nature as well as to find and justify the relationship between them.

CHAPTER 2. DEVELOPMENT OF A METHOD FOR INTEGRATED CONTROL OF THE TECHNICAL CONDITION OF ELECTROMECHANICAL EQUIPMENT

The tasks of methods and techniques for monitoring the technical condition of sets of traction electro-mechanical equipment (hereinafter referred to as TEE) provide for:

1) determining the object of control at a given time; with regard to TEE, it is preferable to have data on the state of specific units or structural elements of the electrical part and individual motion converters (mechanical part);

2) prediction of one of the future states of these nodes.

The diagnosis of an object is based on a comparison of diagnostic features with their threshold values. In the case of assessing the state of one type of assembly or structural element (for example, a gearbox housing), it is necessary to determine the threshold structural values. When evaluating a TEE which has several types of nodes or structural elements with operating processes of different physical nature, the task of determining the threshold values of a diagnostic feature becomes much more complicated.

2.1 Analysis of signs of defects in the main components of electromechanical equipment

Consider the main defects of electromechanical equipment and the signs of their manifestation. Defects in rotating parts can be identified using vibration analysis as well as drive motor current analysis. Table 2.1 presents the types of defects, their causes and effect [103].

Table 2.1

The Types of Defects, Their Causes and Effects

Cause	Defect	Effect
Overload	Surface cracking	Vibration, current ripple
Miscentering	Chafing on the raceways Surface cracking Damage to the cage	
Defects in the fit of the bearing on the shaft	Cracking and spalling of the bearing material	
Wrong installation	Cracking and spalling of the bearing material	
Incorrect bearing clearance	Cracking and chipping Abrasive wear Ring misalignment Incorrect installation	
Unsuitable lubricant	Fatigue spalling Seizures on the raceways Grooves on the raceways	
Poor sealing (pressurization)	Abrasive wear Seizures on the raceways Grooves on the raceways	
Unbalance load	Raceway damage	

Some types of defects, the signs of manifestation of which are associated with the appearance of amplitude or frequency modulation of vibration components, can be detected and identified by a single vibration measurement. At the same time, it should be taken into account that many components of vibration at frequencies that are multiples of the rotor rotation frequency can have components of both mechanical and electromagnetic origin, and their modulation can refer to only one of the components [87].

The stator current is also an informative sign of the manifestation of defects in an induction motor. All characteristic frequencies for vibration analysis can be observed in the stator current spectrum. Each fault type is associated with a corresponding frequency component in the stator phase current [74]. The frequency components of the stator current can be divided into two separate groups:

1) spectral components: excitation frequencies, supply harmonics; spatial harmonics associated with the spatial arrangement of the winding;

2) abnormal spectral components: as a result of stator malfunctions; incorrect installation; load change.

All the main signs of defects and violations of normal motor power conditions are summarized in Table 2.2 [87].

Table 2.2

The Main Defects of Induction Motors

Defect	Low frequency vibration	High frequency vibration	Stator current analysis
Stator winding defects	+	+	+
Rotor winding defects	+	+	+
Static gap eccentricity	+	+	+
Dynamic gap eccentricity	+	+	+
Supply voltage unbalance	+	-	+
Nonlinear voltage distortion	+	+	+

As mentioned in Section 1.1, an object was investigated, which is a typical electromechanical equipment. At JSC "Rīgas elektromašīnbūves rūpnīca", an analysis was made of the malfunctions of the MRM with an asynchronous traction motor (the description of the object is given in Section 5.1) and the external signs of their manifestation (state parameters). The basis for the analysis was the data of the log of acts of work performed, which recorded information about the impacts. The analysis includes data for the period from January 4, 2018 to January 31, 2022.

Despite the listed causes of mechanical failures, most of them are directly related to the electric drive. An analysis of the entire picture of emerging malfunctions of rolling stock electric locomotives showed that it is necessary to introduce control of the condition of mechanical components (wheel sets and traction gearboxes), since these elements are connected with the electric motor by a single energy flow (electrical and mechanical energy) circulating in the drive. The main characteristics of traction MGU are given in Table 5.1.

2.2. Methods for processing diagnostic signals and assessing the technical condition of equipment

2.2.1 Basic provisions for vibration control. Calculation of significant vibration signal frequencies

At present, the frequency spectrum of vibration (vibration velocity, vibration acceleration and vibration displacement) of the assembly is the main input parameter for vibration control. Spectral analysis is based on the selection of the most characteristic and sensitive areas of signal frequencies.

In order to decompose the obtained measurements into the frequency spectrum and identify all the amplitudes of those frequencies at which defects occur, the fast Fourier transformation method (hereinafter referred to as FFT) is used.

Vibration can be divided into three types based on human perceptions: slow motion and visible, invisible but sensible by touching, and insensible by touching but audible as abnormal noise [88]–[94] as shown in Fig. 2.1.
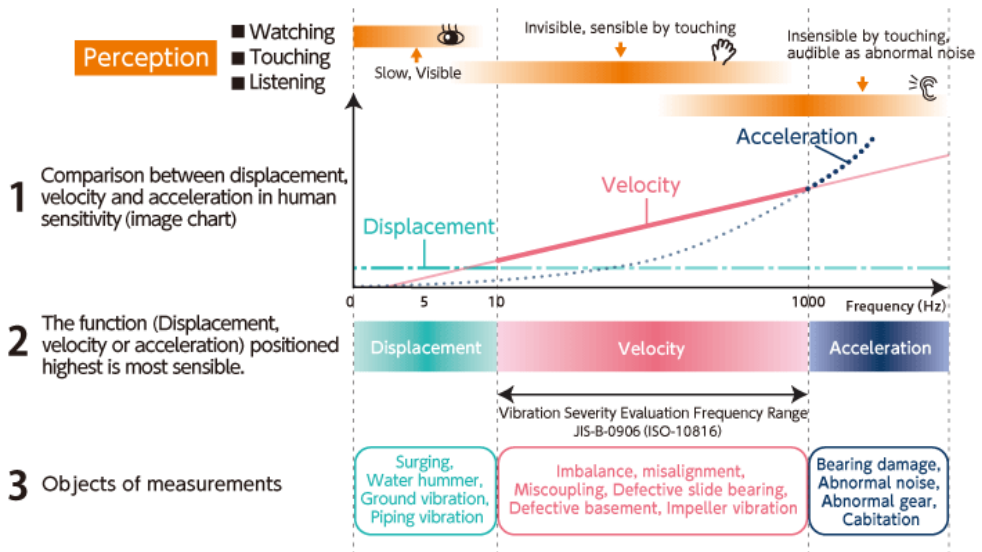

Fig. 2.1. Types of vibration [88]

Identification of increased vibration amplitudes at frequencies coinciding with the frequencies of possible damage in the elements, resonant frequencies of parts, at the frequencies of the working process helps to detect and identify emerging defects at an early stage of nucleation and their development.

Solving the problems of spectral analysis using FFT allows to determine the contribution of individual vibration components to the overall picture of vibration. With the help of FFT, the vibration signal is decomposed into the simplest components of its oscillations of various frequencies and amplitudes [95]. FFT is a method of analysis based on vibration waveform. Generally, waveforms are complicated and difficult to analyse. In FFT, we break waveforms

down into a series of discrete sin waves, (left chart in Fig. 2.2) and evaluate each individually (right chart in Fig. 2.2).
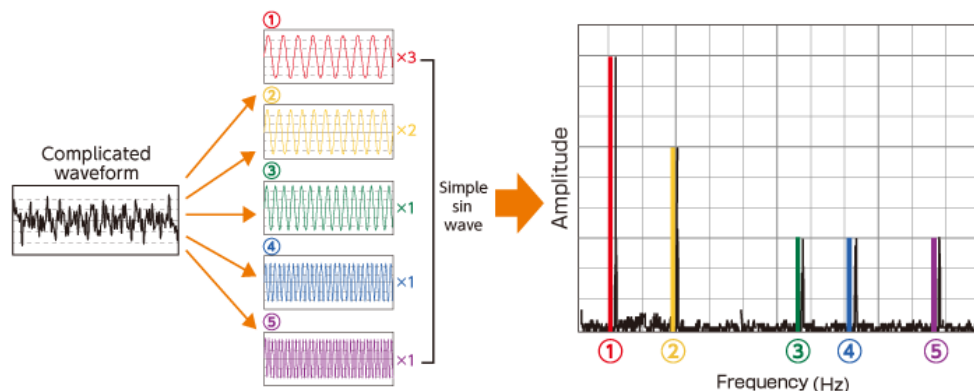

Fig. 2.2. Graphic interpretation of FFT [88]

The higher the rotational speed of the machine, the higher the vibration frequencies will be, the larger the measured frequency range must be in order to cover vibrations at high frequencies.

For machines consisting of mechanisms that contain toothed gears, blades, finger and gear couplings, rolling bearings, the maximum frequency of the measured frequency range is selected by a 3-fold product, for example, of the number of "blades" (fingers, balls, etc.) on the rotation speed of the machine. The resulting maximum frequency in the calculations (vane, finger, ball, outer and inner ring frequencies) is selected as the maximum frequency of the measured frequency range. Usually, a measurement in such a frequency range makes it possible to obtain all the necessary information about the state of a machine or mechanism [95].

To analyse the obtained spectrum of the vibration signal, it is necessary to know which vibrations and at what frequency occur when a particular defect appears. The most common components in the vibration signal spectrum are the following [95]: reverse frequency, harmonics, subharmonics, resonant frequencies, non-harmonic vibrations, sidebands, and broadband noise.

In [95], the basic rules for analyzing the vibration spectrum are described, the main of which is the following: with an increase in the number of harmonics and an increase in the amplitude of oscillations in the spectrum, the state of the machine or mechanism is considered unsatisfactory.

The key characteristics for evaluating an object are the signal frequency and its amplitude, since in the vibration signal spectrum method, the presence of one or another frequency component in the spectrum indicates the occurrence of the corresponding defect, and the amplitude indicates the depth of this defect.

Each mechanical assembly has its own set of frequencies at which one or another defect manifests itself. For example, the frequencies of manifestation of various defects in rolling bearings are determined by expressions from [61], [95].

Separator rotation frequency fq (2.1) (this vibration component appears if one of the rolling elements has a smaller (larger) diameter).

$$f_q = \frac{1}{2} f_r \left(1 - \frac{d_w}{d_q} \cos\phi \right), \tag{2.1}$$

where f_q – separator rotation frequency, Hz;

f_r – frequency of rotation of the shaft (inner ring of the bearing), Hz;

d_w – diameter of rolling elements, mm;

d_q – separator diameter, $d_{sep}=(d+D)/2$, where d, D – internal and external diameter of the bearing, respectively, mm;

ϕ – angle of contact of the rolling elements with the treadmill, in degrees [65].

The rolling frequency of the rolling elements on the outer ring f_0 (2.2) (the presence of this vibration component is determined by the fact that the shaft "jumps" on each rolling element)

$$f_0 = \frac{1}{2} z f_r \left(1 - \frac{d_w}{d_q} \cos\phi \right). \tag{2.2}$$

Rolling element rolling frequency on the inner ring is f_i (2.3). This vibration component appears if the shaft (inner ring of the bearing) is not perfectly round, but, for example, has local wear. Then the shaft "fails" on each rolling element when the latter enters the wear zone:

$$f_i = \frac{1}{2} z f_r \left(1 + \frac{d_w}{d_q} \cos\phi \right). \tag{2.3}$$

Rotation frequency of rolling elements is f_w (2.4). If the rolling body is not round, but has a facet, then with the frequency of its rotation, the shaft either "jumps" or "falls through".

$$f_w = \frac{d_q}{2 d_w} f_r \left(1 - \left(\frac{d_w}{d_q}\right)^2 (\cos\phi)^2 \right). \tag{2.4}$$

Resonant frequency of rolling elements is f_{wr} [65]:

$$f_{wr} = \frac{0{,}848 E}{d_w 2 \rho}, \tag{2.5}$$

where E – modulus of elasticity of the material of the rolling elements, Pa;

ρ – specific density of the material, kg/m^3.

Table 2.3 coresponds defects and the values of the frequencies of their manifestation.

Based on the above expressions (2.1)-(2.5), the maximum frequency of the vibration signal received from the bearings that are subject to control is determined.

After that, according to the Kotelnikov theorem, the sampling frequency and sample size are determined for decomposing the received signals into the frequency spectrum.

If it is known that the analog signal $x(t)$ has a limited spectrum, then it can be reconstructed from its discrete samples taken at a frequency twice the maximum frequency of the spectrum f_{max}: $f_{dis} > 2 f_{max}$ [96].

Table 2.3

The frequency of manifestation of various bearing defects [13]

Bearing defect	Fundamental defect frequency	Presence of harmonics in signal	Strong defect threshold
Distortion of the outer ring during landing	$k \cdot f_0$	$k = 1,2$	16%
Non-uniform radial interference	$k \cdot f_r$	$k = 1,2$	13%
Slippage in the seat	$k \cdot f_r$	$k = 1,2,3$	9%
Bearing loosening	$k \cdot f_r$	$k = 0.5,1,2,3$	13%
Rubbing in the bearing and seals	$k \cdot f_r$	$k = 0.5,1,1.5,2,2.5,3$	13%
Lubrication issues	General vibration background	-	20dB
Increased bearing clearances	$k \cdot f_r$	$k = 1,2,3,4,5,6$	13%
Wear of the outer ring surface	f_0	-	16%
Surface wear of rolling elements	$k \cdot f_w$ или $(k \cdot f_r) - (k \cdot f_w)$	$k = 1,2,3$	15%
Wear on the surface of the inner ring	$k \cdot f_r$	$k = 1,2,3,4,5,6$	13%
Friction surface group defect	$(k \cdot f_0) + (k \cdot f_i)$ $(k \cdot f_0) + (k \cdot f_r)$	$k = 1,2,...$	16%
Sinks (chipped) on the outer ring	$k \cdot f_0$	$k = 1,2,3$	16%
Shells (chipped) on the inner ring	$k \cdot f_i$	$k = 1,2,3$	15%
Shells (chipped) on rolling elements	$k \cdot f_w$	$k = 1,2,3$	15%

When recording vibration signals generated by gears, it is necessary to take into account the main characteristic features of their operation, described in [16].

The main rule: when gearing defects appear, not only does the amplitude of the gearing harmonic increase, but side harmonics appear near the gearing frequency.

The frequency shift between the main peak of the gearing harmonic and the side harmonic tells which gear has the suspected defect. If the frequency shift is equal to the reverse frequency of the input shaft, then the defect is located on it, if the shift is equal to the reverse frequency of the output shaft, then the defect is located accordingly. Sometimes there are lateral harmonics from both shafts, while the most defective will be the shaft, the family of lateral harmonics from which will have large amplitudes [16].

The frequencies of manifestation of various defects in gears are the sum of the frequency of gearing (F_z), as well as the rotational frequencies of the input and output shaft (F_{r1} и F_{r2}).

The gearing frequency F_z is found by the formula [16]:

$$F_z = Fr_n z_n, \qquad\qquad (2.6)$$

where z_n – the largest number of teeth in a tooth pair;
Fr_n – rotational frequency of the wheel with the largest number of teeth, Hz.

The harmonic amplitude at the gear frequency is usually very sensitive to load. When analysing the spectra of vibration signals, the most serious attention should be paid to [16]:

- the presence in the vibration spectrum near the gearing harmonic of lateral harmonics from the main gearing frequency, located to the left and right, in frequency, from the F_z peak;
- the relative magnitude of the amplitude of these lateral harmonics of the gearing frequency in relation to the amplitude of the peak of the main gearing frequency;
- the value of the frequency step of alternation of the lateral harmonics of the toothing frequency: how much they are shifted relative to each other and relative to the main harmonic;
- the presence in the spectrum of a characteristic hump (humps) of "white noise" near the gearing frequency, its average level relative to the harmonic of the gearing frequency itself, and the relative power level concentrated in each hump;
- the presence of peaks and "white noise" in the spectrum in all other frequency bands of the vibration spectrum, located in areas that at first glance are not related to the gearing frequency.

Table 2.4 presents gear defects and their frequency values [26].

Table 2.4

Frequency of occurrence of defects in gear transmission

Gear defect	Fundamental defect frequency	Harmonics	Development of a defect
Gear pair wear (defect on the input shaft)	F_z, $F_z \pm k \cdot F_{r1}$	3 side harmonics, unpaired	"White noise"
Gear pair wear (output shaft defect)	F_z, $F_z \pm k \cdot F_{r2}$	+ (4-5 side harmonics)	"White noise"
Gear eccentricity	$F_z \pm k \cdot F_{r1}$ or $F_z \pm k \cdot F_{r2}$	k = 1,2,3,4,5,...	Side harmonics rise
Gear misalignment	$k \cdot F_z$	k = 1,2,3	The appearance of side harmonics
Cracked (broken) tooth	Timing signal analysis	–	On the oscillogram, it is possible to track the amplitude of the beats

The maximal frequency of the received signal for controlled gears can be quite high. For the object under study, with the maximum number of revolutions - 4653, the frequency value reaches 1.94 kHz for the first and most loaded gear stage ($z = 25$) and 860.1 Hz for output stage ($z = 61$).

When carrying out vibration control of rolling bearings and gears, it is also necessary to determine the sample length. In order to analyze the frequency band up to 2 kHz, it is necessary to take at least 1000 samples per second, in accordance with the Kotelnikov theorem [96].

2.3. General provisions and analysis of methods and means for diagnosing the MGU of electric rolling stock

2.3.1 Diagnosis of MGU as part of the traction and energy assessment of electric rolling stock

Wheel-motor units - must provide the necessary work resource within the specified time limits. The operation of rolling and sliding friction systems, which include ball and roller bearing assemblies, traction gears, the uniformity of the air gap between the motor rotor and stator, and other drive devices, largely depends on their vibration state and the quality of manufacture and assembly. The most important indicators of the technical condition of the power electrical equipment of the electric rolling stock include the parameters of its own hull vibration. The intrinsic hull vibration of traction electric machines and other mechanisms is understood as vibrations of their structural elements caused by their own excitatory forces. Solving the problems of reducing own hull vibration at the design, manufacturing, repair and assembly stages, ensuring the stability of the vibration level during operation is impossible without vibroacoustic diagnostics, predicting the technical condition, a detailed analysis of the processes of formation of driving forces and vibration, taking into account the influence of defects and features of the operation of traction electrical equipment in composition of the train energy system on these processes [97].

Technical diagnostics is the science of recognizing the state of a technical system. Technical diagnostics studies methods for obtaining and evaluating diagnostic information, diagnostic models and decision-making algorithms. The purpose of technical diagnostics is to increase the reliability and service life of technical systems [98]. The tasks of technical diagnostics are: monitoring the technical condition, finding a place and determining the causes of failure (malfunction), predicting the technical condition.

Currently, to determine the technical condition of the nodes of the wheel-motor units of the rolling stock, vibroacoustic diagnostics is most widely used [99].

The purpose of vibroacoustic diagnostics is to assess the degree of deviation of the technical state of the mechanism from the norm by indirect signs, namely, by changing the properties of vibroacoustic processes in the mechanism, depending on the nature of the interaction of its components and parts [100].

Vibroacoustic diagnostics - determination of the internal state of the machine by its vibroacoustic characteristics - is a section of the dynamics of machines associated with the study of their own hull vibrations and noise, which is called the acoustic dynamics of machines [101]–[103].

The vibration of machines that occurs during operation is due to errors in design, manufacture, and assembly, as well as the discreteness of the structure of individual elements (for example, a finite number of grooves of the rotor, stator, rolling elements in bearings, the number of teeth of traction gears, etc.) [104].

The use of vibroacoustic diagnostics as a method for determining the technical condition of bearing assemblies of wheel-motor blocks of a rolling stock requires preliminary studies of the laws of distribution of random variables characterizing the change in the technical condition of a rolling stock unit, classification of faults, development of diagnostic features that determine

the technical condition of a rolling stock unit. The solution of these issues will ensure an increase in the operational readiness of the rolling stock.

The failure of the unit, regardless of its design or functional complexity for the operating personnel, occurs suddenly, although the preparation of this failure sometimes proceeds for a long time: the working surfaces of the parts wear out, fatigue phenomena accumulate in the metal, the properties of lubricants deteriorate, other similar processes occur, which are functions of the conditions and duration of operation [104].

For rotary units and machines with rotational motion, rolling bearings have a low durability and a large scatter. The service life of rolling bearings is difficult to predict due to the large discrepancy between the theoretical and actual endurance limits, errors in the summation of fatigue damage, difficulties in accounting, manufacturing, installation and operation conditions.

Technical diagnostics of machines is a system of methods and tools used to determine the technical condition of a machine without disassembling it. With the help of technical diagnostics, it is possible to determine the condition of individual parts or parts of machines, to search for faults that caused a stop or abnormal operation of the MGU.

The diagnostic object can be considered in two aspects [104]:
– in terms of structure;
– in terms of how it works.

Each of the aspects has its own characteristics, described by its own system of concepts. The structure of an object is determined by the functions assigned to it. In the structural approach, they deal with the dimensions and shape of parts, with gaps in kinematic pairs and other properties of the elements of the object that ensure its normal operation. The main concept of diagnostics associated with the structural aspect will be the state of the object [32].

The properties of the object's structure at some point in time t can be characterized by a set of parameters $x'_1, x'_2,..., x'_n$. Parameters x'_i are variable values. During the manufacture of an object, they depend on various technological factors, and during operation, on the degree of wear and destruction of parts. To set the origin of the parameter x'_i, the concept of an ideal object is introduced. An ideal object is an imaginary system, the structure of which corresponds to the project with absolute accuracy. In an ideal object, there are no violations or defects of any kind. All real objects, to one degree or another, differ from the ideal. If x^0_i is the value of the ideal object state parameter. Then the difference $x_i = x'_i - x^0_i$ will characterize the deviation of the i-th parameter of the diagnosed object from the parameter of the ideal prototype (from the nominal value) [104, 105].

The properties of an object's structure can be characterized by different sets of parameters. Bearing properties can be specified by the shaft diameter d, the diameter of the inner ring D and the gap between them h.

Thus, dependencies of the form $x_i = f(x'_1, x'_2,..., x'_n)$ are possible between some parameters of the object's structure. Thus, the technical condition of machines and mechanisms is characterized by structural parameters, the change of which is the reason for the change in the technical condition. Structural parameters are the parameters of the parts, their relative position - dimensions, gaps, distortions, geometry violation, consumable characteristics, etc. Thus, the technical condition of the object is determined by a set of technical parameters characterizing the possible deviation of the object from normal functioning, leading to failure [106].

In the general case, the minimum condition is imposed on the set of structure parameters x_i. The set of parameters $x_1, x_2,..., x_n$ will be minimal if none of these values can be functionally expressed through the values of other parameters included in the set.

In addition to being minimal, the set of parameters describing the structure of the mechanism must satisfy the condition of completeness. The set of parameters x_i will be complete if the change in the technical state under the given operating conditions is determined by changes in one or more parameters of this set. Knowing their value allows you to make unambiguous decisions about the need for repair and maintenance of the mechanism [106].

The state of an object is the complete minimum set of structure parameters $x_1, x_2,..., x_n$, characterizing the deviation of the object structure from the structure of the ideal prototype.

With a functional approach, an object is considered as a single system that generates various processes. Any working object generates many processes of different physical nature: it gives off mechanical energy, emits heat and acoustic vibrations, etc.

All these processes can be characterized quantitatively by the set of parameters $s_1, s_2,..., s_m$. The value of these parameters depends on the state of the object and on its mode of operation (speed, load, etc.). If the operating mode of an object during diagnostics is strictly regulated, then any change in the value of the indicated parameters should be prescribed to a change in the shape, size, etc., i.e., a change in the state of the object. Based on this, the parameters of the output processes of the object are considered as functions of the state $s_j=s_j(x_1, x_2,..., x_n)$ [106].

A group of state functions based on the performance criteria of an object is a numerical characteristic of the ability of an object to perform a given job, i.e. parameters characterizing the operation of the object. The most commonly used indicators are efficiency (efficiency), productivity, etc.

Another group of state functions includes the numerical characteristics of various processes, i.e., the parameters of the diagnostic signal accompanying the operation of the object (accompanying the operation of the object) and available for direct measurement. By themselves, the processes that form a diagnostic signal, as a rule, are not significant from the point of view of the object's operability, and therefore, in machine science, with the exception of diagnostics, they are usually not studied. But in diagnostics, their role is essential: they serve as a source of information about the state of the object [104].

In the process of troubleshooting, the state of the object is divided into classes of faults that do not differ from each other. The number of classes (hence the number of fault states included in them) determines the detailing of fault locations achieved during troubleshooting. This degree of detail in technical diagnostics is usually called the depth of search or the depth of diagnosis [105].

The characteristics of the diagnostic signal containing information about the parameters of the technical state of the object are called diagnostic signs of the state.

The practical solution of applied problems of diagnostics is to find diagnostic signs that are unambiguously associated with the corresponding structural parameters that determine the main reasons for the degradation of the technical state of the object. These diagnostic features should be practically mutually statistically independent of each other and must correspond to mutually statistically independent classes of faults and object defects. The word "practically" reflects the presence of relationships between all defects and diagnostic features as an objective property of nature. The components of these vectors are considered practically independent,

between which the Linder measure (the square of the correlation coefficient) does not exceed 10% [36].

2.3.2 General provisions of MGU vibration diagnostics

To diagnose the MGU units, a vibrodiagnostic method is used based on the analysis of vibration signals recorded by piezoelectric vibration transducers (vibration sensors). To control the technical condition of the equipment, as a rule, the general level (rms value) of vibration acceleration, vibration velocity and vibration displacement is used, and spectral analysis of the vibration acceleration envelope is used to determine specific faults [107].

The standard indicators are determined on the basis of a statistical method that takes into account the probabilistic processes of changing the technical condition of the MGU. Thus, the statistical determination of diagnostic parameters for bearing assemblies of the MGU rolling stock is one of the foundations of diagnosis.

The reactions of mechanical systems to excitation by mechanical vibrations are determined by complex physical processes, even when measuring on the same element of the unit at points close to each other, a different nature of the studied vibrations can be observed. Therefore, it is important to make vibration measurements at the same places, called vibration measurement control points [108].

To ensure reliable diagnosis, it is necessary that the static load on the bearing acts on those areas of the rolling surfaces on which operational defects are formed. When hanging the wheelset on jacks, the load on the rolling surface changes direction, due to which the measured vibration signal may not show signs of defects in the outer ring of the bearing. To avoid such a situation, the rotational speed of the wheelset must be large enough so that the centrifugal forces acting on the rolling elements of the bearings significantly exceed their gravity and perform the functions of a static load. At the same time, the rotational speed of the wheelset should not be too high, so that the centrifugal forces acting on the unbalanced wheelset are significantly lower than its gravity. Then, during the rotation of the wheelset, additional shock loads will not appear in the bearings with a gap, distorting the vibration diagnostic signs of a number of defects.

The most important condition for obtaining a reliable diagnosis is the correct choice of points and directions of vibration control. In this case, the following basic rules should be observed [99]:
- the bearing vibration control point should be as close as possible to the point of action of the static load on the bearing;
- there should be a minimum of contact surfaces between the control point and the place of formation of high-frequency oscillatory forces and there should not be sharp changes in the cross section of those elements of the bearing unit through which high-frequency vibration propagates;
- vibration at medium and low frequencies is measured mainly in the direction of the static load;
- the place where the sensor is to be installed must be level, free from paint and dirt, and covered with grease.

2.4. Main results and conclusions of Chapter 2

Currently, there are many different means of technical diagnostics, differing in the type of measuring instruments, the method of processing the obtained data, and the rule for solving the diagnostic problem.

Depending on the type of execution, stationary, portable and combined means of technical diagnostics are distinguished. Stationary systems are local and distributed, in which the elements of the diagnostic system are separated in space and communication between them is carried out via data transmission channels. Portable systems are characterized by their portability with a limited number of measuring channels.

Depending on the level of automation, expert and automatic diagnostic systems are distinguished. In expert systems, the decision on the technical condition of the object is made by a person, in automatic systems, the decision is made by the diagnostic system.

Depending on the type and form of the diagnostic experiment, there are test, functional and functional-test diagnostic systems. In test diagnostic systems, the impact on the diagnosed object comes from the diagnostic tools. In systems of functional diagnostics, the impacts coming to the diagnosed object are set by the working algorithm of functioning.

According to the type of vibration signal acquisition, systems with parallel and serial measurement are distinguished.

As practice shows, it is not advisable to reduce the number of measuring points, and, consequently, the number of vibration sensors, since there is no strongly pronounced correlation between different measuring points.

It is possible to increase the reliability of diagnosis by reducing instrumental, methodological and subjective errors. It is possible to reduce the instrumental error by using measuring equipment with higher metrological characteristics in the vibration diagnostics system. It is possible to reduce the instrumental error by using measuring equipment with higher metrological characteristics in the vibration diagnostics system. To eliminate subjective error (human factor), it is necessary to completely exclude the influence of the operator on the diagnosis.

CHAPTER 3. INVESTIGATION OF THE STATIC STRENGTH OF THE TRACTION GEAR IN THE MOTOR BOGIE COMPOSITION

3.1. Development of a model of an electromechanical drive system

The operation of the traction gearbox drive almost all the time occurs in dynamic modes. Intensive conversion of electrical energy into mechanical energy on the motor shaft, transfer of kinetic energy in the elements of the gearbox and in the elastic system of the gearbox-wheel pair determines the continuity of the loads. The magnitude of dynamic loads that occur in the elements of the MGU depends on the energy and kinematic characteristics of the drive: motor power, drive speed and acceleration, inertia of rotational units, and external influences, including shock loads on the wheelset.

To study the influence of external conditions and drive characteristics (kinematic and energy) on the load of the gearbox elements, it is necessary to develop a traction drive model, which is a single electromechanical system in which the electrical and mechanical parts in the dynamic modes of operation of the mechanism are in continuous interaction. When developing a model, one should strive to use design schemes that adequately describe the dynamic system and avoid using coefficients that are difficult to determine.

Most often, to solve the problems of the dynamics of electromechanical systems of the traction electric drive of rolling stock, two- and three-mass design schemes are used, which reflect the processes occurring in them with a sufficient degree of accuracy [110, 111]. Using this approach, we represent the traction drive system with a three-mass design scheme (Fig. 3.1).
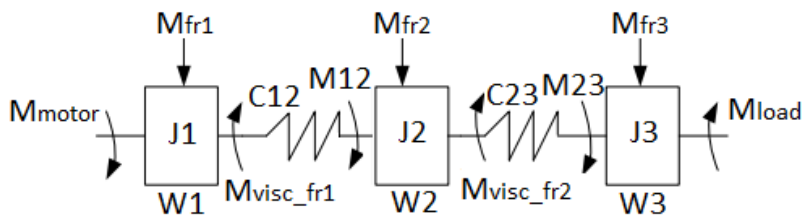

Fig. 3.1. Calculation scheme of traction gear

The elastic moment M_{12} can be represented as $M_{12} = c_{12} \cdot \delta_1$, where δ_1 - deformation of the elastic element, defined as $\delta_1 = \varphi_1 - \varphi_2$ (φ_1 and φ_2 - coordinates of the first and second mass, respectively). When developing the model, the following assumptions were made:
- the masses are concentrated;
- mechanical connections have no mass;
- the rigidity of the mechanical bonds is constant [110].

For a mathematical description of the processes in the system, taking into account that the elastic shafts and the resistance forces act on the masses in the form of viscous friction, we will take the Lagrange equation as the initial equation for the system motion:

$$\frac{d}{dt}\frac{dL}{dq_i} = \frac{dL}{dq_i} + \theta_i + F_{qi} \tag{3.1}$$

where L - Lagrange function, $L = T - P$ (T – kinetic energy of the system; P – potential energy of the system); q_i – the generalized coordinate of the system; θ_i – the generalized force; $F_{qi} = -k_i \cdot \dot{q}_i$ – the friction force; k_i – the coefficient of viscous friction [112].

Assuming that the shafts have no mass, a system with three degrees of freedom is obtained. The kinetic energy of the system in generalized coordinates is determined by the expression [110]:

$$T = \frac{1}{2}\left(J_1\dot{\varphi}_1^2 + J_2\dot{\varphi}_2^2 + J_3\dot{\varphi}_3^2 \right) \tag{3.2}$$

Potential energy is given by:

$$P = \frac{1}{2}[c_{12}(\varphi_1 + \varphi_2)^2 + c_{23}(\varphi_2 + \varphi_3)^2] \tag{3.3}$$

Substituting formulas (3.2) and (3.3) into equation (3.1), a system of equations in angular mass deviations is obtained:

$$\begin{cases} J_1\ddot{\varphi}_1 = -c_{12}(\varphi_1 - \varphi_2) + M_d - k_1\dot{\varphi}_1 \\ J_2\ddot{\varphi}_2 = -c_{12}(\varphi_1 - \varphi_2) - c_{23}(\varphi_2 - \varphi_3) - k_2\dot{\varphi}_2 \\ J_3\ddot{\varphi}_3 = -c_{23}(\varphi_2 - \varphi_3) - k_3\dot{\varphi}_3 - M_c \end{cases} \tag{3.4}$$

Taking into account the moment of internal friction M_{in_i} the system can be written in the form:

$$\begin{cases} J_1\ddot{\varphi}_1 = -c_{12}(\varphi_1 - \varphi_2) + M_d - k_1\dot{\varphi}_1 - M_{in\_1} \\ J_2\ddot{\varphi}_2 = -c_{12}(\varphi_1 - \varphi_2) - c_{23}(\varphi_2 - \varphi_3) - k_2\dot{\varphi}_2 + M_{in\_1} - M_{in\_2} \\ J_3\ddot{\varphi}_3 = -c_{23}(\varphi_2 - \varphi_3) - k_3\dot{\varphi}_3 + M_{in\_2} - M_c \end{cases} \tag{3.5}$$

Determining $M_{in\_i} = b_i(\omega_i - \omega_{i+1})$ and $M = c(\varphi_i - \varphi_{i+1})$ and replacing $d/dt = p$, a system of differential equations in operator form describing the movement of coordinates in a three-mass calculation scheme is obtained [110]:

$$\begin{cases} J_1 p\omega_1 = M_d - M_{12} - M_{frict\_1} - M_{in\_1} \\ J_2 p\omega_2 = M_{12} - M_{23} - M_{frict\_2} + M_{in\_1} - M_{in\_2} \\ J_3 p\omega_3 = M_{23} - M_{frict\_3} + M_{in\_2} - M_c \end{cases} \tag{3.6}$$

The block diagram, compiled on the basis of differential equations (3.6), is shown in Fig. 3.2.
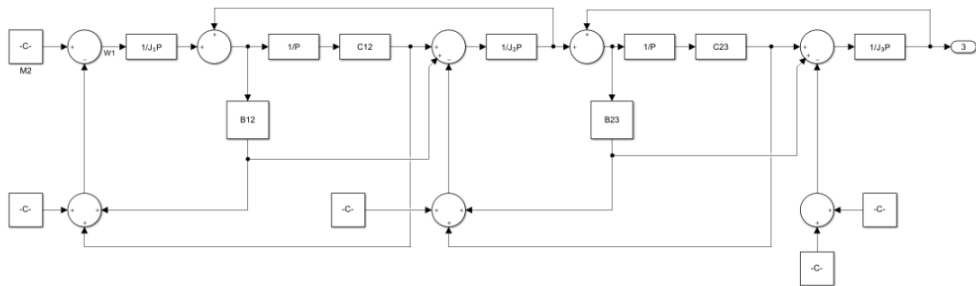
Fig 3.2. The block diagram of the mechanical part of the traction drive

Due to the fact that the rigidity of the gearing is greater than the torsional rigidity of the shafts, the inertial masses are combined in the following way:

- the pinion shaft and the wheel, which are in engagement with the elements rigidly attached to it, are a single mass;

- the stiffness between the combined masses is equal to the stiffness of the shaft connecting them.

The developed model makes it possible to study the loads that occur in the least reliable elements of the gearbox - gear shafts, depending on the speed, the forces generated by the drive, and the external load on the wheelset. The loads on the pinion shafts are determined by the moments M_d and M_{12}.

The determination of the moments of inertia of the gear shafts and gears reduced to the motor was carried out according to the formula [111]:

$$J = \frac{M \left(\frac{mz}{2}\right)^2 \cdot 10^{-6}}{\sum i^2}, kg \cdot m^2 \tag{3.7}$$

where M - gear (wheel) mass, kg; m - engagement module, mm; z - number of teeth; i - gear ratio of the driven stage of the gearbox. For the first gear stage i_1: $z = 25$, $m = 5.5$; i_2: $z = 26$, $m = 7$; i_3: $z = 56$, $m = 5.5$; i_4: $z = 61$, $m = 7$. The moment of inertia reduced to the motor was determined by the expression: $J = \frac{M_w \left(\frac{D_w}{2}\right)^2 \cdot 10^{-6}}{\sum i^2}$, kg $\cdot$ m^2, where M_w – mass of suspended wheelset, kg; D_w – wheel diameter, mm.

The moment of inertia of an unloaded wheelset reduced to the motor is calculated by the expression: $J = M_w (V_w / \omega_r)^2$, kg $\cdot$ m^2, where V_w – is the nominal speed of the wheelset, m/s; ω_r – nominal motor rotor speed, min^{-1}. In the model, the moment of inertia is calculated for a loaded motor bogie.

The electrical part of the drive consists of a control system and a power unit. The traction drive control system is built according to the subordinate principle with an external circuit in speed, average current and internal voltage. Each circuit has its own regulator. The speed circuit is a proportional P-regulator, the current circuit is a proportional-integral PI controller, the voltage circuit is a proportional-integral PI controller.

3.2. Study of the static strength of the gearbox elements

The power electrical circuit of the motor coach of the suburban electric train is shown in fig. 3.3. Each motor car (train lineup of 11 cars has 5 motor cars) has two motor bogies, each of which contains two MGU controlled by a traction converter. The power controll circuit for the traction MGU by means of converters is shown in Fig. 3.4.
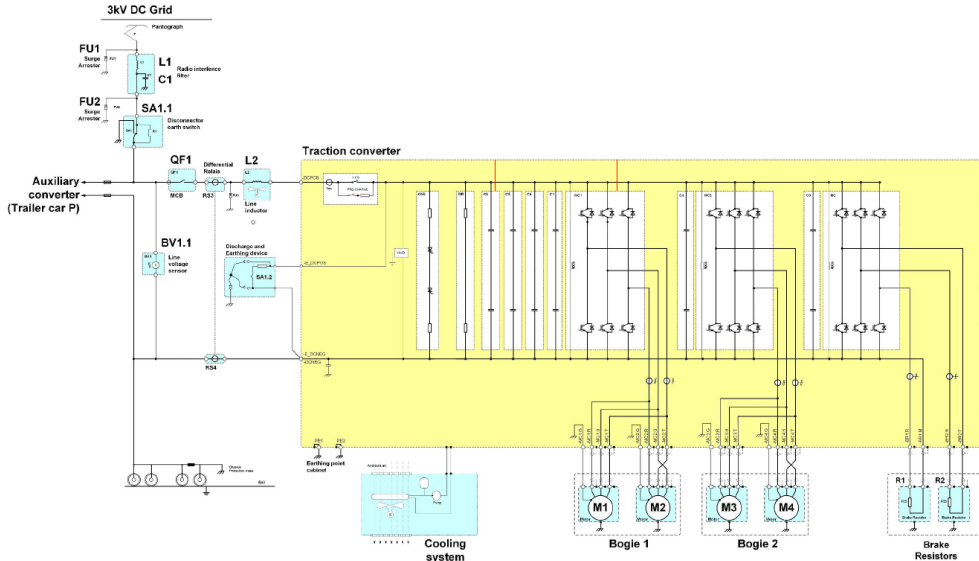

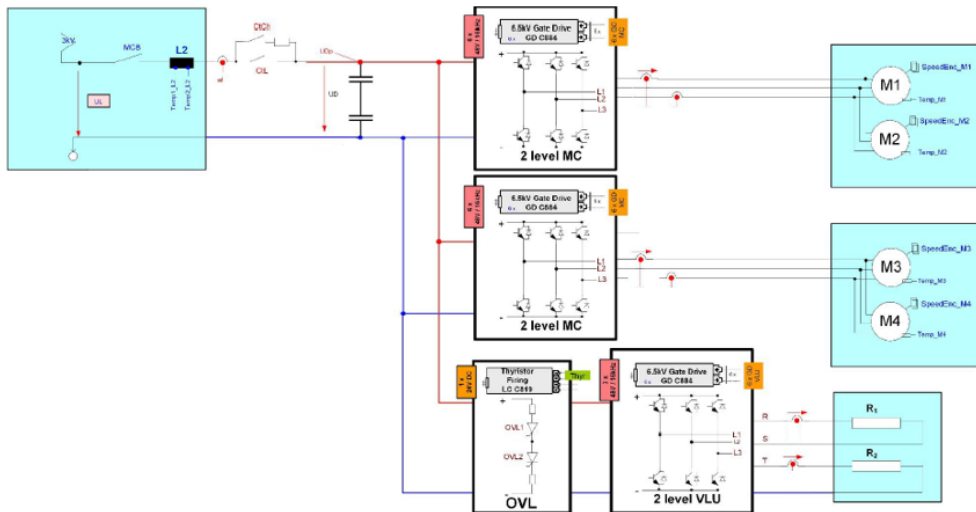Fig. 3.3. Structural diagram of the electrical part of the drive of a motor coach

Fig. 3.4. Control scheme of traction MGU by means of inverters [114]

L2 – input line choke; 2 level MC – two-level converter on IGBT transistors; OVL and 2 level VLU – braking control system on power thyristor; M1 and M2 – traction MGU of motor bogie No. 1; M3 and M4 – traction MGU of motor bogie No. 2; R1 and R2 – braking resistors.

The power section is a system of two MGUs with asynchronous motors functionally made according to the "generator-motor" structure with twin control by means of a converter on IGBT transistors. The block diagram of the electrical part of the electromechanical system, created in the MATLAB Simulink program, is shown in Fig. 3.5.
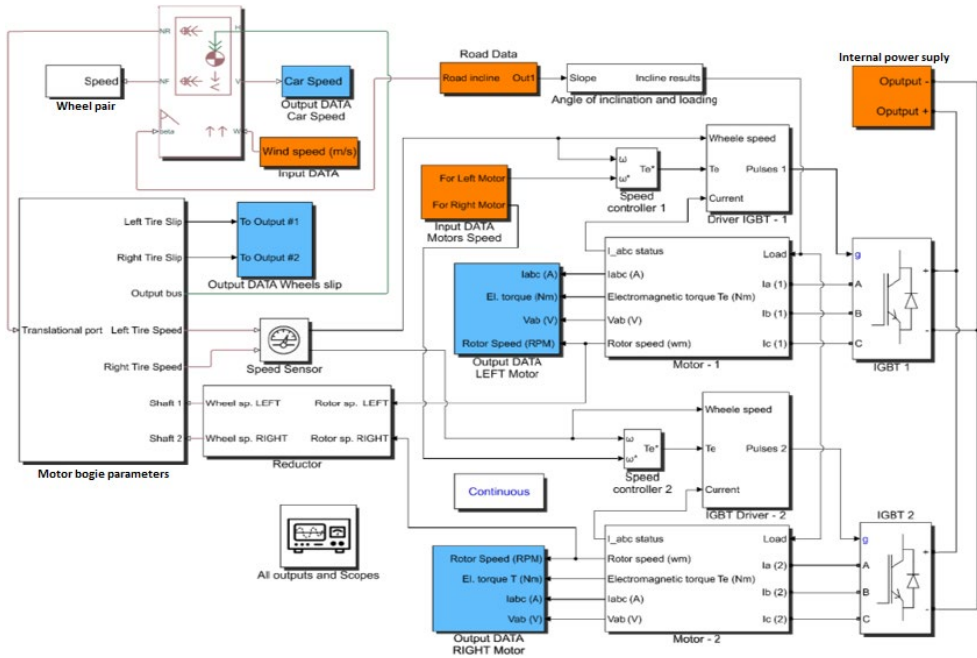

Fig. 3.5. Implementation of the researched TL mathematical model and variable identification system MATLAB Simulink [114]

The reference signal Uinput is fed to the speed controller VR, from which the error signal is fed to the current controller IR through the IMAX limiting block (current cutoff). The current regulator IR gives a reference signal to the voltage regulator UR, the output from which goes to the IGBT converter that feeds the winding of the loaded motor (RIGHT Motor), which, by controlling the current in the winding, determines the set voltage level. Next, the voltage is applied to the load motor (LEFT Motor), which is represented by an aperiodic link with EMF feedback. Feedback signals proportional to speed, current and voltage via sensors V_S, I_S and U_S are fed to their respective regulators.

Modeling of the electromechanical block diagram was also performed using the MATLAB software in the Simulink calculation module [114]–[118]. The obtained parameters of the transient process of reaching the nominal parameters for a mutually loaded pair of MGU are shown in Fig. 3.6., and traction – power energy characteristics of the drive shown in Fig. 3.7. and EMU output torque cyclogram on Fig. 3.8.
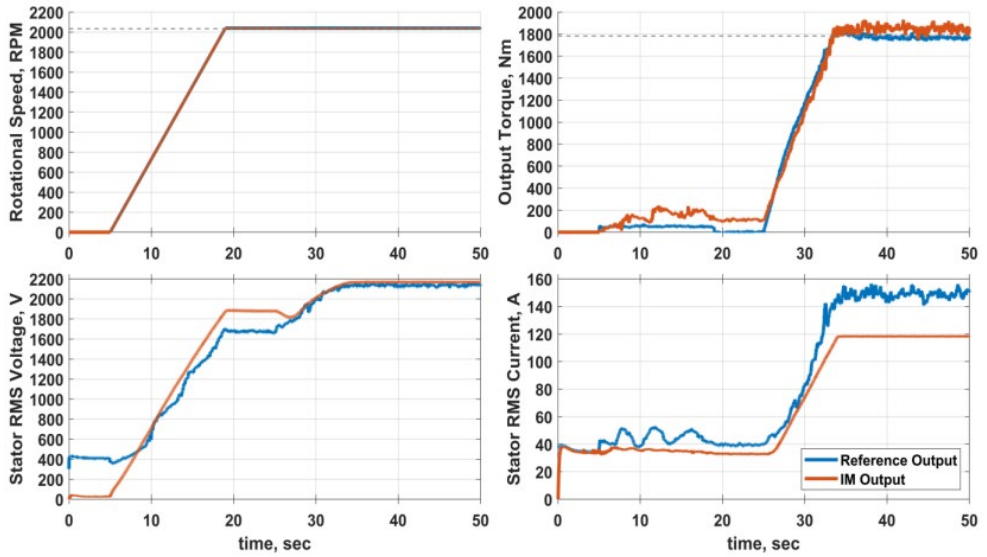
Fig. 3.6. Transient process reaching the nominal parameters for a mutually loaded MGU
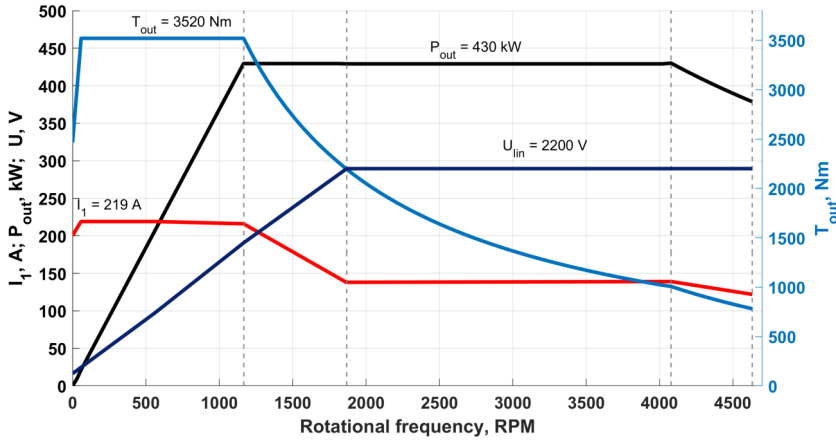

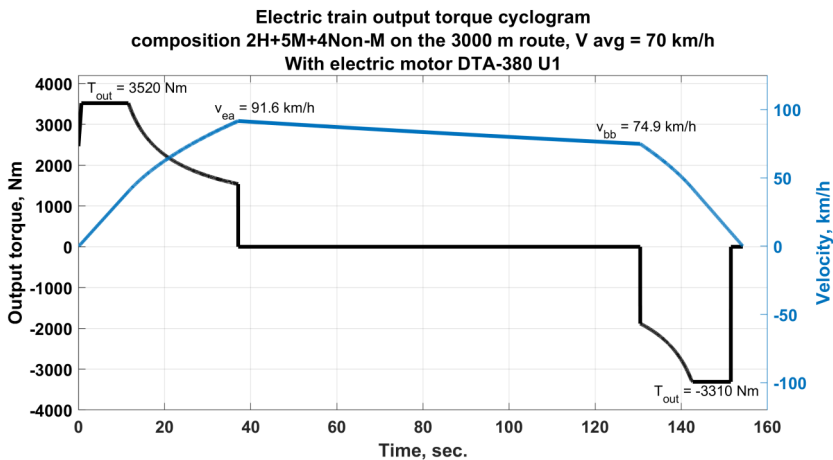Fig. 3.7. Traction – power energy characteristics of the drive

Fig. 3.8. EMU output torque cyclogram with 380 kW MGU

Due to the fact that the main modes of operation of the motor bogie drive are starting and braking, studies of the loading of the elements of the thrust reducer were carried out for these modes. When modeling, it is assumed that there are no gaps in the mechanism, the stiffness is $c_{12} \gg c_{23}$, and the first two masses are practically a single whole, according with Fig. 3.1. The assessment of the loading of the gearbox elements was carried out according to the following indicators [45]:

- $M_{d\_max} = max \,|(t)|$ - maximum load;
- $\int M_d = \frac{1}{T} \int_0^T |M_d(t)| dt$ - integral load.

The value M_{d_max} reflects the maximum value of the dynamic moment in the node under consideration, and the integral value $\int M_d$ – reflects the duration of its impact. The values of the moments were measured in relative terms and are given to the motor.

The preliminary verification of the model was carried out in two stages. The first stage: starting the motor at a speed of $0.5\omega_{nom}$ with a load moment $M_c = 0.3 M_{nom}$ and locking the drive with $M_{stop} = 2 M_{nom}$. The maximum M_{d_max} and integral $\int M_d$ values of the moments of the motors M_d, the gear shafts S_2 $M_{s-g} = M_{12}$ and on the wheelsets $M_w = M_{23}$ were registered.

Stage 2: starting the motor at a speed of 0.5 ω_{nom} with a load moment $M_c = M_{nom}$ and stopping with $M_{stop} = 2 M_{nom}$.

The results of a preliminary check of the operability of the circuit in the modes of starting and stopping with different loads showed:
- in the start mode with $M_c = 0.3 M_{nom}$, the load on the motor is the largest in terms of integral and maximum values, their minimum values are on the output shaft;
- when starting with $M_c = M_{nom}$, the load on the motor is the largest, the minimum value is on the gear shaft S_2;
- the loads that occur on the gear shaft S_2 and on the shaft of the wheelset in start-up modes with $M_c = 0.3 M_{nom}$ and $M_c = M_{nom}$ are comparable and practically do not differ;
- integral indicators of the load moment on the gear shaft S_2 in the locking mode are 15–30 % higher compared to the motor and depend on the load moment on the output shaft of the wheelset;
- the integral load on the gear shaft S_2 is less than on the output shaft of the wheelset, the difference is 7 %, the value of the maximum load on the gear shaft S_2 is less than on the output shaft by 3 %.

Oscillograms of the speed, current and torques of the motor, gear shaft in the start mode for Stage 1 and Stage 2 of simulation are shown in Figs. 3.6 and 3.7.

An analysis of the results of the studies carried out allows us to conclude that the loads that occur on the gear shaft in the gearbox in locking modes are commensurate with the loads on the working body, and in terms of the magnitude and duration of the load, the most loaded element in the thrust reducer is the gear shaft that engages with wheel. At the same time, the greater the load on the working body, the faster the motor stops and the greater the load on the elements of the gearbox housing.

3.3. Calculation of stresses of the MGU structure

Statistical analysis of the reliability of the MGU hull allows us to establish that a significant part of its failures is associated with the development of fatigue cracks in the area of the end of the splined joint and fillet. To assess the danger of stresses arising in dynamic modes, it is necessary to evaluate their magnitude and determine the places of dangerous concentration. Numerous studies of the reliability of elements of railway machines have shown that the initiation and development of fatigue cracks occurs in places of significant stress concentration, which are sharp changes in cross sections, surface roughness, chips, scratches and scuffs.

The degree of danger of the influence of stress concentrators is determined by calculating the stresses arising in them when the maximum loads occur in the element. The most informative method for determining the stress-strain states of parts with stress concentrations is the finite element method [119], [120].

The development of a finite element model of the hull was carried out in the Ansys program in the Workbench calculation module [5], [6], [94]. The geometric model of the body, made in SolidWorks 2021.

Determination of the physical conditions of simulation. The conducted studies of the loading of the gearbox elements, performed on the electromechanical model of the MGU drive, made it possible to establish the maximum loads that occur on the housing in dynamic modes. In this regard, it is necessary and sufficient to calculate the stress-strain state in a static loading model. For this purpose, the FEMAP static strength analysis is used. The model uses the following coordinate system:

- the force that acts in the X-axis direction is defined as the tangential force F_t (N)
- the force that acts in the Y-axis direction is defined as the axial force F_r (N)
- the force that acts in the Z-axis direction is defined as the radial force F_x (N).

The next step is to set the properties of the material. The body is made of structural ductile iron EN-GJS-350-22-LT with the following strength properties:

- modulus of elasticity E = 169 000 MPa;
- Poisson's ratio μ = 0.275;
- yield strength σ_y = 220 MPa.

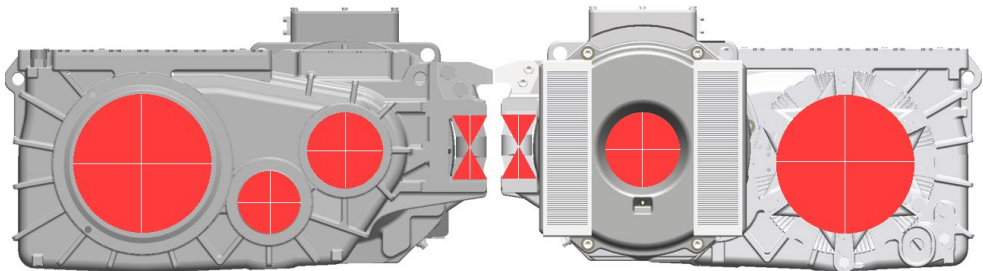The resulting model for analyzing the stress-strain state of the hull is shown in Fig. 3.9.

Fig. 3.9. Mesh of the finite element model of the hull

The supports for the housing (the location of the bearings) and the moment transmitted to the housing from the motor (applied to the seat of the bearing) are set, the kinematic diagram of the gear shaft is shown in Fig. 3.10. As a result, we obtain a numerical model prepared for the solution.
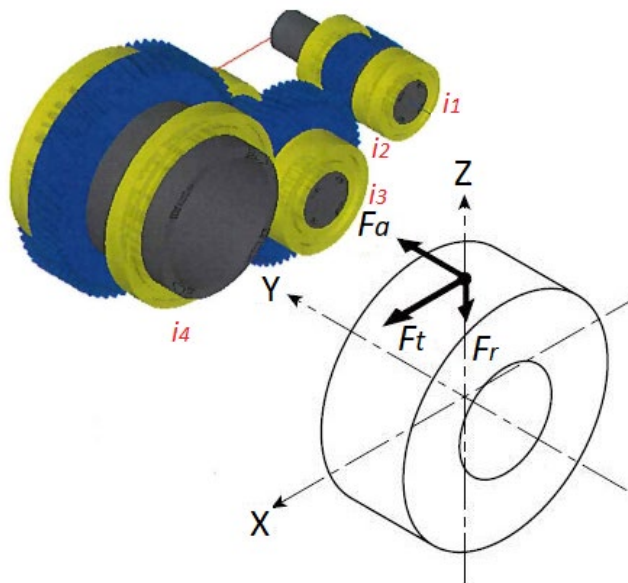

Fig. 3.10. Kinematic diagram of the pinion shaft
i_1: $z = 25$, $m = 5.5$; i_2: $z = 26$, $m = 7$; i_3: $z = 56$, $m = 5.5$; i_4: $z = 61$, $m = 7$

As a result of the performed calculations with further analysis of the results, it was possible to establish that the seating surface is a place of significant stress concentration.

The reliability of the stresses obtained in the finite element model is confirmed by the analytical solution [26]. Stresses were calculated according to the formula: $\sigma_{max} = k \cdot \sigma_{eq}$, where σ_{max} - the maximal stress; k - stress concentration factor; σ_{eq} - equivalent stresses.

Calculation of equivalent stresses on the fillet of the gear shaft is performed by the formula:

$$\sigma_{eq} = \sqrt{\sigma_{flex}^2 + 3\tau_{tw}^2},$$ (3.8)

where

$$\sigma_{flex} = \frac{M_{flex}}{0{,}1d^3}.$$ (3.9)

Here M and T are the bending and torque moments in the dangerous section during overload. The bending moment of the shaft is: $M_{flex} = F_M \cdot c$, where $F_M = 250\sqrt{T}$, where T - is the torque on the pinion shaft, Nm; c - distance from the center of application of the load to the place of the dangerous section (Fig. 3.11).
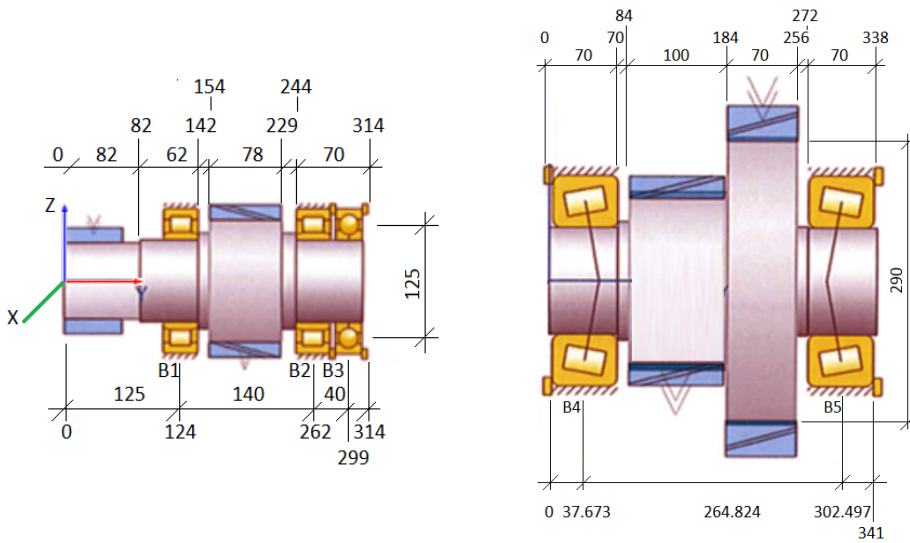
37

Fig. 3.11. Distance between 1st and 2nd stage bearings, dimensions in [mm]

The increase in stress due to the presence of a concentrator geared shaft was taken into account by the coefficient k [26]. Its value was determined as follows:

$$k = c_1 + c_2 \frac{2h}{D} + c_3 \left(\frac{2h}{D}\right)^2 + c_4 \left(\frac{2h}{D}\right)^3 \qquad (3.10)$$

where coefficients c_1, c_2, c_3, c_4 are taken for the torsion stress.

The geometric dimensions in the calculation were taken as follows: $D = 290$ mm; $h = 70$ mm. Calculated values of coefficients in torsion: $c_1 = 1.75$; $c_2 = -2.02$; $c_3 = 2$; $c_4 = -0.72$. The stress concentration factor was $k = 1.52$. Under bending conditions: $c_1 = 2.22$; $c_2 = -2.77$; $c_3 = 2.21$; $c_4 = -0.68$. The stress concentration factor was $k = 1.9$.

The performed studies of dynamic loads that occur on the most loaded element of the gearbox - the geared shaft z = 25, m = 5.5, showed that their magnitude can reach the values shown in Fig. 3.12.

The scheme for fixing the gearbox housing is shown in Fig. 3.13. At the installation site of the suspension, the fastening is made using a rotating connection. In the place of holes for axial bearings, a rotating link is used. The forces resulting from the acceleration of the motor rotor mass are transferred to the bearing reactions. The rest of the drive mass is calculated in the central acceleration settings for the entire model. The forces generated in the gearing cause reaction forces in the bearings according to the data presented in Table 3.1. [119].
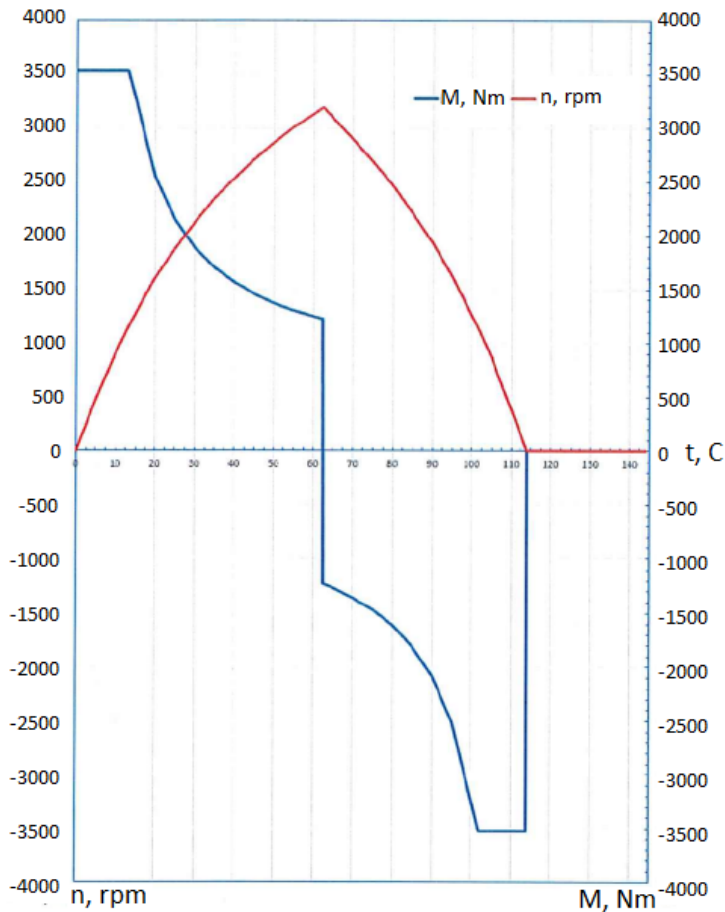
Fig. 3.12. Input geared shaft (1st atage with $z = 25$, $m = 5.5$) loading characteristics

Table 3.1

Initial Model Data

Parameter	Designation	Meaning
Traction motor shaft power in continuous mode (kW)	P_N	380
Maximum starting torque of the traction motor (Nm)	M_{max}	3551
Rated drive motor starting torque (Nm)	M_N	1176
Maximum clutch slip torque (Nm)	M_S	11000
Traction motor rotor speed, maximal constructive value (min^{-1})	n	4774
Place of application of the acceleration	Direction of acceleration	Acceleration values, g
Acceleration on gear housing and traction motor for strength (g)	Vertical transverse longitudinal	15 15 15
Acceleration on gearbox housing and traction motor for fatigue (g)	Vertical transverse longitudinal	5.4 4.7 2.5

The model contains a gearbox housing and a traction motor housing. The electrical part of the stator is replaced by a weight at the centre of gravity, as shown in Fig. 3.13. Traction silent blocks are replaced by a spring element. Finite element sizes vary from 6 to 12 mm. The model includes 773 125 elements and 1 296 304 nodes. The structure is modelled by finite elements of the types like "TETRA 10" and "Springs"

Fig. 3.13. Fixing scheme for load modes I, II, III.

Determination of the static strength of the MGU structure in the Thesis is proposed to be carried out in 3 modes with forward and reverse directions of rotation for each mode.

Mode I (forward direction of rotation)
Mode I is calculated for the maximum motor torque when starting from a standstill of 3 551 Nm. The torque is transferred to the gear in the form of forces:

tangential force $F_t = 2M_{rot}/D_0 = 49\ 891$ N (graphic discription of D_0 see in APPENDICES I and II);

radial force $F_r = F_t \cdot tg\alpha\ /\ cos\beta = 18800$ N, where $\alpha = 20\ °$, $\beta = 15°$;

axial force $F_a = F_t \cdot tg\beta = 13\ 368$ N, where $\beta = 15°$.

Further on Fig. 3.14 shows a diagram of the 1st gear bearings, and Table 3.2 shows the load values in the 1st gear bearings in the coordinate system.
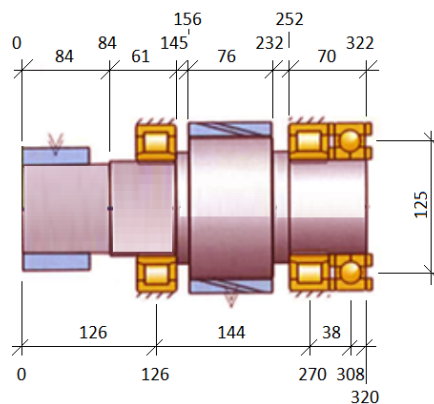

Fig. 3.14. Distance between 1st stage bearings, dimensions in [mm].

Table 3.2

Load in Bearings of the 1st Stage in the Coordinate System

Bearing No.	Force [N]						
	x'		y'	z'		xz'	
Direction	forward direction of rotation	reverse direction of rotation	forward direction of rotation / reverse direction of rotation	forward direction of rotation	reverse direction of rotation	forward direction of rotation	reverse direction of rotation
B1	11 876	−27 763	0	20 301	−15 391	23 478	31 746
B2	-31	−14 993	0	29 979	−18 283	29 973	23 649
B3	0	0	13 389 / −13 389	0	0	0	0

On Fig. 3.15 shows a diagram of the 2nd gear bearings, and Table 3.3 shows the load values in the gear bearings in the coordinate system.
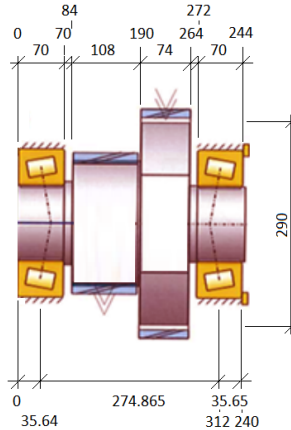

Fig. 3.15. Distance between 2nd stage bearings, dimensions in [mm].

Table 3.3

Load in Bearings of the 2nd Stage in the Coordinate System

Bearing No.	Force [N]						
	x'		y'	z'		xz'	
Direction	forward direction of rotation	reverse direction of rotation	forward direction of rotation / reverse direction of rotation	forward direction of rotation	reverse direction of rotation	forward direction of rotation	reverse direction of rotation
B4	7 847	−41 149	−21 060 / −21 878	−77 050	57 861	77 436	70 982
B5	−27 093	27 361	28 832 / 19 017	−65 999	44 047	71 276	51 853

On Fig. 3.16 shows a diagram of the 3rd stage bearings, and Table 3.4 shows the load values in the transmission bearings in the coordinate system.
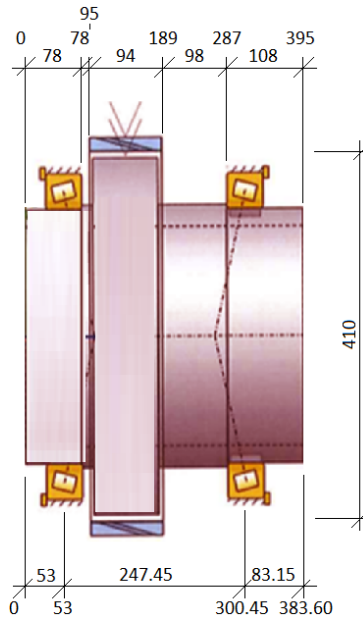

Fig. 3.16. Distance between 3rd stage bearings, dimensions in [mm].

Table 3.4

Load in Bearings of the 3rd Stage in the Coordinate System

Bearing No.	Force [N]							
	x'		y'		z'		xz'	
Direction	forward direction of rotation	reverse direction of rotation	forward direction of rotation / reverse direction of rotation	forward direction of rotation	reverse direction of rotation	forward direction of rotation	reverse direction of rotation
B6	0	0	−31 293 / −21 078	0	0	0	0
B7	0	0	10 154 / 42 221	0	0	0	0

Further, the mode includes impacts in all directions of X, Y and Z coordinates with accelerations:

$a_x = \pm 15$ g;

$a_y = \pm 15$ g;

$a_z = \pm 15$ g.

Mode I (forward rotation)

On Fig. 3.17 - 3.24 shows the resulting radial, axial loads, as well as the inertial radial loading of bearings and the reaction of the accelerating force in the labyrinths for simulated Mode I for forward rotation.
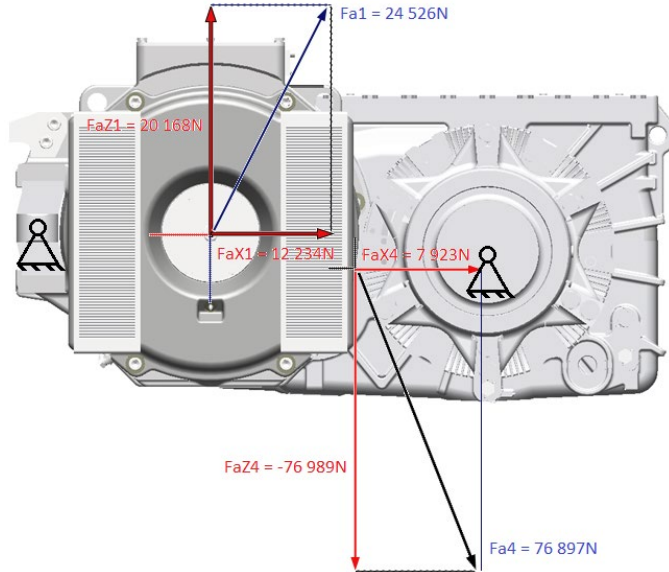

Fig. 3.17. Radial load of the 1st and 4th bearings in simulated Mode I.
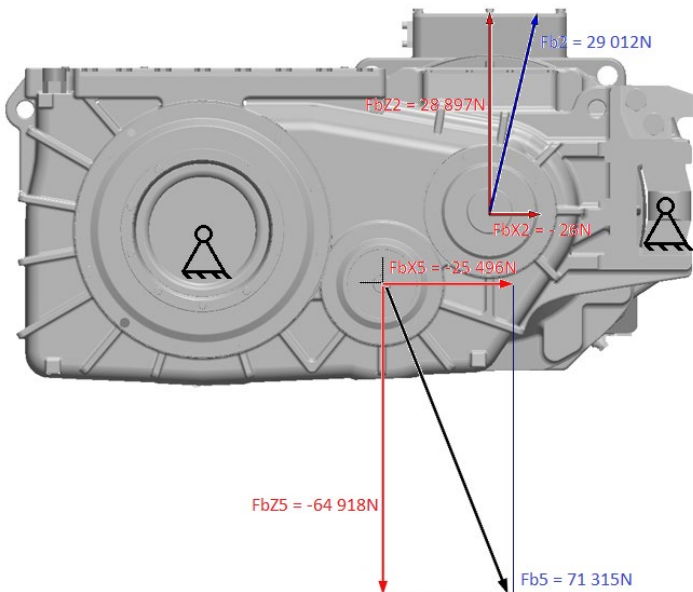

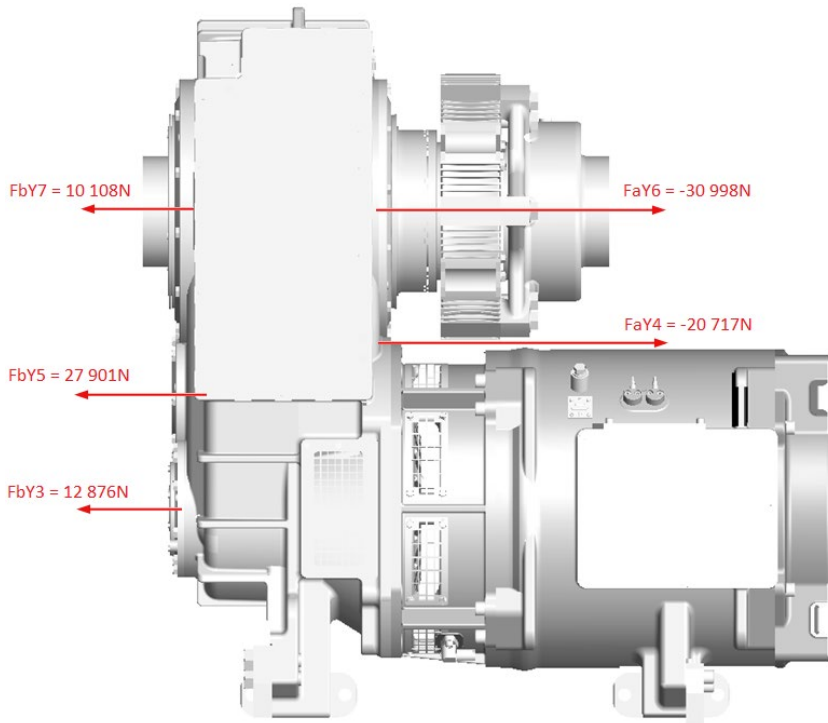Fig. 3.18. Radial load of the 2nd and 5th bearings in simulated Mode I.

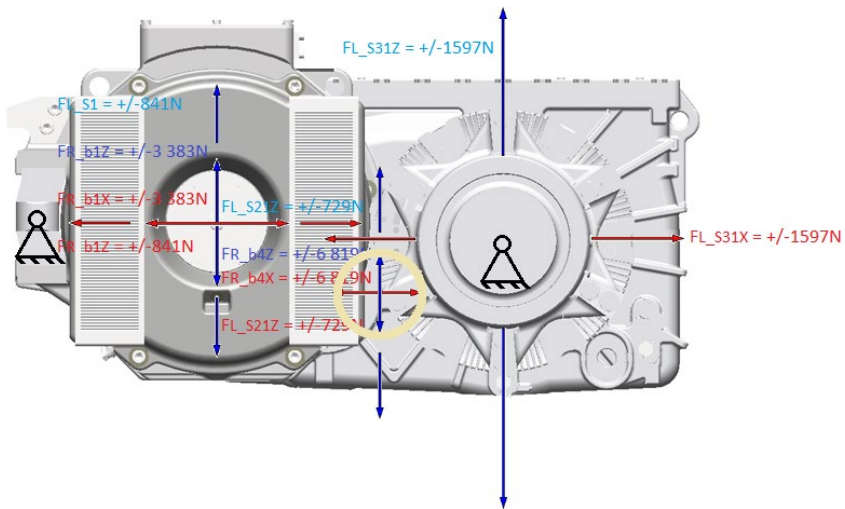Fig. 3.19. Axial load of the 3rd, 4th, 5th, 6th and 7th bearings at simulated Mode I.

Fig. 3.20. Inertial radial loading of bearings No. 1 and No. 4 and the reaction of the accelerating force in the labyrinths S1-1, S2-1 and S3-1 for simulated Mode I.
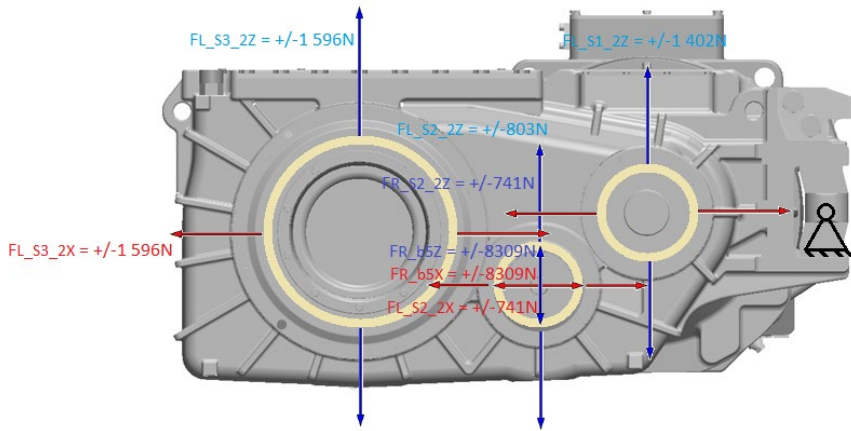
Fig. 3.21. Inertial radial load bearing No. 5 and the reaction of the accelerating force in the labyrinths S1-2, S2-2 and S3-2 for simulated Mode I.
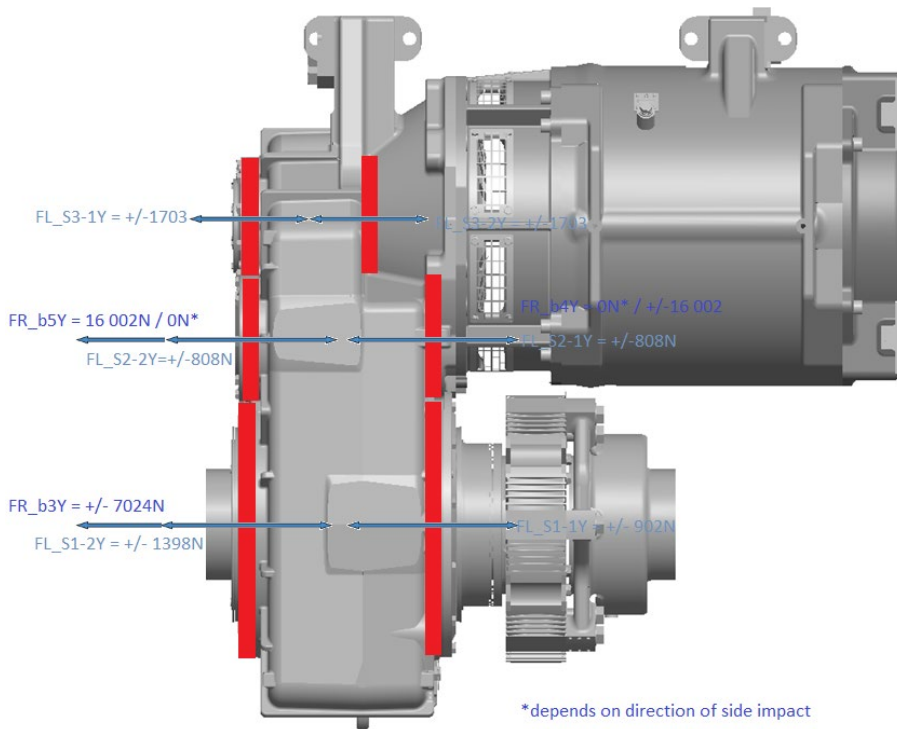

Fig. 3.22. Inertial axial load of bearings No. 3, No. 4 and No. 5 and axial force response to acceleration in labyrinths S1-1, S1-2, S2-1, S2-2, S3-1 and S3-2 for simulated Mode I.
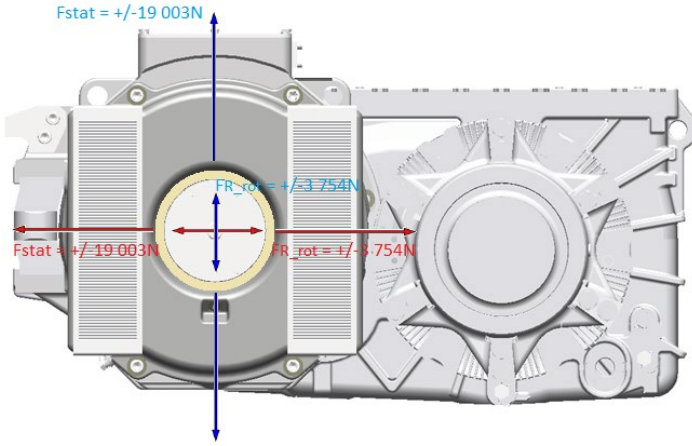
Fig. 3.23. Inertial radial load on the motor bearing and accelerating force reactions in the motor labyrinth for simulated Mode I.

Fig. 3.24. Inertial axial load of the motor for simulated Mode I.

Mode I (reverse rotation)

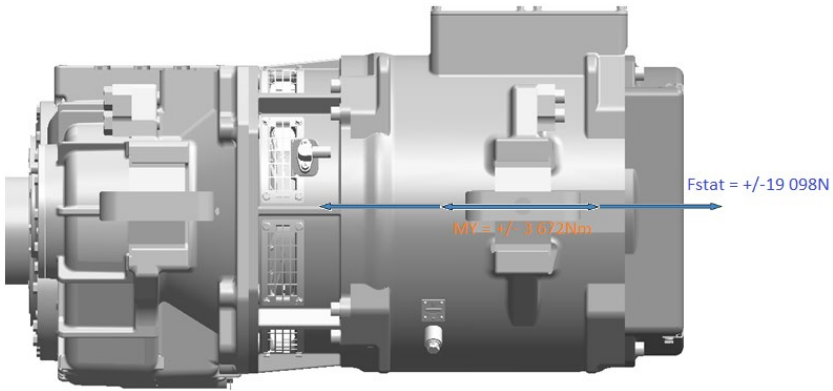On Fig. 3.25 - 3.27 shows the resulting radial, axial loads, as well as the inertial radial loading of bearings and the reaction of the accelerating force in the labyrinths for simulated Mode I for reverse rotation.

Fig. 3.25. Radial load of the 1st and 4th bearings in simulated Mode I.

Fig. 3.26. Radial load of the 2nd and 5th bearings in simulated Mode I.
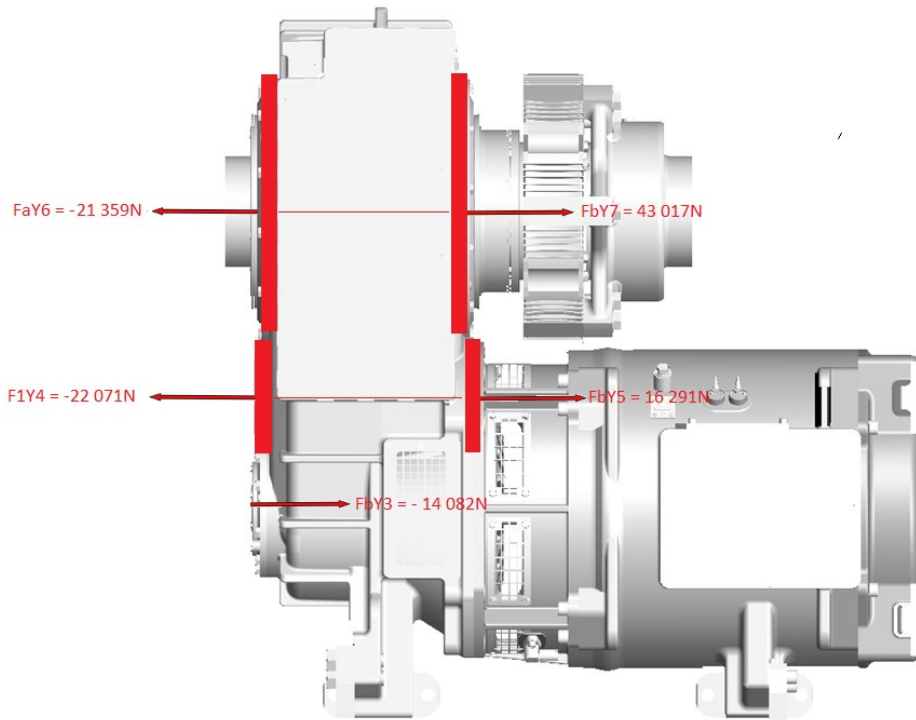
Fig. 3.27. Axial load of the 3rd, 4th, 5th, 6th and 7th bearings in simulated Mode I.

Mode II (forward rotation)

Mode II is calculated for a maximum starting torque of 11 000 Nm. The torque is transferred to the gear in the form of forces:

- tangential force $F_t = 2M_{rot} / D_0 = 154\ 549$ N;
- radial force $F_r = F_t \cdot tg\alpha / \cos\beta = 58\ 235$ N, where $\alpha = 20\ °$, $\beta = 15°$;
- axial force $F_a = F_t \cdot tg\beta = 41\ 411$ N, where $\beta = 15°$.

Table 3.5 below shows the load values in the 1st stage bearings in the coordinate system.

Table 3.5

Load in Bearings of the 1st Stage in the Coordinate System

Bearing No.	Force [N]						
	x'		y'	z'		xz'	
Direction	forward direction of rotation	reverse direction of rotation	forward direction of rotation / reverse direction of rotation	forward direction of rotation	reverse direction of rotation	forward direction of rotation	reverse direction of rotation
B1	36 731	−86 102	0	68 531	−41 931	77 734	95 667
B2	−103	−46 513	0	90 793	−58 612	90 799	74 795
B3	0	0	41 439 / −41 439	0	0	0	0

Table 3.6 shows the load values in the bearings of the 2nd stage in the coordinate system.

Table 3.6

Load in Bearings of the 2nd Stage in the Coordinate System

Bearing No.	Force [N]						
	x'		y'	z'		xz'	
Direction	forward direction of rotation	reverse direction of rotation	forward direction of rotation / reverse direction of rotation	forward direction of rotation	reverse direction of rotation	forward direction of rotation	reverse direction of rotation
B4	24 317	−127 397	−65 054 / −67 979	−238 039	179 967	239 278	220 473
B5	−283 376	84 743	89 145 / 43 867	−203 534	137 399	219 931	161 436

Table 3.7 shows the load values in the 3rd stage bearings in the coordinate system.

Table 3.7

Load in Bearings of the 3rd Stage in the Coordinate System

Bearing No.	Force [N]						
	x'		y'	z'		xz'	
Direction	forward direction of rotation	reverse direction of rotation	forward direction of rotation / reverse direction of rotation	forward direction of rotation	reverse direction of rotation	forward direction of rotation	reverse direction of rotation
B6	0	0	−97 101 / −65 073	0	0	0	0
B7	0	0	31 673 / 131 117	0	0	0	0

On Fig. 3.28 - 3.30 shows the resulting radial, axial loads, as well as the inertial radial loading of bearings and the reactions of the accelerating force in the labyrinths for calculated Mode II.
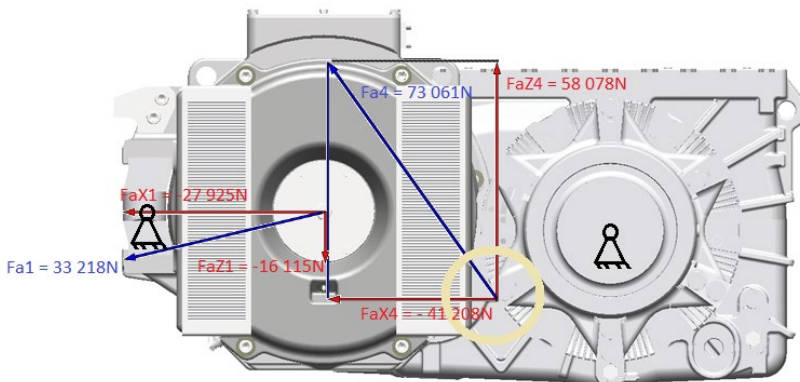

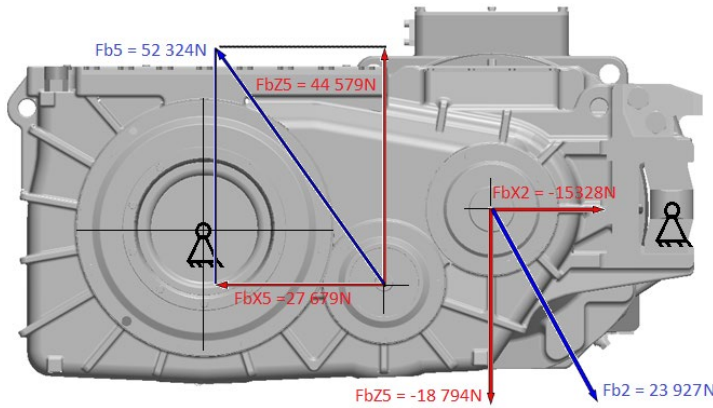Fig. 3.28. Radial load of the 1st and 4th bearings in calculated Mode II.

Fig. 3.29. Radial load of the 2nd and 5th bearings in calculated Mode II.

Fig. 3.30. Axial load of the 3rd, 4th, 5th, 6th and 7th bearings in calculated Mode II.

Mode II (reverse rotation)

On Fig. 3.31 - 3.33 shows the resulting radial, axial loads, as well as the inertial radial loading of bearings and the reaction of the accelerating force in the labyrinths for simulated Mode II for reverse rotation.
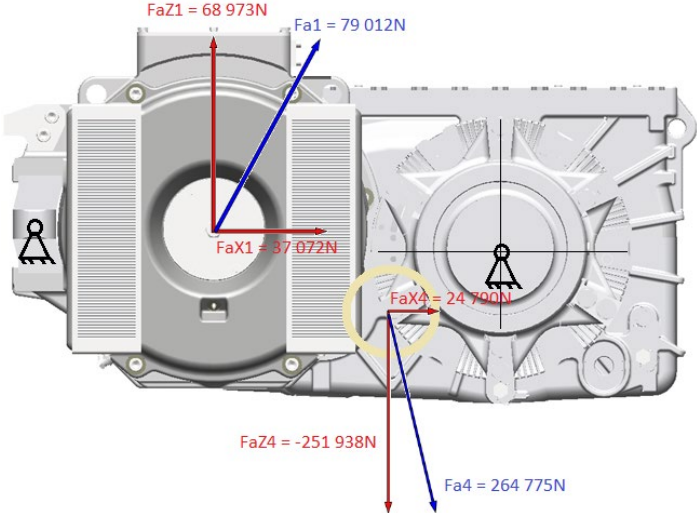

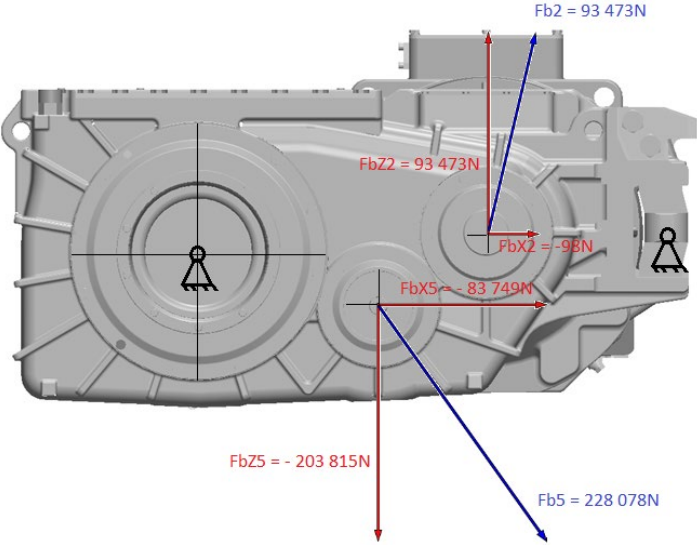Fig. 3.31. Radial load of the 1st and 4th bearings in simulated Mode II.

Fig. 3.32. Radial load of the 2nd and 5th bearings in simulated Mode II.
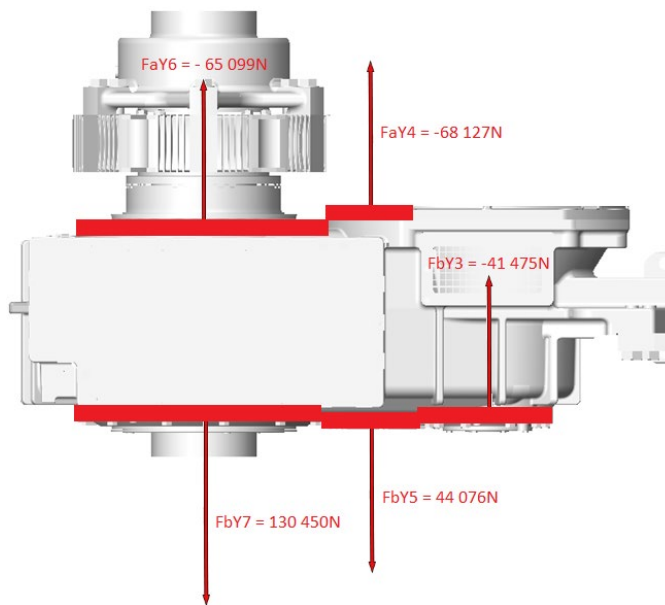
Fig. 3.33. Axial load of the 3rd, 4th, 5th, 6th and 7th bearings in simulated Mode II.

Mode III (forward rotation)

Mode III is calculated for motor torque up to 1 176 Nm and impacts. The magnitude of the forces arising in the gearing are equal to:

- tangential force $F_t = 2M_{rot} / D_0 = 24\ 953$ N;
- radial force $F_r = Ft \cdot tg\alpha / \cos\beta = 9402$ N, where $\alpha = 20$ °, $\beta = 15°$;
- axial force $F_a = F_t \cdot tg\beta = 6686$ N, where $\beta = 15°$.

Further, shocks in all directions of coordinates with accelerations are included in the Mode III:

$a_x = \pm 2{,}5$ g (longitudinal impact);

$a_y = \pm 4{,}7$ g (axial impact);

$a_z = \pm 5{,}4$ g (impact in the vertical direction).

Further in Tables 3.8, 3.9 and 3.10 the load values in bearings of the 1st, 2nd and 3rd stages are given in the coordinate system.

Load in Bearings of the 1st Stage in the Coordinate System

Bearing No	Force [N]						
	x'		y'	z'		xz'	
Direction	forward direction of rotation	reverse direction of rotation	forward direction of rotation / reverse direction of rotation	forward direction of rotation	reverse direction of rotation	forward direction of rotation	reverse direction of rotation
B1	6 103	−14 179	0	9 102	−9 143	10 757	16 701
B2	−102	−7 573	0	15 997	−8 759	15 625	11 687
B3	0	0	6 902 / −6 902	0	0	0	0

Load in Bearings of the 2nd Stage in the Coordinate System

Bearing No	Force [N]						
	x'		y'	z'		xz'	
Direction	forward direction of rotation	reverse direction of rotation	forward direction of rotation / reverse direction of	forward direction of rotation	reverse direction of rotation	forward direction of rotation	reverse direction of rotation
B4	4 079	−20 876	−10 729 / −10 998	−38 943	28 876	39 046	35 514
B5	−13 543	13 734	14 703 / 7 103	−33 477	21 918	35 984	26 001

Load in Bearings of the 3rd Stage in the Coordinate System

Bearing No.	Force [N]						
	x'		y'	z'		xz'	
Direction	forward direction of rotation	reverse direction of rotation	forward direction of rotation / reverse direction of rotation	forward direction of rotation	reverse direction of rotation	forward direction of rotation	reverse direction of rotation
B6	0	0	−16 901 / −11 002	0	0	0	0
B7	0	0	32 137 / 21 993	0	0	0	0

On Fig. 3.34 - 3.41 shows the resulting radial, axial loads, as well as the inertial radial loading of bearings and the reactions of the accelerating force in the labyrinths for simulated Mode III.

Fig. 3.34. Radial load of the 1st and 4th bearings in simulated Mode III.

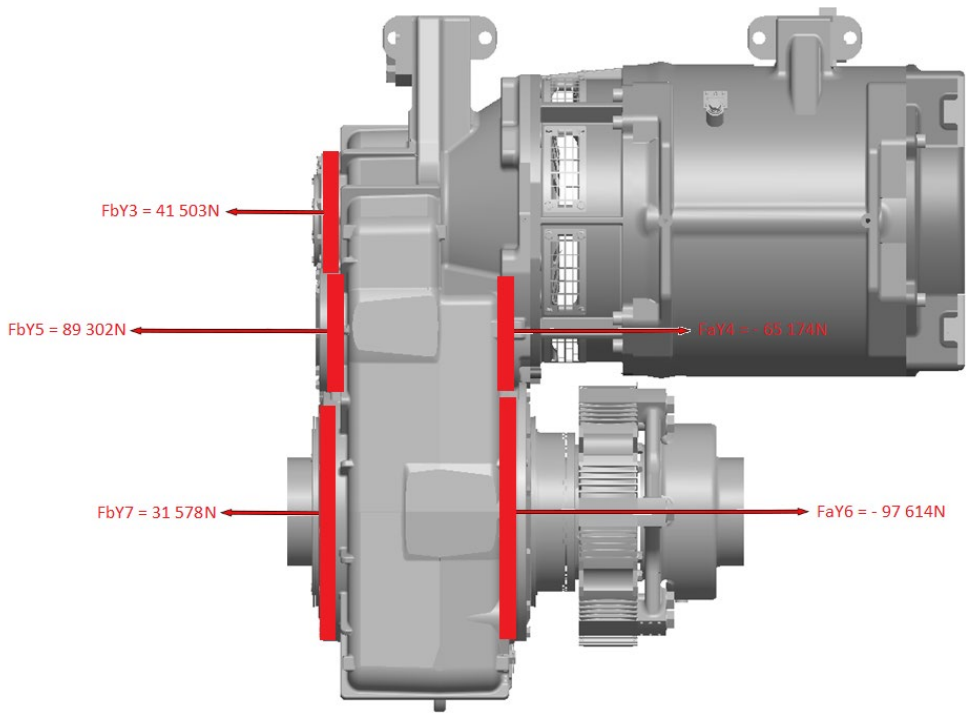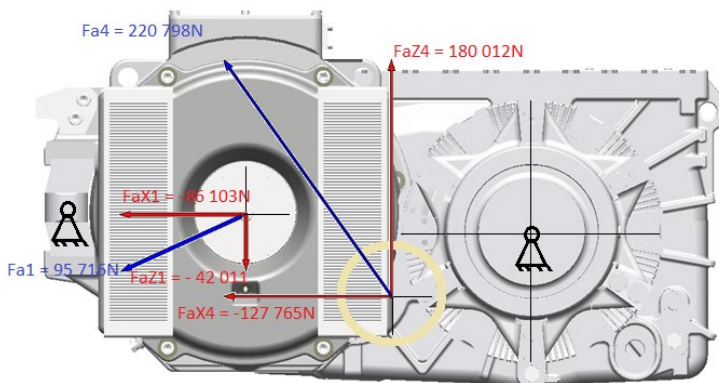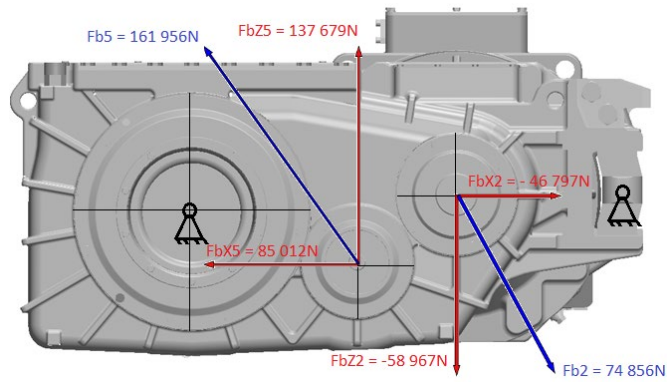Fig. 3.35. Radial load of the 2nd and 5th bearings in simulated Mode III.

Fig. 3.36. Axial load of 3rd, 4th, 5th, 6th and 7th bearings in simulated Mode III.
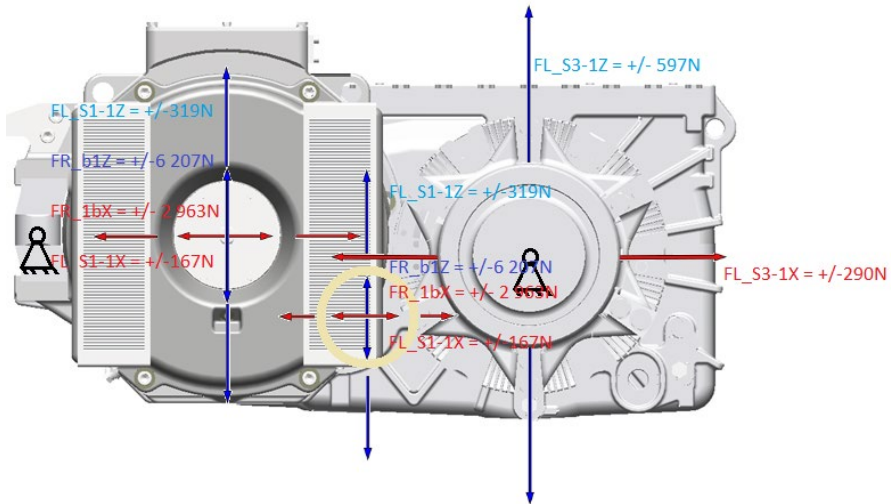
Fig. 3.37. Inertial radial loading of bearings No. 1 and No. 4 and the reaction of the accelerating force in the labyrinths S1-1, S2-1 and S3-1 for simulated Mode III.
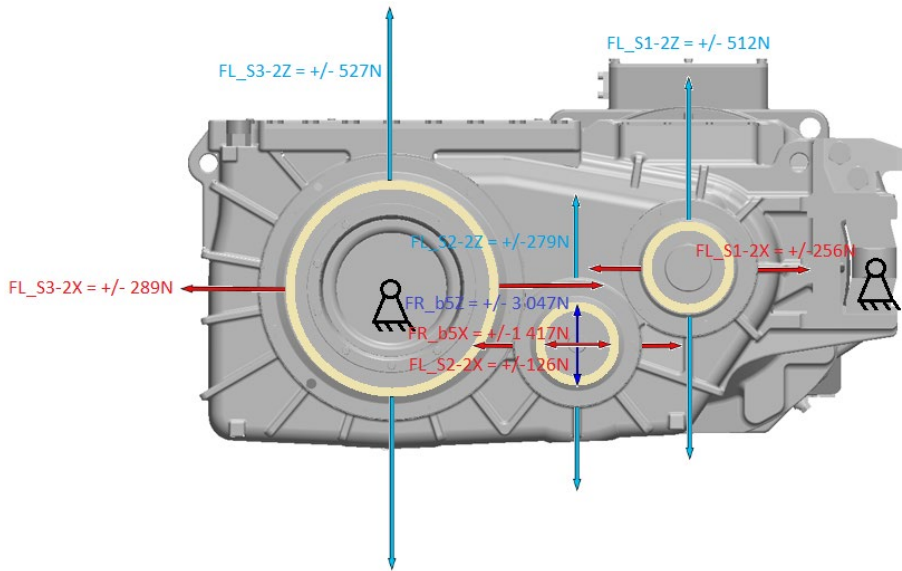
Fig. 3.38. Inertial radial load bearing No. 5 and the reaction of the accelerating force in the labyrinths S1-2, S2-2 and S3-2 for design Mode III.
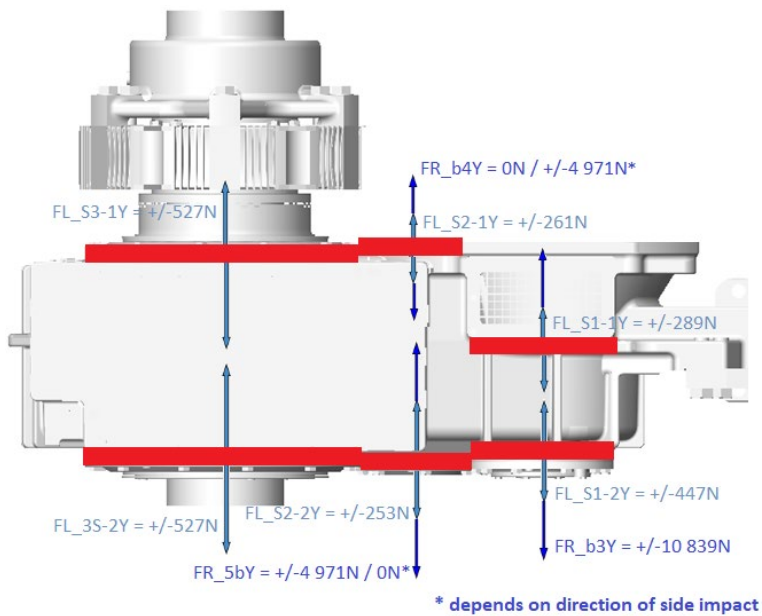
Fig. 3.39. Inertial axial load of bearings No. 3, no. 4 and No. 5 and axial force response to acceleration in labyrinths S1-1, S1-2, S2-1, S2-2, S3-1 and S3-2 for simulated Mode III.
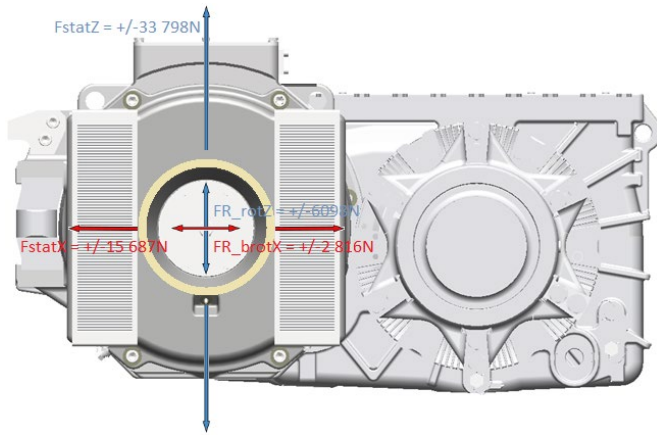
Fig. 3.40. Inertial radial load on the motor bearing and accelerating force reactions in the motor labyrinth for simulated Mode III.
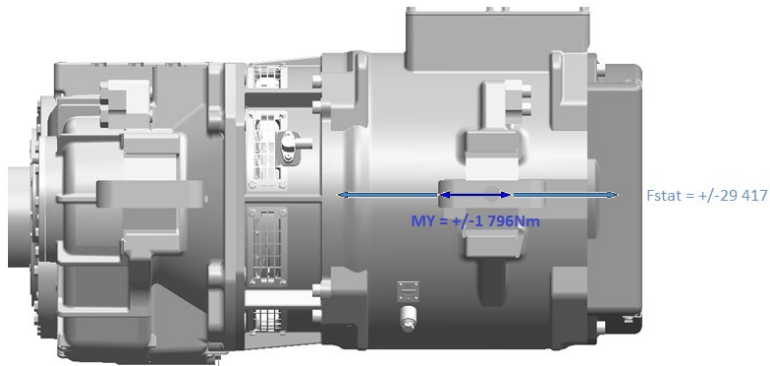
Fig. 3.41. Inertial axial load of the motor for simulated Mode III.

Mode III (reverse rotation)

On Fig. 3.42 - 3.44 shows the resulting radial, axial loads, as well as the inertial radial loading of bearings and the reaction of the accelerating force in the labyrinths for simulated Mode III for reverse rotation.
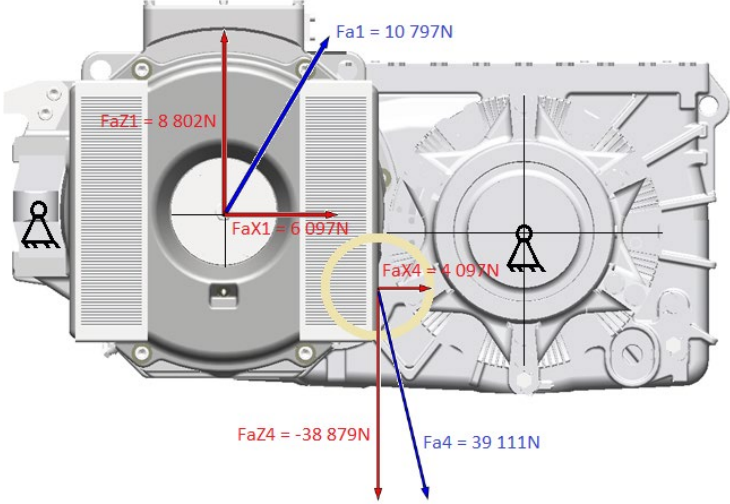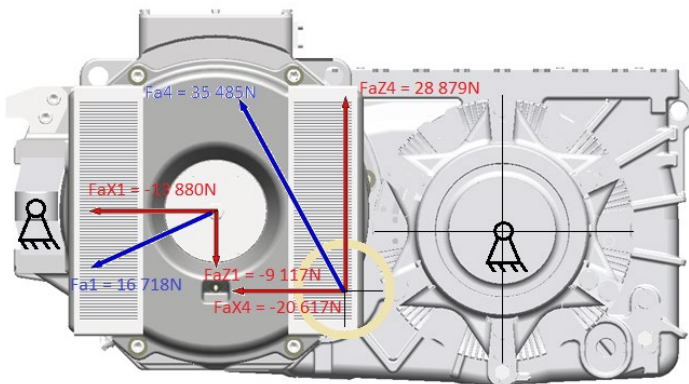

Fig. 3.42. Bearing radial load No.1 and No. 4 at simulated Mode III.
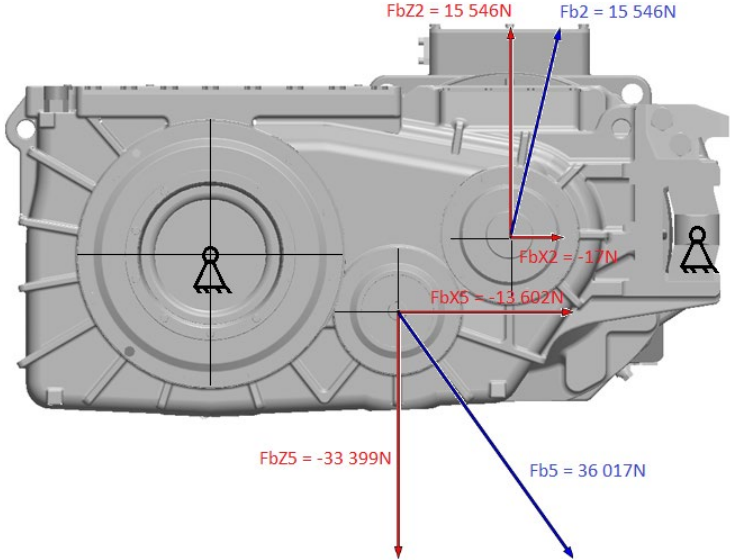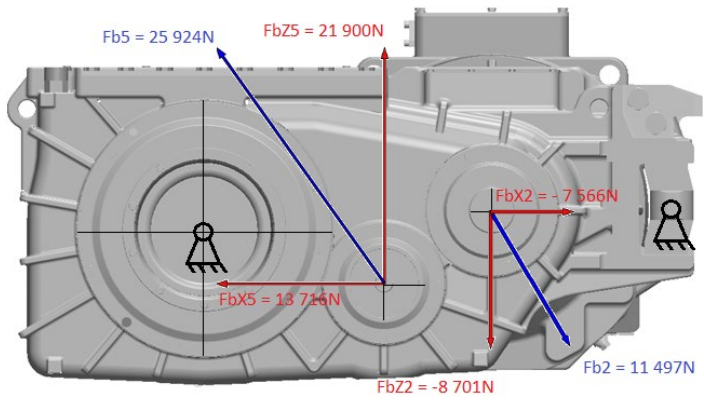
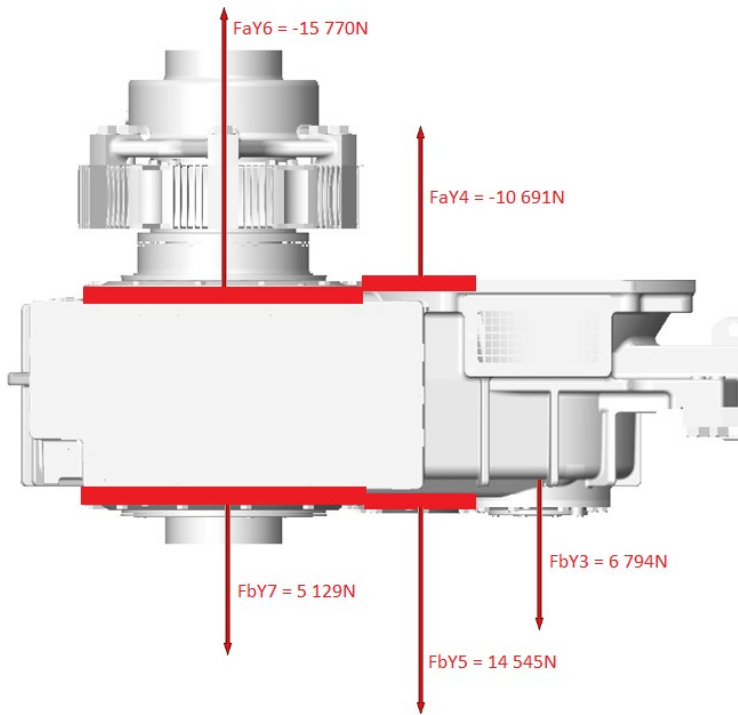Fig. 3.43. Radial load of the 2nd and 5th bearings in simulated Mode III.
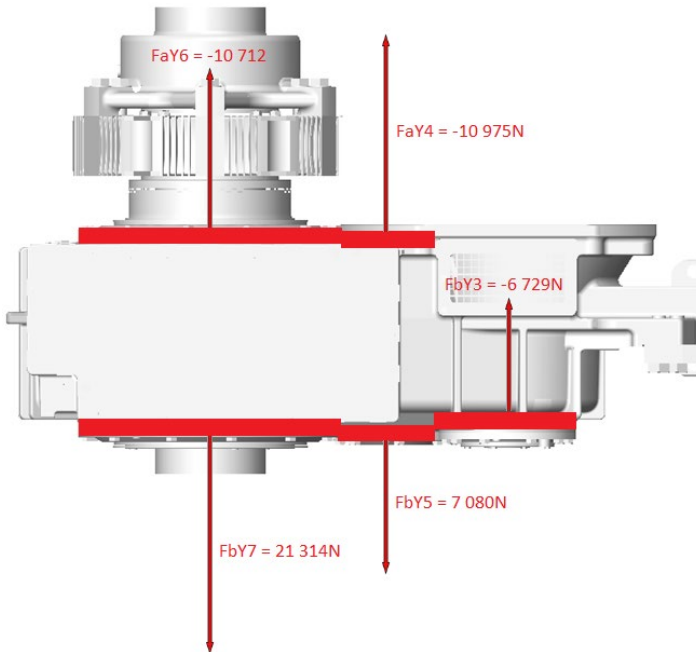
Fig. 3.44. Axial load of 3rd, 4th, 5th, 6th and 7th bearings in simulated Mode III.

3.4. Main results and conclusions of Chapter 3

1. A traction drive model has been developed, which is a single electromechanical system in which the electrical and mechanical parts in dynamic modes are in continuous interaction.
2. The developed model allows to study the maximum and integral load indicators on the most loaded transmission elements – gear shafts: primary shaft i_1: $z = 25$, $m = 5.5$; intermediate shaft i_2: $z = 26$, $m = 7$; i_3: $z = 56$, $m = 5.5$; and output shaft i_4: $z = 61$, $m = 7$.
3. During the simulation, it was found that the value of the integral load on the gear shaft $z = 61$, $m = 7$ is less than on the primary stage by 24.7 %. Primary shaft $z = 25$, $m = 5.5$ is the most loaded element in the drive gearbox.
4. A finite element model of the gearbox housing at the points of rotation of the gear shaft has been developed. The places of maximum loads are found, the calculation of stresses is carried out taking into account the maximum values. The maximum stresses are concentrated in the seating area of the 7th bearing. The reliability of the model is confirmed by an analytical solution.

CHAPTER 4. INFLUENCE OF LOADS ON THE RESOURCE OF THE GEAR BEARING ELEMENTS

4.1. Determination of stresses on the gearbox housing under different operating modes of the drive

The operation of the drive mainly consists of two modes: acceleration and deceleration. The loads that occur on the elements of the gearbox in these modes determine the intensity of their wear. In this regard, it is necessary to know the magnitude of the stresses that appear on the elements of the gearbox when the specified loads are applied, and the ability of the housing to resist destruction.

Further, it is considered how the loads on the hull change under various modes of operation of the MGU, the end of which will be the locking of the wheelset. In the analysis, we will use the developed drive model and the finite element model of the housing.

Load studies were carried out when the drive was started at a speed of $0.5\omega_{nom}$, then gradual loading and locking with different values of the locking torque. The dynamic coefficient was defined as the ratio of the maximum torque on the drive shaft to the stop torque value Mstop in static modes. Further, using the finite element model of the hull, stresses were calculated at the place of their maximum concentration.

The calculations of stresses on the fillet of the gear shaft showed that their values vary from 6 686 N to 41 411 N and depend on the operating modes of the mechanism. To assess the degree of influence of loads on the resource of the housing, it is necessary to determine the ability of the element to resist fatigue failure at different levels in the mechanism.

The ability of a part to withstand loads and resist destruction is determined by technological factors, such as: the quality of cast billets, the accuracy of machining, the quality of hardening work, and design features: the presence of transitions with changing sections, holes, etc., which are places of local concentration stresses [114].

Based on the results of modeling studies, it is advisable to consider the gear case as the most loaded structural element, the most susceptible to possible technological deviations during manufacture.

To determine the level of stresses that reduce the resource of a part, it is necessary to calculate the value of the average endurance limit. The median value of the fatigue limit of the part σ_{-1dyn} (MPa), corresponding to the probability of failure of 50 %, is determined taking into account the coefficient of reduction of the fatigue limit K_{end} [117], [118], [119]:

$$\sigma_{-1dyn} = \frac{\sigma_{-1}}{K_{end}}, MPa \tag{4.1}$$

The coefficient K includes technological and design factors that lead to a decrease in the endurance limit, and is calculated by the formula:

$$K_{end} = \left(\frac{K_\sigma}{K_{dyn\_\sigma}} + \frac{1}{K_{F\sigma}} - 1 \right) \frac{1}{K_V K_A} \tag{4.2}$$

where $\frac{K_\sigma}{K_{dyn\_\sigma}}$, $K_{F\sigma}$ – effective stress concentration factor and surface roughness influence factor; K_V, K_A – coefficients taking into account hardening and anisotropy of metal properties, respectively.

The effective stress concentration factor $\frac{K_\sigma}{K_{dyn\_\sigma}}$ is calculated by the formula:

$$\frac{K_\sigma}{K_{dyn\_\sigma}} = a_\sigma F(\theta, v_\sigma) \tag{4.3}$$

where a_σ was determined according to GOST 25.504-82 according to the nomogram $F(\theta, v_\sigma)$, where F – is a function of the fatigue fracture similarity criterion θ depending on the value v_σ. Calculation of values for determining the coefficient according to the nomogram was carried out as follows. According to the geometric dimensions (see Fig. 3.11), the coefficient a_σ is determined.

For the transitional flange connection dimensions $D_1 = 300$ mm, $D_2 = 133.4$ mm, $\rho = 16.5$ mm. $D_1 / D_2 = 300/133.4 = 2.25$, $\rho / D_2 = 16.5 / 133.4 = 0.12$. Obtained value $a_\sigma = 1.5$.

The value of the relative gradient of the first principal stress is defined as $G = \frac{2,3(1+\varphi)}{\rho} + \frac{2}{D_1}$, where $\varphi = \frac{1}{4\sqrt{t/p+2}}$, but $t = \frac{D_1 - D_2}{2}$. Obtained values $t = 83,3$ mm, $\varphi = 0.059$, $G = 0.154$ mm^{-1}.

On the next step, the similarity criterion for fatigue failure is calculated $\theta = L / G \cdot 1 / 88.3$, where $L = \pi D_1$ when bending with torsion of a round shaft, $L = 942$ mm. Similarity criterion $\theta = 942/0.154 \cdot 1/88.3 = 69.12$.

For high-strength cast iron EN-GJS-350-22- LT (EN 1563-2011), the coefficient of metal sensitivity to stress concentration and scale factor

The value of the function (θ, v_σ) with coefficients $\theta = 69.12$ and $v_\sigma = 0.0809$ is calculated by the formula: $F = 2 / 1 + \theta^{-v\sigma} = 1,131$.

As a result, the value (4.3) $K_\sigma / K_{dyn\_\sigma} = a\sigma \cdot \theta = 1.8 \cdot 1.131 = 2.03$.

The coefficient of influence of surface roughness characterizes the decrease in the endurance limit depending on the tensile strength and the quality of the surface treatment, and is determined by the expression [119]:

$$K_{F\sigma} = 1 - 0,22 \cdot log_{10} R_z \cdot \left(log_{10} \frac{\sigma_b}{20} - 1 \right) \tag{4.4}$$

and is $K_{F\sigma} = 0.87$, with surface roughness $R_z = 6 - 10$ µm. The gearbox housing is not subjected to hardening, therefore the coefficient $K_V = 1$, the anisotropy of the material properties does not appear $K_A = 1$.

The value of the fatigue limit reduction coefficient at the place of the shaft support in the bearing was $K_{end} = 1.8$.

The value of the endurance limit for smooth laboratory specimens, manufactured and large-sized forgings of high-strength cast iron EN-GJS-350-22-LT is $\sigma_{-1} = 350$ 360 MPa [118].

The endurance limit of iron EN-GJS-350-22-LT in the place of greatest stresses, taking into account technological and design factors, was: $\sigma_{-1} = 360 / 1.8 = 199$ MPa.

Comparison of the stresses arising on the fillet of the gear shaft with the endurance limit of steel showed that the accumulation of fatigue damage does not occur at loads not exceeding $1.4 \cdot M_{nom}$. To determine the effect of loads on the uptime of the gear shaft, it is necessary to choose a hypothesis for calculating the resource, taking into account the specifics of the traction drive.

4.2. Choosing a hypothesis for determining the resource of the gear shaft

Any crystalline material initially contains many imperfections. These are point (crystal lattice vacancies) and linear imperfections (dislocation loops), foreign inclusions, microcracks, etc. [1]. Under the action of tangential stresses, dislocations move, multiply, according to the Frank-Read source [2], go to microcracks and expand them, which ultimately leads to destruction. Under cyclic influences, the same processes occur at a faster rate. The study of the mechanism of destruction makes it possible to give an explanation of the process, however, the determination of the duration of the material's resistance to cyclic influences can be determined only as a result of an appropriate experiment. The scatter of experimental data on the number of cycles to failure is very large and different types of probability distributions are accepted for it: normal distribution [3], [4], Pearson distribution [5], Weibull distribution [3], [6], etc. Below we will consider the averaged values of the number of cycles to destruction N corresponding to the conditions of cyclic action (load). During the operation of structures, the conditions of cyclic loading are usually not constant; as a rule, loading alternates with unloading.

The cyclic operation of the traction drive, the random nature of the loading, depending on the quality of the track and atmospheric conditions during the movement of the electric train, indicate different levels of loads in the gearbox that do not depend on time.

Under irregular loading, the actual change in stresses can be represented by a block [35], which contains r loading steps and the corresponding stress amplitudes σ_{ai}, with the number of their repetition for each step $\nu_i = 1, 2, 3 \ldots k$ (see Fig. 4.1).
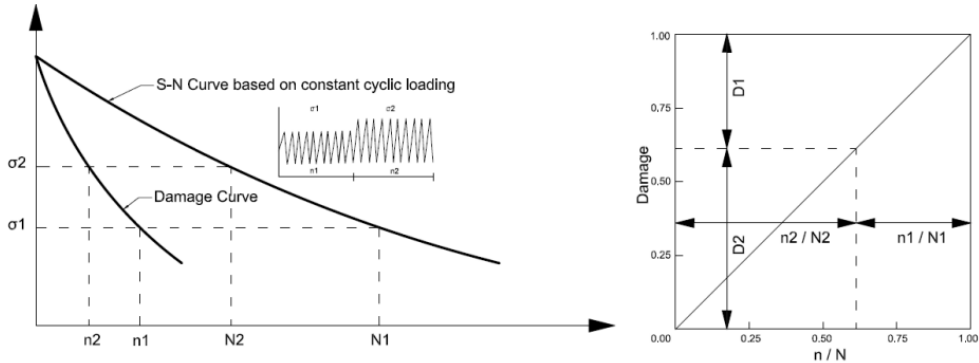

Fig. 4.1. The linear cumulative damage rule

With the number of loading blocks λ for the entire time of the part to failure or crack formation, the number of loading cycles with amplitude σ_{ai} will be $n_i = \lambda \cdot v_{ib}$. If the number of cycles to failure along the fatigue curve at σ_{ai} is equal to N_i, then at this stress amplitude the part will work out a share of its resource equal to n_i / N_i. Failure under block loading occurs when the sum of the specified durability reaches the limiting value a_p. Satisfactory results are obtained by the corrected fatigue damage summation hypothesis and for a fatigue curve with a horizontal section it is expressed by the equation [35]:

$$\sum_{(\sigma_{ai} \geq \sigma_{-1d})i=1}^{r} \frac{n_i}{N_i} = a_p \tag{4.5}$$

where:

$$a_p = \frac{\sigma_{a\_max}\varepsilon - 0{,}5\sigma_{-1d}}{\sigma_{a\_max} - 0{,}5\sigma_{-1d}} \tag{4.6}$$

when $a_p \geq 0.1$.

$$\varepsilon = \sum_{(\sigma_{ai} \geq 0{,}5\sigma_{-1d})i=1}^{r} \frac{\sigma_{ai}}{\sigma_{a\_max}} t_i = a_p \tag{4.7}$$

where

$$t_i = \frac{v_i}{v_b} \tag{4.8}$$

where v_b – the number of cycles in the loading block without considering the amplitudes $\sigma_{ai} \leq 0.5\sigma^{-1d}$. The corresponding entry under the sum sign in the expression for ε indicates that the amplitudes that satisfy this condition are summed.

The calculation of the safety margin was carried out at stress values σ_i, taking into account the obtained value of the average endurance limit σ_{-1d}. Probabilistic diagrams of fatigue of ductile iron EN-GJS-350-22-LT [118], were used, the number of cycles N before failure with a probability $pN = 50\%$ is determined by the expression: $\ln(N \cdot 10^{-3}) = 6.28 - 10.4 \cdot \ln(\sigma/\sigma^{-1}) + 0.65$ $\ln \cdot pN$. As a result, an exponential dependence of the hull resource in cycles was obtained, on the magnitude of the emerging loads $N_{case} = {}^{(-3.02+Kd)/-0.1614}$. To determine the degree of danger of the occurrence of overloads, the values of relative durability were determined n_i / N_i for each amplitude value σ_i and their contribution to the total a_p with a traction drive loading sequence diagram consisting of $v_b = 100\ 000$ cycles [118].

Considering the values of relative durability n_i-N_i, we can conclude that stresses of 330-350 MPa and more, arising in the modes of hard locking of the MGU shaft, intensively reduce the life of the housing, despite the fact that they appear quite rarely. So the share of cycles with $\sigma_{ai} = 351$ MPa is 4.3 % from the rest of the load. The increase in the cycles of hard locking of the working body by 2 times, which is typical for the operation of the MGU in the winter season

(when motor bogie moves to the skid), increases the total value to $\sum_{(\sigma_{ai} \geq \sigma_{-1d})i=1}^{r} \frac{n_i}{N_i} = 0.337$ (increase by 9 %), in this case, the frequency of occurrence of overloads is 6.7 % of the loading block. Stresses on the housing appear in a relatively small area and depend on the position of the pinion shaft at the moment of application of the maximum load.

In order to increase the service life of the gear housing in severe operating conditions with heavy traffic and changing operating conditions of the traction drive, it is necessary to strive to reduce overloads in the transmission elements to a level that provides an acceptable resource while maintaining sufficient overload capacity of the drive, and also to limit the time of exposure to the maximum load on the transmission elements, those tends to the shortest possible stop of the drive.

4.3. Evaluation of the safety margin of the gear housing according to the allowable stresses

The assessment of safety margin by allowable stresses is carried out by calculation for the cases of the most unfavourable possible combination of simultaneously acting standard loads in accordance with the design modes. The total stresses obtained as a result of the calculation should not exceed the allowable values presented in Table 4.1 for the corresponding simulated modes [119].

Table 4.1

Permissible Stresses for the Housing of Gearbox Elements

Simulated Mode	Permissible stress for constructive elements
Mode I	$0.9\sigma_y$
Mode II	$0.9\sigma_y$
Mode III	$0.9\sigma_y$

where σ_y – conditional material yield strength EN-GJS-350-22-LT (according to EN 1563-2011).

The gearbox housing equivalent stress values in Mode I are shown in Figs. 4.1., 4.2. and 4.3. Data and calculated safety factor for Mode I are presented in Tables 4.2, 4.3 and 4.4 [119].

Table 4.2

Equivalent Stresses and Safety Margin for Mode I
Forward Rotation

σ_{ekv}		σ_y	$0.9\sigma_y$	Safety margin $0.9\sigma_y / \sigma_{eq}$
(15; 15; 15) g	137.0	220	198	1.445
(-15; -15; -15) g	132.4	220	198	1.495
(-15; -15; 15) g	134.7	220	198	1.470
(-15; 15; 15) g	133.9	220	198	1.479
(15; -15; 15) g	139.9	220	198	1.415
(15; 15; -15) g	134.9	220	198	1.468
(15; -15; -15) g	138.3	220	198	1.432
(-15; 15; -15) g	132.2	220	198	1.498

The minimal value of safety factor $n = 0.1$ for Mode I.

Forward rotation

(15; 15; 15) g

(-15; -15; -15) g

(-15; -15; 15) g

(-15; 15; 15) g

(15; -15; 15) g

(15; 15; -15) g

(15; -15; -15) g

(-15; 15; -15) g
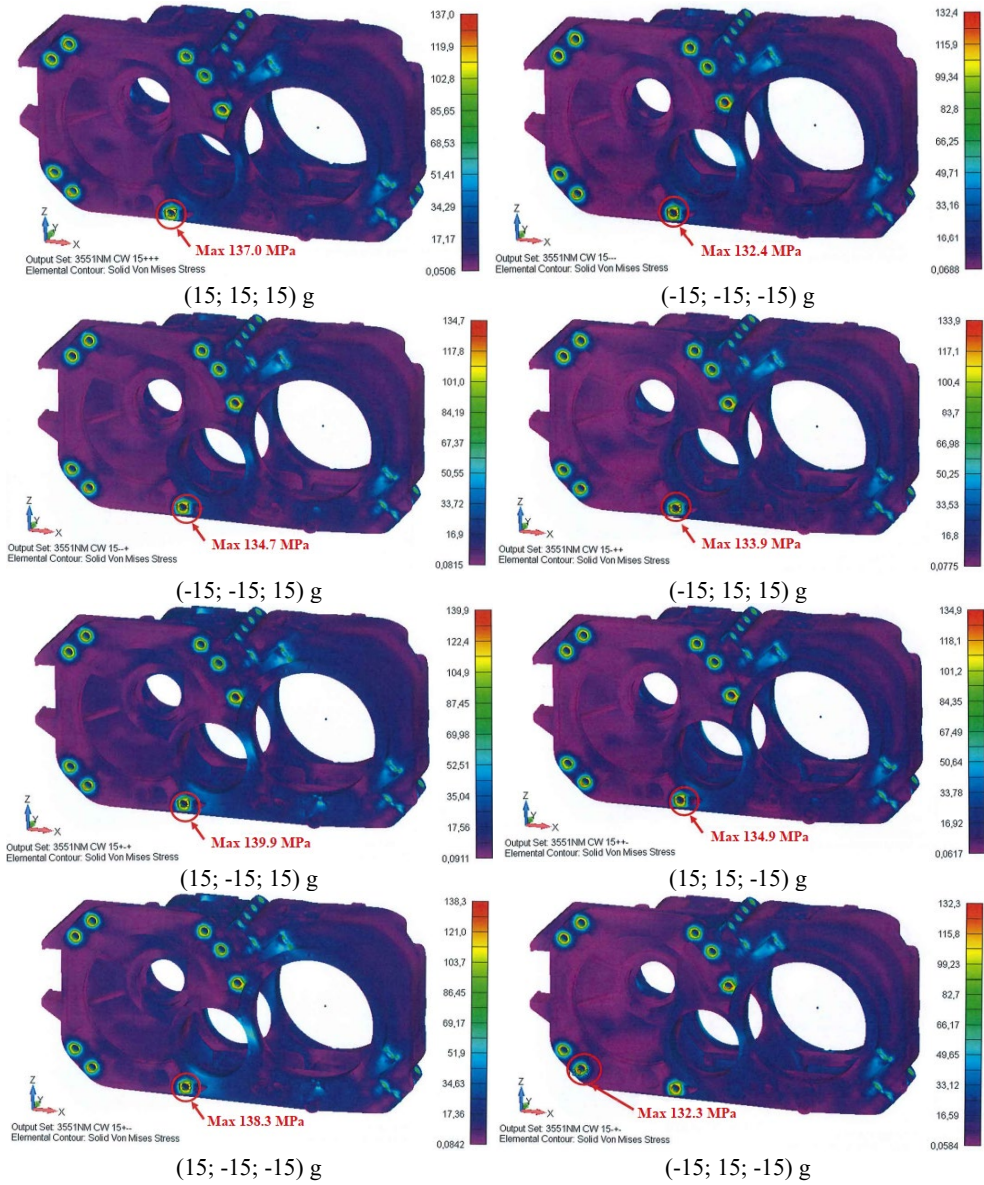
Fig. 4.1 Equivalent housing stresses in Mode I for forward rotation.

Fig. 4.2 Equivalent housing stresses in Mode I for reverse rotation.

Table 4.3

Equivalent Stresses and Safety Margin for Mode I. Reverse rotation

σ_{ekv}		σ_y	$0.9\sigma_y$	Safety margin $0.9\sigma_y / \sigma_{eq}$
(15; 15; 15) g	133.5	220	198	1.483
(-15; -15; -15) g	137.5	220	198	1.440
(-15; -15; 15) g	137.7	220	198	1.438
(-15; 15; 15) g	141.3	220	198	1.401
(15; -15; 15) g	135.9	220	198	1.457
(15; 15; -15) g	134.2	220	198	1.475
(15; -15; -15) g	137.1	220	198	1.444
(-15; 15; -15) g	138.1	220	198	1.434

The minimal value of safety factor $n = 0.1$ for Mode I.
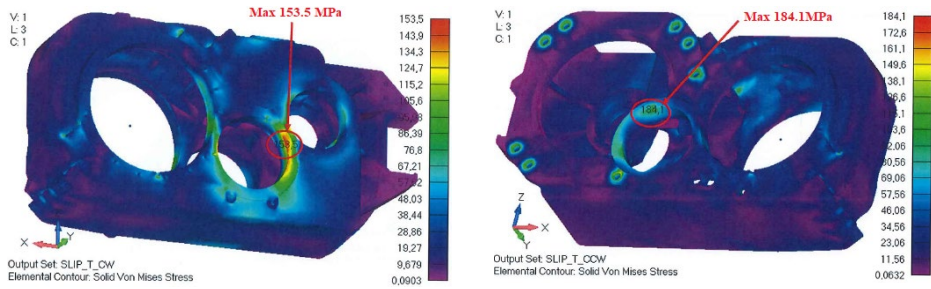
Fig. 4.3 Equivalent housing stresses in Mode II for forward rotation.

Table 4.4
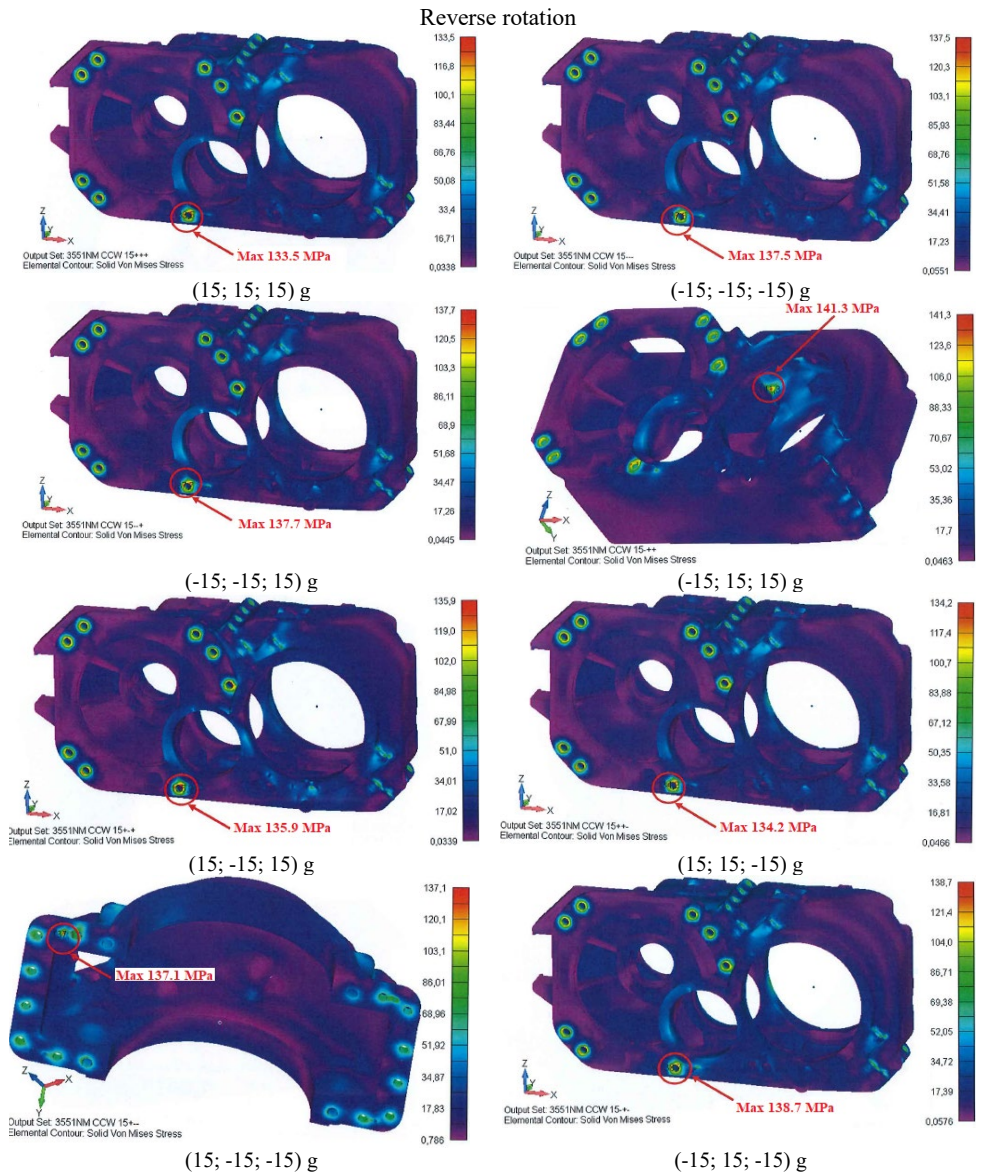
Equivalent Stresses and Safety Factor Values for Mode II

σ_{eq}		σ_y	$0.9\sigma_y$	Safety margin $0.9\sigma_y / \sigma_q$
Forward rotation	153.5	220	198	1.291
Reverse rotation	184.1	220	198	1.083

The minimal value of safety factor $n = 0.1$ for Mode II.

4.4. Evaluation of Structural Fatigue Resistance

The assessment of the fatigue resistance of load-bearing elements is made depending on the available information regarding the loading of the element and the parameters of the material fatigue curve.

In the absence of a histogram of the distribution of stress amplitude values that characterizes the strength of the element for the designated service life, and in the absence of parameters of the material fatigue curve, the fatigue resistance should be evaluated using the formula [112]:

$$n = \frac{\sigma_{-1p}}{K_\sigma \sigma_a + \Psi_\sigma \dfrac{\sigma_m}{\alpha_\sigma}} \tag{4.9}$$

where σ_{-1p} – endurance limit of a standard sample in tension-compression with a symmetrical loading cycle, according to standards $\sigma_{-1p} = 157$ MPa;

K_σ – concentration coefficient characterizing the decrease in the endurance limit of a structure in relation to the endurance limit of a standard sample;

σ_a – amplitude of stresses (maximum in the concentration zone) of the cycle, MPa;

σ_m – average cycle stress, MPa;

Ψ_σ – the coefficient characterizing the effect of cycle asymmetry is taken as $\Psi_\sigma = 0.3$ for $\sigma_m > 0$; $\Psi_\sigma = 0$ for $\sigma_m < 0$;

The coefficient of reduction of the endurance limit of the structure K_σ is calculated by the formula [112]:

$$K_\sigma = \frac{K_1 K_2}{K_m} K_3 \tag{4.10}$$

where K_1 – coefficient that takes into account the influence of the inhomogeneity of the detail material. For rolled, forgined and stamped details $K_1 = 1.1$, for casted details it is taken equal to $K_1 = 1.25$:

K_2 – coefficient that takes into account the influence of internal stresses of the detail, depending on the largest transverse size of the detail. With a detail size from 2500 to 1000 mm the coefficient is proportional to values from 1.0 to 1.2.

K_m – coefficient that takes into account the state of the surface of the detail and, depending on the processing method, is taken:

1.0 – for polished surface;

0.9 – for finished machined surfaces;

0.8 – for surfaces after rough machining, surfaces with dross and surfaces of steel castings after sandblasting;

γ – coefficient that takes into account the influence of the exchange factor and is selected depending on the largest transverse size of the section of the part h. The value of the coefficient is selected:

0.8 – for a cross-section height h – 100 mm inclusively;

0.75 – for a cross-section height h from 100 mm to 50 mm inclusively;

0.7 – for a cross-section height over h – 250 mm;

K_3 – correction factor used for weld zones. The gearbox housing presented in the desartation study is cast (not welded), therefore the coefficient K_3 is not included in the calculation of structural fatigue.

Further, in Fig. 4.4 shows the main maximum forces of the gearbox housing in Mode III for the forward direction.
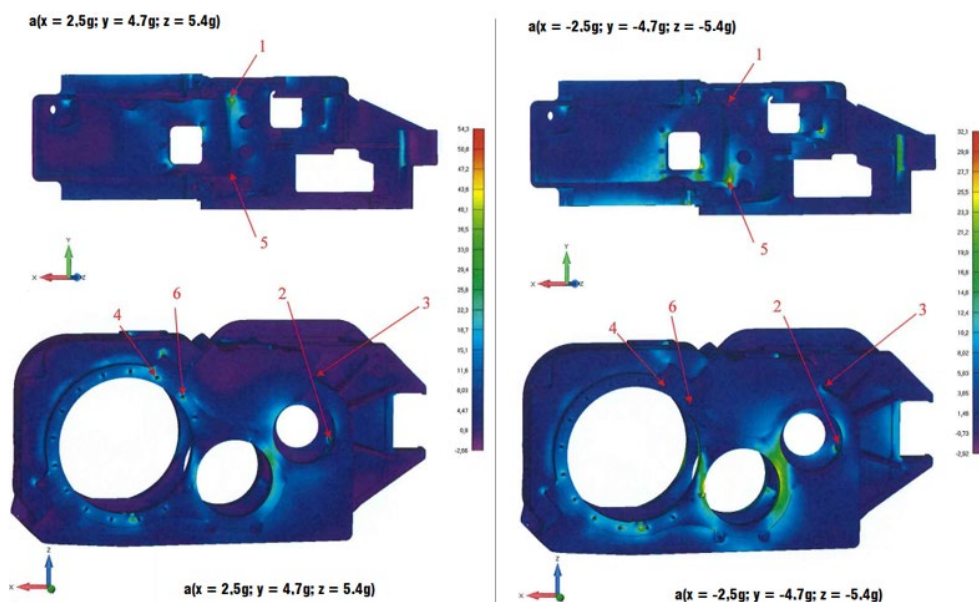
Fig. 4.4 Maximal gear housing forces in Mode III.

On Fig. 4.5 shows the maximal values of the main stresses of the gearbox housing at the points shown in Fig. 4.4 obtained by finite element analysis.
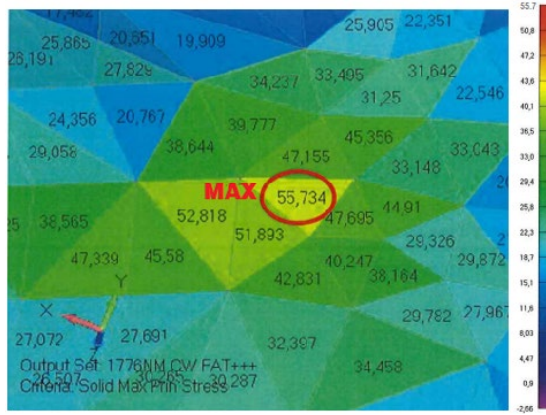
Fig. 4.5 Maximal main stresses at point "1" for Mode III.

Fig. 4.6 Maximal principal stresses at point "2" for Mode III.

The force field for the values of the maximum main stresses of the gearbox housing in Mode III for the forward direction for the forces of gearing and gravitational acceleration is shown in Fig. 4.7, and for point No. 4 in Fig. 4.8.
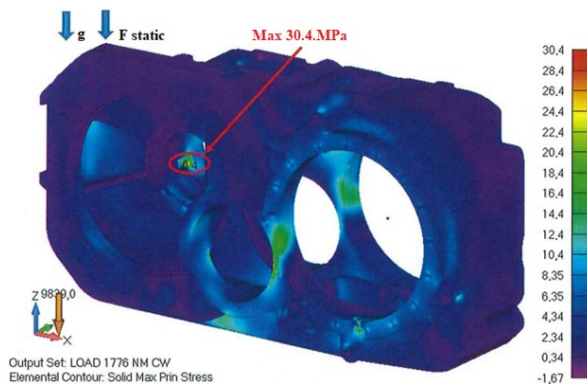
Fig. 4.7 Maximal main stresses of the gearbox housing in Mode III for forward direction for gearing forces and gravitational acceleration.

68

Output Set: LOAD 1776 NM CW
Elemental Contour: Solid Max Prin Stress

Fig. 4.8 Maximal main stresses of the gearbox housing in Mode III for forward direction for gearing forces and gravitational acceleration at point No. 4.

The calculated on model values for the fatigue safety factor for the forward direction are given in Table 4.5.

<div align="right">Table 4.5</div>

Calculated Values of the Fatigue Resistance Safety Margin
Direct rotation

Indicator	Values					
Stress point No. (MAX)	1	2	3	4	5	6
σ_{max}	55.9	75.2	49.9	41.8	35.8	42.1
σ_{min}	−3.8	18.1	3.4	1.1	−3.3	4.9
$\sigma_m = (\sigma_{max} + \sigma_{min})/2$	26.05	46.65	26.65	21.45	16.25	23.5
$\sigma_a = \sigma_{max} - \sigma_m$	29.85	28.55	23.25	20.35	19.55	18.60
Ψ_σ	0.3	0.3	0.3	0.3	0.3	0.3
α_σ	1	1	1	1	1	1
K_σ	1.83	1.83	1.83	1.83	1.83	1.83
n	2.55	2.41	2.85	3.64	3.95	3.87

On Fig. 4.9 shown the main maximum forces of the gearbox housing in Mode III for the reverse direction of rotation.
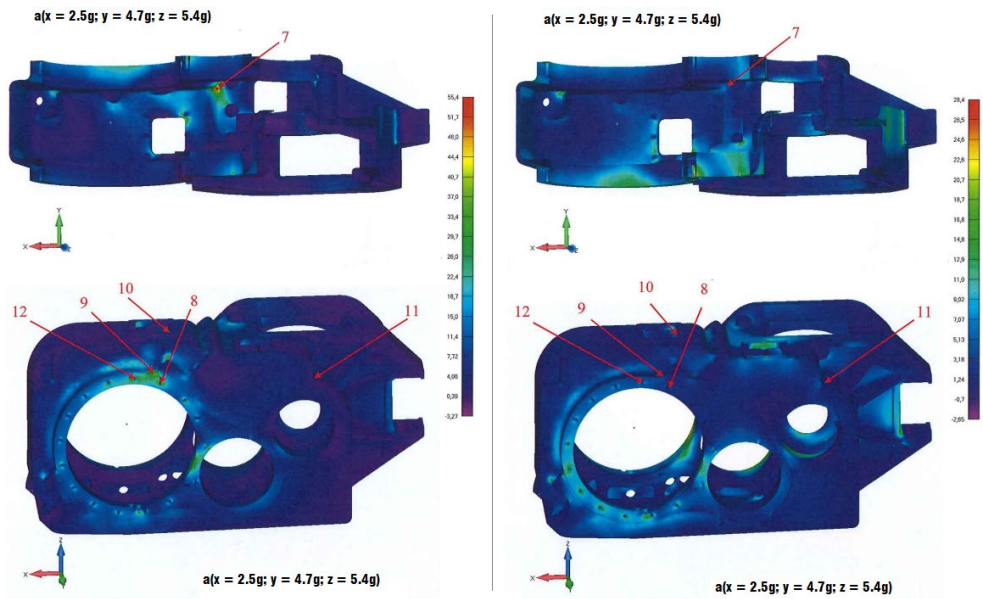
Fig. 4.9 Maximum main stresses of the gearbox housing in Mode III for reverse direction.

Fig. 4.10 shows the maximal values of the main stresses of the gearbox housing at the points shown in fig. 4.9 obtained by finite element analysis.
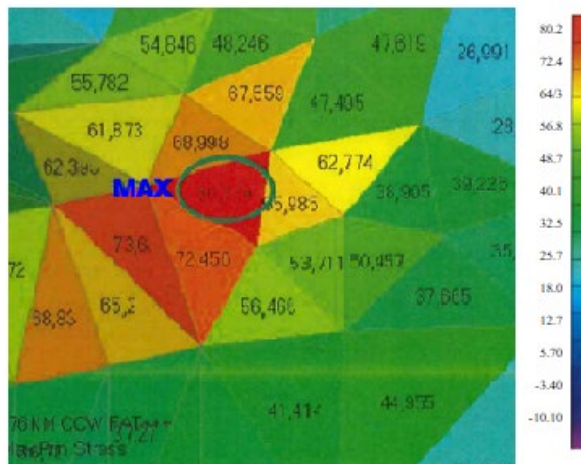
Fig. 4.10 Maximal main stresses at point "7" for Mode III (reverse rotation).
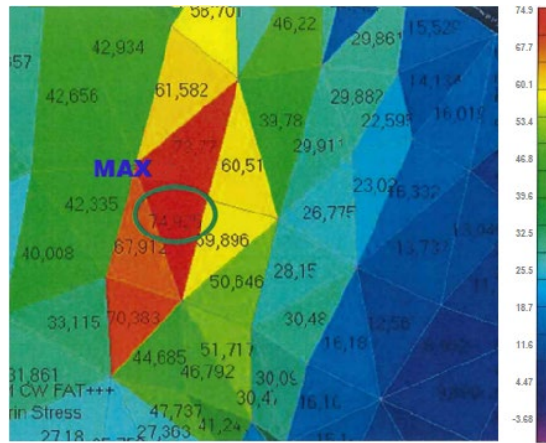
The force field for the values of the maximal main stresses of the gearbox housing in Mode III for the forward direction of rotation for the forces of gearing and gravitational acceleration is shown in Fig. 4.11, and for point No. 7 in Fig. 4.12.
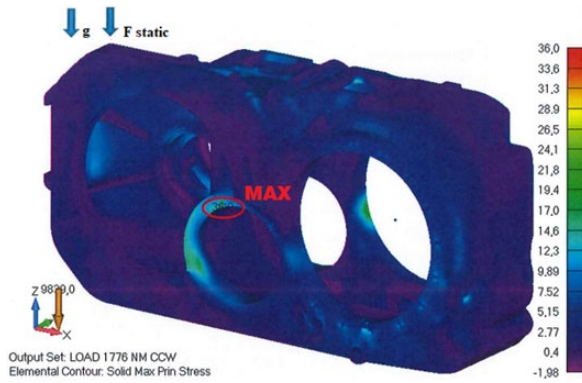
Fig. 4.11 Maximal principal stresses of gearbox housing in Mode III for reverse direction of rotation for gearing forces and gravitational acceleration.
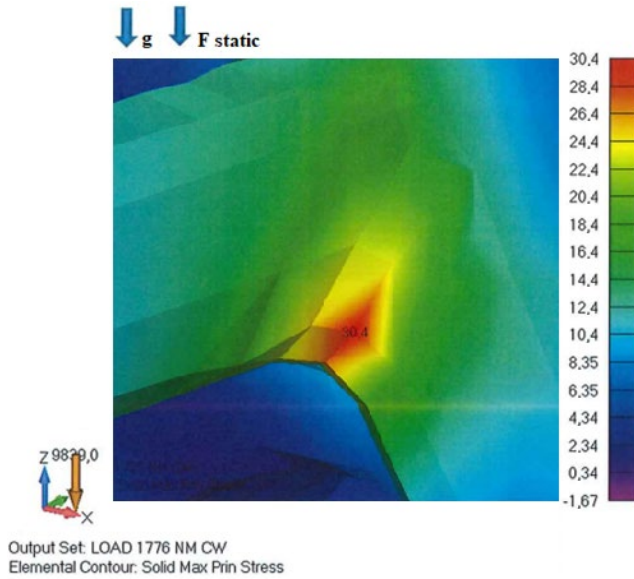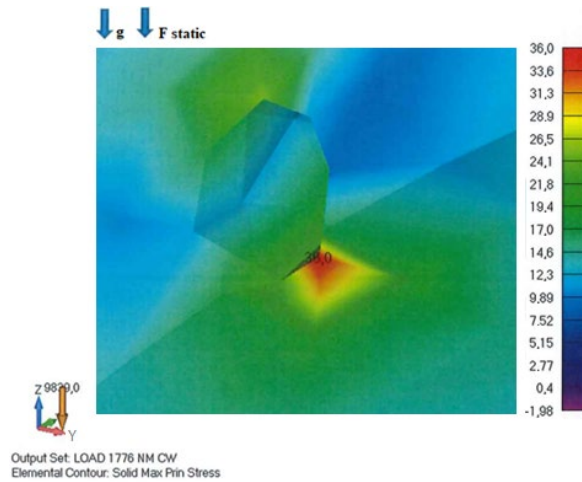

Fig. 4.12 Maximal principal stresses of the gearbox housing in Mode III for forward direction of rotation for gearing forces and gravitational acceleration at point No. 7

The calculated on model values for the fatigue safety factor for the forward direction of rotation are given in Table 4.6.

<div align="right">Table 4.6</div>

Calculated Values of the Fatigue Resistance Safety Margin
Direct rotation

Indicator	Values					
Stress point No. (MAX)	1	2	3	4	5	6
σ_{max}	80.9	55.1	54.6	46.7	41.1	54.6
σ_{min}	11.0	6.7	6.8	−0.3	−5.3	11.6
$\sigma_m = (\sigma_{max} + \sigma_{min})/2$	45.95	30.9	30.7	23.2	17.9	33.1
$\sigma_a = \sigma_{max} - \sigma_m$	34.95	24.2	23.9	23.5	23.2	21.5
Ψ_σ	0.3	0.3	0.3	0.3	0.3	0.3
α_σ	1	1	1	1	1	1
K_σ	1.82	1.82	1.82	1.82	1.82	1.82
n	2.05	2.97	3.01	3.24	3.37	3.25

4.5. Main results and conclusions of Chapter 4

For working Mode I, the minimal allowable margin of safety in the calculation of strength for allowable stresses is $[n] > 1.0$. Data on simulated modes are summarized in Table 4.7.

Values of safety factors for allowable stresses

Simulated mode	n_{min} (calculated)	$[n]$	Safety margin for the selected construction
Mode I (forward rotation)			
(15; 15; 15) g	1	1.445	sufficient
(-15; -15; -15) g	1	1.595	sufficient
(-15; -15; 15) g	1	1.47	sufficient
(-15; 15; 15) g	1	1.479	sufficient
(15; -15; 15) g	1	1.415	sufficient
(15; 15; -15) g	1	1.468	sufficient
(15; -15; -15) g	1	1.432	sufficient
(-15; 15; -15) g	1	1.98	sufficient
11 000 Nm	1	1.291	sufficient
Mode I (reverse rotation)			
(15; 15; 15) g	1	1.483	sufficient
(-15; -15; -15) g	1	1.44	sufficient
(-15; -15; 15) g	1	1.438	sufficient
(-15; 15; 15) g	1	1.401	sufficient
(15; -15; 15) g	1	1.457	sufficient
(15; 15; -15) g	1	1.475	sufficient
(15; -15; -15) g	1	1.444	sufficient
(-15; 15; -15) g	1	1.434	sufficient
11 000 Nm	1	1.083	sufficient

Values of safety factors for allowable stresses

Simulated mode	n_{min} (calculated)	$[n]$	Safety margin for the selected construction
Mode III (forward rotation)			
1	2	2.55	sufficient
2	2	2.41	sufficient
3	2	2.85	sufficient
4	2	3.64	sufficient
5	2	3.95	sufficient
6	2	3.87	sufficient
Mode III (reverse rotation)			
7	2	2.05	sufficient
8	2	2.97	sufficient
9	2	3.01	sufficient
10	2	3.24	sufficient
11	2	3.37	sufficient
12	2	3.25	sufficient

To calculate the strength for allowable stresses, the minimum calculated margin of safety is n = 1.40, which is more than the minimal allowable value. The design of the gearbox housing complies with the requirements of GOST R 55513.

For calculated Mode III, according to the assessment of the fatigue resistance of load-bearing elements, the minimal allowable margin of safety is [n] > 2.0. Data of calculated points for fatigue assessment are summarized in Table 4.8.

For the remaining calculated points of fatigue strength, the minimum margin of safety is higher than the minimum allowable coefficient when assessing fatigue resistance, which corresponds to the fatigue requirements in accordance with the norms.

CHAPTER 5. DETERMINATION OF THE LEVEL OF VIBROACTIVITY OF THE TRACTION MGU CONSIDERING THE INTERRELATIONS WITH THE DRIVE ARCHITECTURE

5.1. Determination of the traction drive model parameters

For the normal operation of the rolling stock, it is necessary that the resonant frequencies appear, at best, beyond the operating speed range, or at speeds below 60 km/h. So, with some residual imbalance of the engine rotor for a train speed of 120 km/h (corresponding to 155 Hz), resonant oscillations of the MGU will appear, which is unacceptable. In order to shift the resonance to the region of speeds less than 60 km/h, it is necessary that the natural frequency of the MGU and the bogie be less than 50 Hz.

To analyse vibration disturbances from the side of the MGU, an analysis of the equations of oscillations of the "bogie frame – MGU" system was carried out to determine the equivalent method of fixing the MGU on a vibration test bench. Under these conditions, the MGU oscillations along the X, Y, Z coordinates will be independent when the coordinates of the MGU fixing points change.

The proposed scheme of the damping system ensures that when the shock-absorbing MGU moves in the direction of one of the degrees of freedom, there is no movement in the direction of the other degree of freedom. This condition is satisfied if the general coefficients connecting different types of MGU oscillations in differential equations describing its motion are equal to zero. Provided that the ratio of linear stiffnesses in the direction of the X, Y, Z axes are equal for all shock absorbers, this can be written as [114]:

$$\sum k_{iz}x_i = 0; \ \sum k_{iz}y_i = 0; \ \sum k_{iz}z_i = 0;$$
$$\sum k_{iz}x_iy_i = 0; \ \sum k_{iz}x_iz_i = 0; \ \sum k_{iz}y_iz_i = 0 \tag{5.1}$$

where k_{iz} – stiffness of the i-th shock absorber along the Z axis;
x_i, y_i, z_i – coordinates of the i-th shock absorber relative to the center of mass.

In the considered version of the drive, a skew-symmetric arrangement of traction MGU on the bogie frame is adopted, and such a scheme is characterized by two bending modes of oscillation of the bogie frame together with the drives: relative to its longitudinal and transverse axes. At the same time, as the analysis of studies shows, the equivalent masses of the frame and drives oscillate in antiphase. With an equivalent frame stiffness of 6,731·108 N/m the natural frequency of this shape can be approximately determined by the formula for two masses connected by a spring [116]:

$$f_z = \frac{1}{2\pi} \sqrt{G_{eq} \frac{M_{frame} + 2M_{drive}}{M_{frame} \cdot 2M_{drive}}}, \tag{5.2}$$

where M_{frame} – frame mass;
$2M_{drive}$ – mass of two drives (MGU);

G_{eq} – equivalent stiffness of the frame, determined by the natural frequency for one of the curved modes of its vibrations by the formula:

$$G_{eq} = M_{frame}\left(2\pi f_{frame}\right)^2,$$ (5.3)

where f_{frame} – frame bending frequency.

The test bench control function is implemented in Matlab / Simulink software. The system shown in the Fig. 3.9. was implemented in Simulink. The electrical (fpower and control) part of electrical traction drive was modeled in the main library of the MATLAB / Simulink software package using the mathematical description published in Chapter 3. The electrical part is connected to the mechanical part of the traction drive. The control system included blocks that implement the defined control curves and algorithms, namely speed and load. The subsystems of the model contain various components of the models (differential equations, logic blocks, functions defined in the form of tables), which are arranged according to the principle of belonging according to the components of the energy equipment.

The test bench is controlled by Code Composer Studio (CCStudio). The interface of the complex electromechanical model subsystems will be discussed below. CCStudio provides unique interfaces for combining the electrical and mechanical subsystems of a complex model. It is a built-in tool of MATLAB Coder: a single integrated development software for all TI processors that use real-time data exchange. The utility generates C / C ++ code that can be compiled and executed using Texas Instruments processors. The built-in encoder allows you to customize the code generated from MATLAB text or Simulink block algorithms to control program interfaces, optimize performance and minimize memory consumption. This approach assumes that the control system model developed in MATLAB / Simulink software is first compiled into a subroutine, and then this library is connected to the mechanical part subsystem using the capabilities of the Simulink and CCStudio software package. Using the special wizard "Links to external libraries" available in CCStudio, the MATLAB / Simulink dynamic library connection is implemented.

In an orthogonal fixed coordinate (α, β) system, the stator energy conversion processes of a three-phase asynchronous motor can be described as follows [116]:

$$\left.\begin{aligned}
\pi_{s\alpha} &= -k_1 i_{s\alpha} + k_3 \Psi_{r\alpha} + k_4 \omega_r \Psi_{r\beta} + u_{s\alpha} / L_\sigma \\
\pi_{s\beta} &= -k_1 i_{s\beta} - k_4 \omega_r \Psi_{r\alpha} + k_3 \Psi_{r\beta} + u_{s\beta} / L_\sigma \\
p\Psi_{r\alpha} &= k_2 R_r i_{s\alpha} - \Psi_{r\alpha} / T_r - \omega_r \Psi_{r\beta} \\
p\Psi_{r\beta} &= k_2 R_r i_{s\beta} - \Psi_{r\beta} / T_r - \omega_r \Psi_{r\alpha} \\
M &= 1{,}5 z_p k_2 \left(\Psi_{r\alpha} i_{s\beta} - \Psi_{r\beta} i_{s\alpha} \right)
\end{aligned}\right\},$$ (5.4)

where:

u – line voltage;

i – stator current;

Ψ – flux linkage;

M – electromagnetic moment;

R, L – active resistance and inductance;

s, r, m – the indices correspond to the values of the stator, rotor and magnetization circuit;

ω_r – rotor rotation angular frequency;

p – differentiation operator;

$T_r = L_r/R_r$ – time constants;

$\tau_r = \sigma T_r$, $\tau_s = L_\sigma/R_s$ – rotor and stator circuit time constants;

$k_1 = 1/\tau_s + (1-\sigma)/\tau_r$; $\quad k_2 = L_m/L_r$; $\quad k_3 = L_m/(L_s\tau_r)$; $\quad k_4 = k_2/L_\sigma$; $\quad L_\sigma = \sigma L$;

$\sigma = L_m^2/(L_s L_r)$ – asynchronous motor scattering coefficient (diffusivity).

After differentiation of (5.4), an equation is obtained that describes the dynamics of the change of the electromagnetic moment depending on the control voltage.

$$pM = -M/T_0 + k_M U + k_M W_1, \tag{5.5}$$

where: $T_0 = (1/\tau_s + 1/\tau_r)$; $k_M = 1{,}5 z_p k_2/L_\sigma$; U, W_1 – effects of torque control loop control and excitation;

$$U = \Psi_{r\alpha} u_{s\beta} - \Psi_{r\beta} u_{s\alpha}, \tag{5.6}$$

$$W_1 = -\omega_r \left(M_\Psi/k_M + k_2 \Psi_r^2 \right)/k_M, \tag{5.7}$$

$$M_\Psi = 1{,}5 z_p k_2 \left(\Psi_{r\alpha} i_{s\alpha} + \Psi_{r\beta} i_{s\beta} \right). \tag{5.8}$$

Multiplying equation (5.6) by $\Psi_{r\alpha}$, but (5.8) by $\Psi_{r\beta}$ and summing the result gives:

$$(T_r/2) p\Psi_r^2 = -\Psi_r^2 + k_\Psi M_\Psi, \tag{5.9}$$

where $k_\Psi = 2L_r/3z_p$; $\Psi_r^2 = \Psi_{r\alpha}^2 + \Psi_{r\beta}^2$ – the square of the rotor flow coupling vector module.

Differentiating (5.8) by (5.4), find

$$pM_\Psi = -M_\Psi/T_0 + k_M V + k_M W_2, \tag{5.10}$$

where V, W_2 – the effects of torque control loop control and excitation;

$$V = u_{s\alpha} \Psi_{r\alpha} + u_{s\beta} \Psi_{r\beta}, \tag{5.11}$$

$$W_2 = M\omega_r/k_M + k_2 \Psi_r^2/T_r + k_2 R_r L_\sigma I_s^2, \tag{5.12}$$

here $I_s^2 = i_{s\alpha}^2 + i_{s\beta}^2$ – is the square of the stator current module.

The differential equations (5.5), (5.9) and (5.10) allow the rotation and torque control of the rotor flow, see block diagram in Fig. 5.1.

In the converter, the adjustment is delayed for a time equal to the IPM period. In the diagram shown in Figure 5.1, the setpoints are indicated by "*".

Proportional-integral regulators of torque and rotor flow circuits are described by transmission functions [116]:

$$W_{Psk}(p) = 1/(2T_\mu), \tag{5.13}$$

$$W_{Pm}(p) = K_1 (T_0 + 1/p), \tag{5.14}$$

where $K_1 = (2k_M \Psi_s T_\mu)^{-1}$; $T_\mu^{-1} = f_{IPM}$.
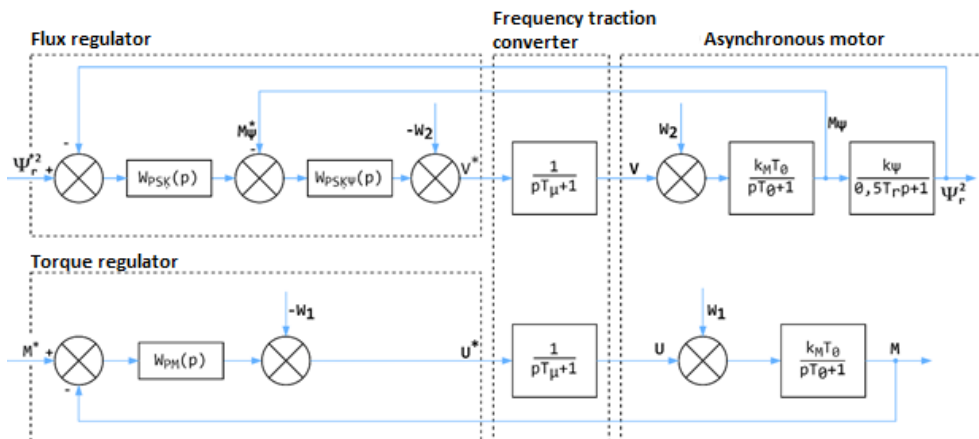
Fig. 5.1. Closed loop block diagram for flow and rotor torque control
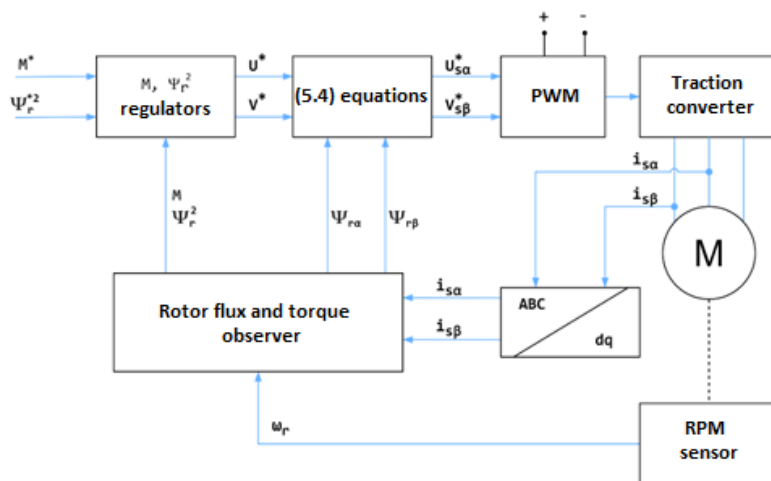
Fig. 5.2. Functional diagram of the asynchronous motor direct torque control system [113]

The functional diagram shown in Fig. 5.1 corresponds to the functional diagram shown in Fig. 5.2, where control signals U^* and V^*, are formed at the outputs of the torque and flow regulators, according to which the voltage values of $u_{s\alpha}^*$ and $u_{s\beta}^*$ for the converter are determined:

$$
\begin{aligned}
u_{s\alpha}^* &= \frac{V^* \Psi_{r\alpha} - U^* \Psi_{r\beta}}{\Psi_r^2} \\
u_{s\beta}^* &= \frac{U^* \Psi_{r\alpha} - V^* \Psi_{r\beta}}{\Psi_r^2}
\end{aligned}
. \qquad (5.15.)
$$

The traction motor parameters for entering them into the MATLAB/Simulink model for checking the natural vibration of an **uncoupled and unloaded MGU** are presented in Table 5.1, and the characteristics of the motor for idle running are shown in Fig. 5.3.

Table 5.1

Typical No-load MGU Characteristics at 155.1 Hz

U_0	$I_{0\ min}$	$I_{0\ max}$	$P_{0\ min}$	$P_{0\ max}$	$\cos\varphi_{min}$	$\cos\varphi_{max}$
V	A	A	kW	kW	r.u.	r.u.
2280	27.6	34.1	11.7	14.4	0.096	0.119
2200	26.0	32.2	11.2	13.8	0.101	0.125
2020	22.6	27.9	9.8	12.1	0.111	0.137
1725	17.4	21.5	7.8	9.6	0.135	0.166
1525	14.3	17.7	6.7	8.3	0.159	0.196
1425	12.9	16.0	6.2	7.7	0.173	0.214
1225	10.4	12.8	5.4	6.6	0.216	0.267
1025	8.3	10.2	4.6	5.6	0.282	0.348
725	5.9	7.2	3.8	4.7	0.461	0.569
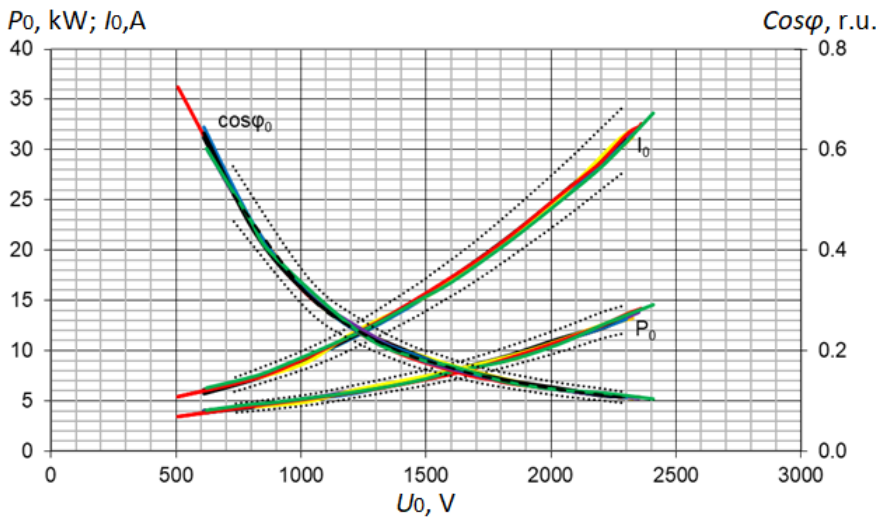
Fig. 5.3. Typical no-load MGU characteristics at 155.1 Hz.

The motor parameters for entering into the MATLAB/Simulink model for checking vibration in the **mutual load mode for coupled and mutually loaded MGU** are presented in Table 5.2, and the motor characteristics for the traction mode are shown in Fig. 5.4.

Table 5.2

Typical Operating MGU Characteristics at 155.1 Hz

M	I_{min}	I_{max}	$\cos\varphi_{min}$	$\cos\varphi_{max}$	s_{min}	s_{max}	η_{min}	η_{max}
Nm	A	A	r.u.	r.u.	%	%	%	%
217	32.3	39.8	0.767	0.947	0.20	0.27	87.1	95.5
318	44.4	54.8	0.795	0.982	0.30	0.41	89.3	98.0
418	57.3	70.7	0.802	0.990	0.40	0.53	89.9	98.6
520	71.0	87.7	0.798	0.985	0.54	0.67	90.2	99.0
622	85.7	105	0.788	0.972	0.65	0.80	90.3	99.0
726	102	126	0.769	0.950	0.80	0.99	89.9	98.5
831	122	150	0.739	0.913	0.99	1.23	89.4	98.0

Fig. 5.4. Typical operating characteristics at 155.1 Hz.

The running traction and energy parameters of the motor for determining the vibration activity of the MGU in the mode of long-term mutual loading using MATLAB/Simulink are presented in Table 5.3.

<div align="right">Table 5.3</div>

Motor Data

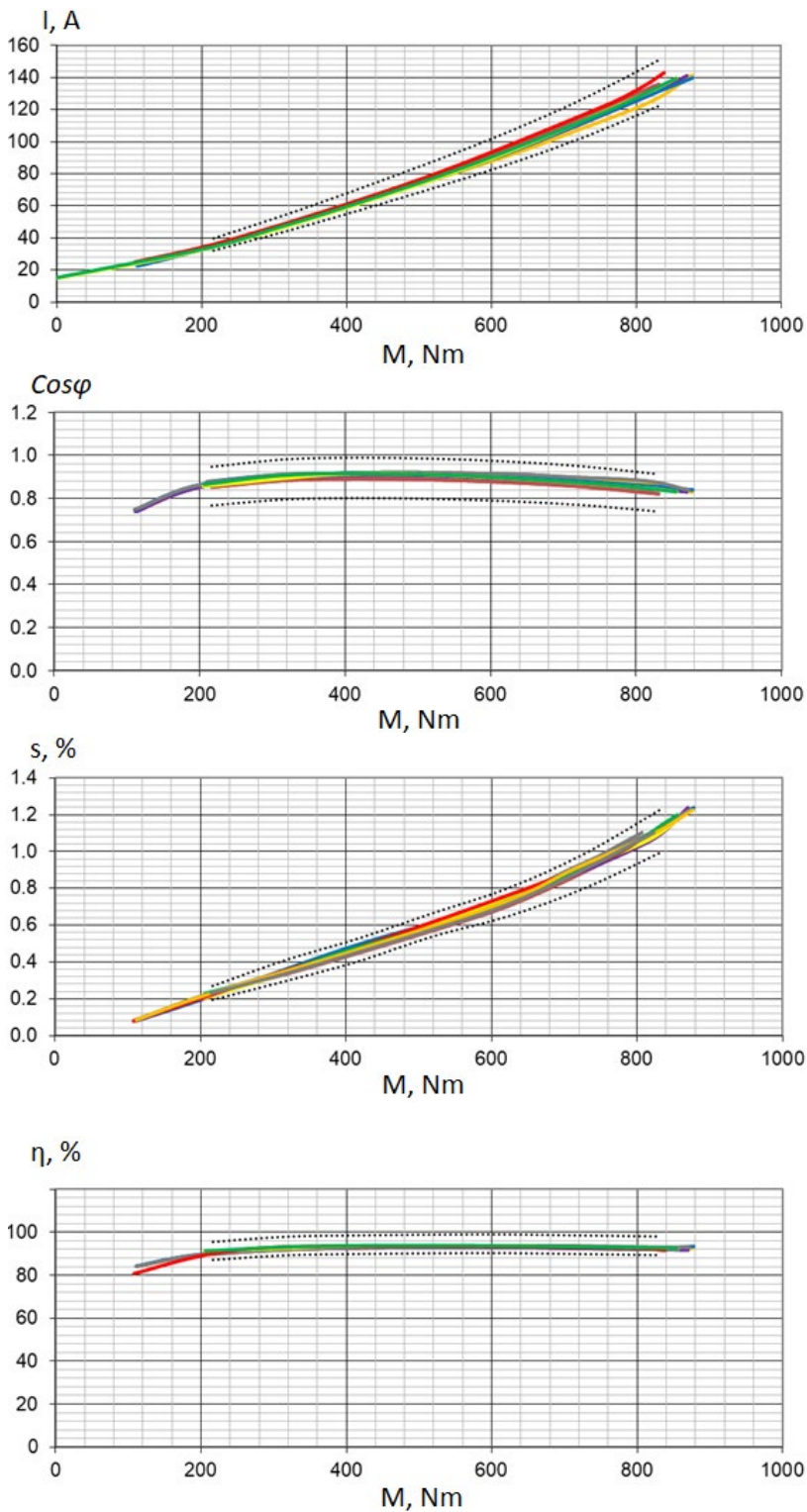| Type:									
Project:									
Mode:		Traction		When powered by a sinusoidal current source					
# of motors	pcs	16			# of poles		4		
Gearbox efficiency	%	0.97			Connection		Y		
Wheel diameter new/worn	m	0.957	0.88						
Gear ratio	r.u.	5.255							
		start	1/v	U/f	1/vv	V max	n max	Vmax Test	S1
Shaft power	kW	207	430	430	430	376	376	376	380
Line voltage	V	740	1450	2200	2200	2200	2200	2200	2200
Current	A	219	216	138	139	121	125.3	125	121
Power factor	r.u.	0.88	0.87	0.856	0.85	0.855	0.82	0.82	0.86
Frequency	Hz	20	40.0	63.0	137.8	157.0	171.0	173.0	68.5
Slip	%	6.4	3.1	1.17	1.36	1.2	1.3	1.3	1
RPM	min^{-1}	562	1 167	1 868	4 078	4 661	5 069	5 127	2034
Shaft torque	Nm	3 520	3 520	2 198	1 007	771	709	701	1 783
Maximum moment	Nm	4982	5466	5297	1255	964	813	795	4515
Multiplicity Mmax	r.u.	1.42	1.55	2.41	1.25	1.25	1.15	1.13	2.53
Total losses	kW	42.40	44.61	22.16	23.11	18.35	19.22	19.39	18.32
Efficiency	%	83.0	90.6	95.1	94.9	95.4	95.1	95.1	95.4
Traction force	kN	600	600	375	172	131	131	119	304
Velocity	кm/h	19.3	40.0	64	140.0	160.0	160.0	176.0	70
R1 @ 20 C	MΩ	113	113	113	113	113	113	113	113
R2` @ 20 C	MΩ	82	82	82	82	82	82	82	82
X1	MΩ	230	572	904	2055	2342	2565	2580	1005
X2`	MΩ	212	529	842	1964	2241	2316	2470	933
Xm	Ω	5.9	14.3	22	74	84	90	93	27.5
I idling	A	57	57	56	17	15	13.5	13	46
Data:		–							
Revision:		–							

The purpose of the study is to determine the vibration characteristics of a MGU to identify the reasons for its premature failure under operating conditions. The study of the amplitude-frequency characteristics of the MGU vibration has been carried out. The developed technique is intended for use at the vibration characteristics research stand. Based on the measurements obtained, an analysis of the results was made, which showed the presence of electromechanical resonance and the rotor imbalance.

By its purpose, the MGU is connected to a converter, which inherently is a powerful source of harmonics with smooth regulation of the supply voltage of traction motors in the

traction mode and smooth regulation of the inverter back EMF in the regenerative braking mode.

The test at an increased speed of rotation was carried out at a speed of (5600 ± 30) min^{-1} for (2 ± 0.1) min.

Measurement of the motor vibration level was carried out in idle mode with a steady speed in the range from (800 ± 30) min^{-1} to (4650 ± 30) min^{-1} on the bearing shield along coordinates X (horizontal axis) and Y (vertical axis) when powered by a traction converter. The root-mean-square value of the vibration velocity in the specified range of rotational speeds should be no more than 2,2 mm/s.

The own level of vibration of the MGU was determined by controlling the rotation by means of an autonomous traction converter with a nominal operating voltage of 3 kV DC and a PWM frequency of 2 kHz.

To determine the level of vibration activity, the ISO 10816 standard allows one of the following values to be used as a measured value [8]:
- vibration displacement, in micrometres (μm);
- vibration velocity, in millimetres per second (mm/s);
- vibration acceleration, in metres per second squared (m/s^2).

According to ISO 10816, the maximum measured vibration level is up to 5 mm/s. in the direction transverse to the output shaft and 2.5 mm/s. in the direction along the output shaft. All components must withstand vibration and shock without damage, according to M27 GOST 30631, sinusoidal vibration with maximum acceleration amplitude of 150 m/s^2 in the frequency range of 0.5–100 Hz. The specified effect is assumed acting from the side of the wheel pair on the wedge plate clutch [9].

Acceptance testing for MGU includes three identical cycles. Parameters such as vibration level, noise, heating temperature of the motor and gearbox bearings in the final – third cycle. At this stage of testing, the main task is to determine the intrinsic vibration activity of MGU and to identify possible resonance through spectral analysis.

The first step is to determine the self-vibration of the first MGU. The scope of dynamic tests consists of three cycles, each of which includes two speed modes – at a continuous speed of 3000 min^{-1} +/- 10 min^{-1} in a clockwise and counterclockwise direction (CW/CCW). Then the rotation speed is increased to the maximal 4 653 min^{-1} +/- 10 min^{-1}, and tests are also carried out for two directions of rotation.

The power test bench includes:
- tested MGU (number of gear stages: 2; gear ratio: 5.25; maximum input torque: 3580 Nm; power: 370 kW);
- traction converter, which allows to realize traction drive control modes, the power regulator of which is controlled on the basis of the TMS320F28335 microprocessor;
- autonomous analyser of the level of vibration velocity and vibration acceleration SKF CMXA 80;
- YOKOGAWA WT1800 precision power analyser connected to the output of the traction converter;
- personal computer for the test bench control.

The change in the value of the RMS vibration speed is carried out in the following mode for CW and CCW directions: acceleration – maximal construction speed – maintaining of the maximum speed – braking – coasting – stopping, shown in Table 5.4 and Fig. 5.5.

Table 5.4

Unlaoded MGU MGU Speed Test Parameters

No.		Speed test parameters		
	Part	Duration [min]	Position	Speed point [RPM]
1	t_1, t_{11}	15	n_1, n_4	300
2	t_2, t_{10}	5	n_2, n_6	4 653
3	t_3, t_9	2	n_3, n_5	3 000
4	t_4, t_6, t_8	10	Speed direction	CW/CCW
5	t_5, t_7	10		
Total:		94		

The appearance of the maximum value of RMS short-term vibration is acceptable when the design speed is reached and at the initial moment of the motor transition to the braking mode [114].
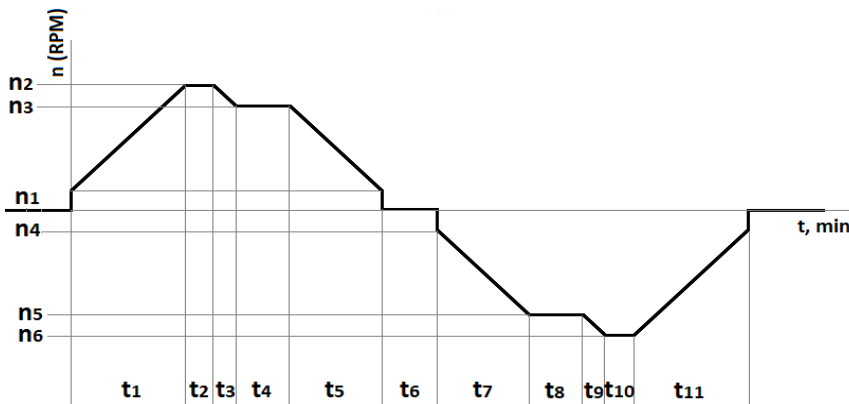

Fig. 5.5. The diagram of the full cycle of MGU dynamic own-vibration test [116].

The test cycle corresponds to the continuous mode S1 with a variable load value. The functional block diagram of the test bench is shown in Fig. 5.6. Thus, the supply voltage of the stator winding of the traction motor is a rectangular-step signal approximating the sinusoidal one with the specified values of the effective voltage and frequency. This form of supply voltage leads to a significant expansion of the spectrum of magnetic vibration-inducing forces, which has a significant effect on the vibroactivity of the MGU. The MGU is powered by a voltage inverter with PWM. The voltage and current readings of the oscilloscope are shown in Fig. 5.7.
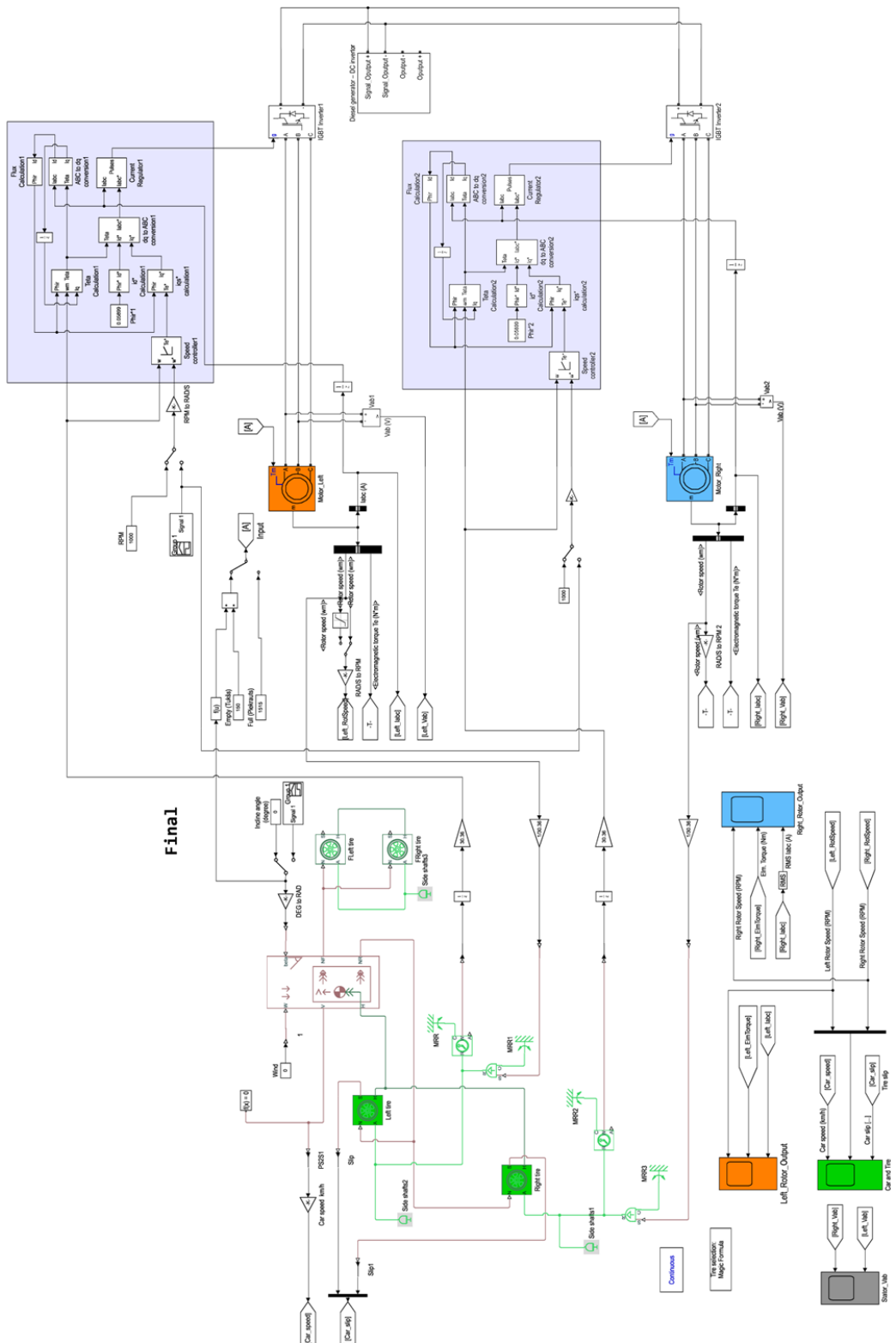
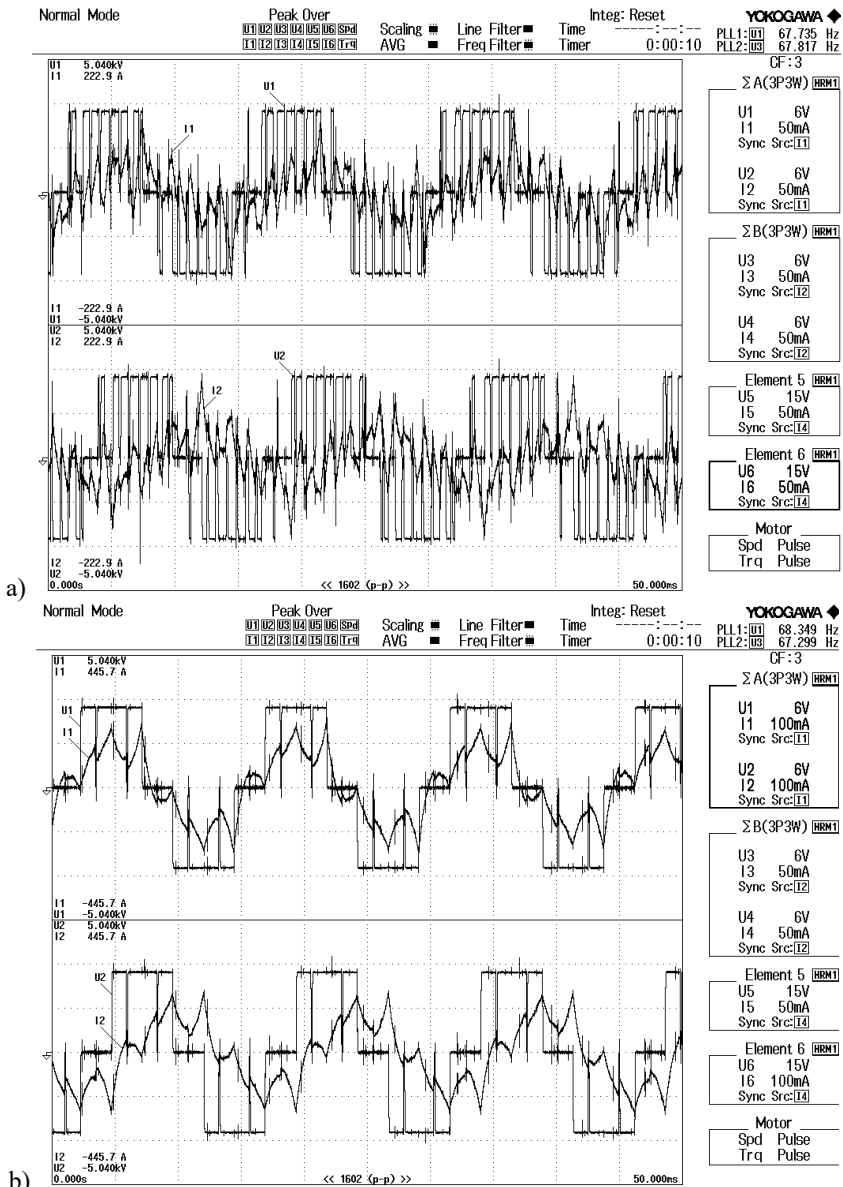Fig. 5.6. Schematic depiction of the test infrastructure setup.

a)

b)

Fig. 5.7. Oscilloscope print screen of motor converter voltage and currents as function of time at DC link a) without lode mode; b) nominal load mode.

The following example considers the case of deviation from the production technology, identified through the methodology presented in this dissertation. With a decrease in the rotor speed in the coasting mode, vibration cannot depend on the PWM of the traction converter control system and is not associated with the load of the MGU. At the same time, in the coasting mode, the possible presence of resonance can be determined. Figures 5.8 and 5.9 shows a distinct resonance of the traction motor, when the rotor speed is within the limited construction speed and at rated speed. The results of the spectral analysis were obtained by means of the fast Fourier transformation. A decomposition of vibration signature leads to speed-dependent engine orders, speed-independent components and speed related off-zero harmonics. The last two components are due to the inverter [116].
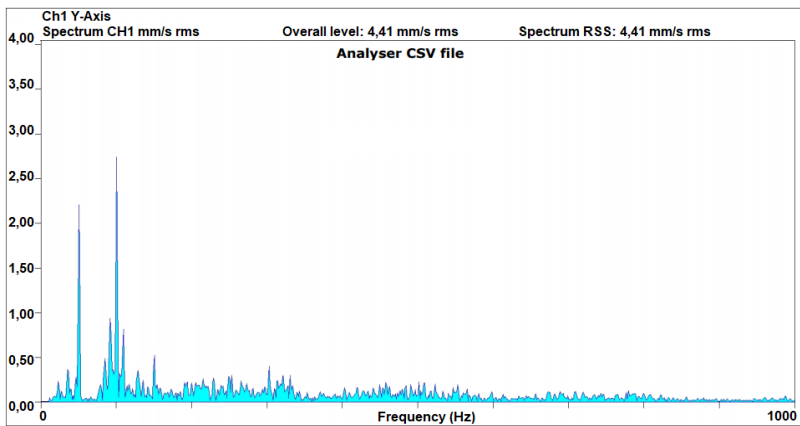
Fig. 5.8. The waveform of the vibration velocity at maximal speed of 4 653 min^{-1}.
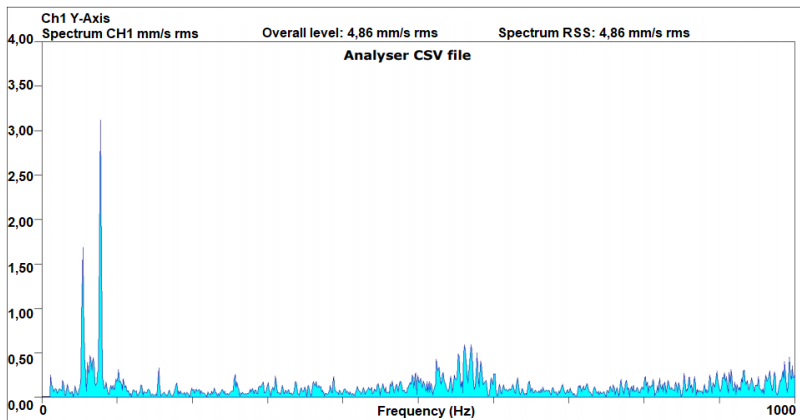

Fig. 5.9. The waveform of the vibration velocity at continuous speed of 3 000 min^{-1}.

For a rotation speed of 4 653 min^{-1}, in the range of 50.0 – 100.0 Hz (step 1.75 Hz), an increase in the RMS vibration speed up to 4.41 mm/s, in the direction of the Y axis, is fixed. For a rotation speed of 4 653 min^{-1}, in the range of 50.0 – 75.0 Hz (step 1.75 Hz), an increase in the RMS vibration speed up to 4.86 mm/s, in the direction of the Y axis, was fixed.

As a result of determining the possible reasons for the appearance of resonance, a violation of the technology of heat treatment of the rotor shaft was revealed, as well as modelling of the shaft stiffness for these conditions was carried out. To ensure the basic hardness of the shaft, the technological process provides for the removal of mechanical stress on the shaft by means of high-temperature tempering at 70 ° C for 24 hours. The traction motor shaft has one support, and is connected to the gearbox shaft by a flanged diaphragm coupling. The support bearing of the rotor shaft is a single-row ball bearing and does not take axial loads. Shaft deflection in the middle of the rotor is defined as $f = f_g + f_d + f_m$, where f_g – is shaft deflection due to gravity, f_d – is shaft deflection due to transmission reaction, and f_m – is shaft deflection due to magnetic pull [120].

Due to the fact that the profile of the shaft has a stepped configuration, it can be represented by sections and the moment of inertia for each can be determined in accordance with $J_i = \pi d_i^4 / 64$, where d_i – section diameter.

Shaft deflection in the middle of the rotor core due to gravity is $f_g = (G/3El^2) \cdot (a^2S_b + b^2S_a)$ $\cdot 10^6 = 0.0049$ mm, where G – gravity (weight) of the rotor [10]; $E = 2.12 \cdot 10^{11}$ Pa – elastic modulus for 20XH3A steel; a, b and l – rotor shaft sections, m.

The stiffness of the shaft is determined as and is equal to $k = G/f_g = 0.55 \cdot 10^6$ kgs/cm.

The specific magnetic force is $0.0213 \cdot 10^6$ kgs/cm, and the steady-state magnetic attraction force is 3 210 N. The distribution of the load on the rotor of the motor, taking into account the above parameters, is shown in Fig. 5.10 [117].
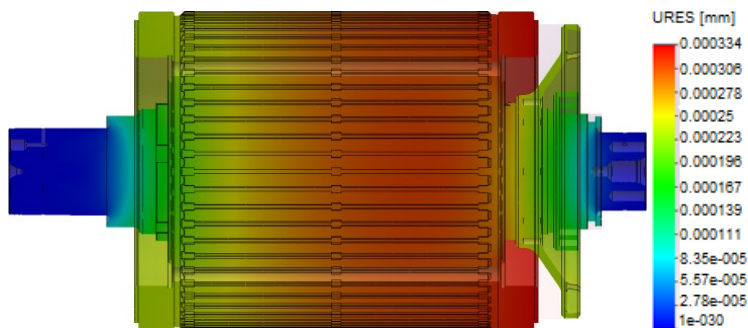
Fig. 5.10. The distribution of the load field on the rotor.

In the case of uneven distribution of the load along the motor rotor shaft, the increased load falls on the place where the motor and gearbox flanges meet. In this case, when the motor is single-bearing, the vibration activity in the bearing assembly increases.

At the same time, measurements were made of the helical meshing area of the gears stages of the gearbox, see Fig. 5.11.

Fig. 5.11. The area of helical gearing of gears.

Further, the fixed value of the vibration acceleration of the MGU corresponding to the test modes will be given with the auto-spectrum of vibration acceleration and vibration velocity with vector control of the PWM. Fig. 5.12 show vibration velocity level on 3 000 min^{-1} on X, Y, Z axes for motor and Y for gearbox side.

Fig. 5.12. Vibration velocity of MGU fixed at 3 000 min^{-1} on motor bearing shell on X, Y, Z axes and on gearbox shell on the Y axis.

The fixed values of vibration velocity on Y axis for 3 000 min^{-1} on motor bearing shell ans gearbox side were 4.52 and 4.18 mm/s, which is 1.5 times more than the allowable limit of 2.8 mm/s. Fig. 5.13 show vibration velocity level on 4 653 min^{-1} on X, Y, Z axes for motor and Y for gearbox side.
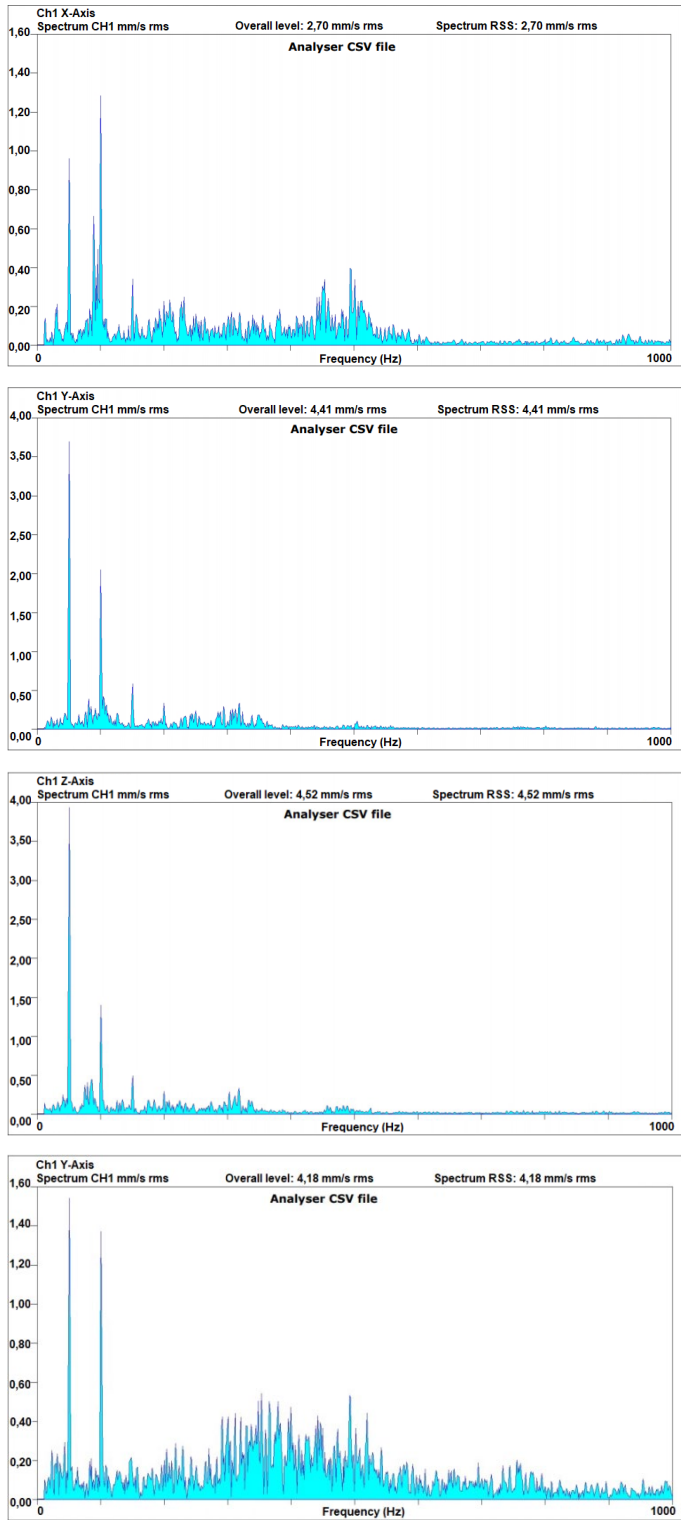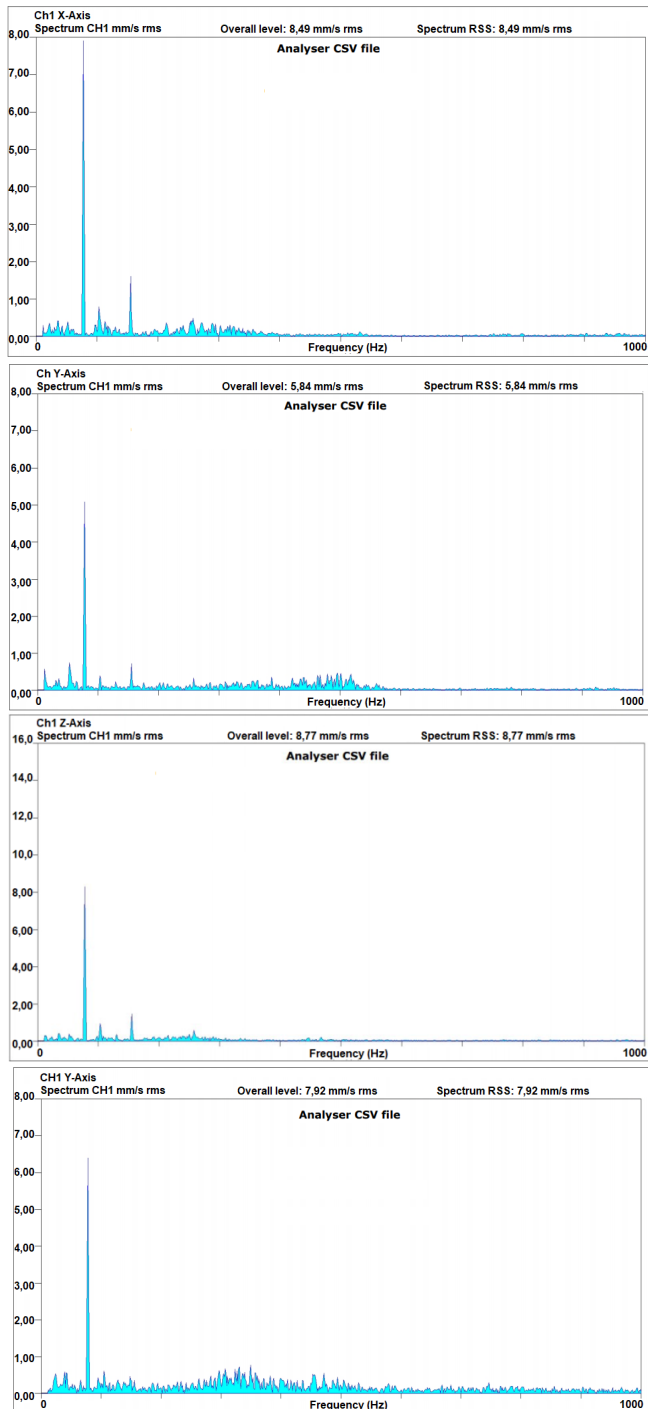

Fig. 5.13. Vibration velocity of MGU fixed at 4 653 min^{-1} on motor bearing shell on X, Y, Z axes and on gearbox shell on the Y axis.

The fixed values of vibration velocity on Y axis were 5.84 and 7.92 mm/s, which is more than twice the allowable limit of 2.8 mm/s. Measurements are carried out for 21 control points on the traction motor and gearbox housing along X, Y and Z axes for rotation speeds of 3 000 min^{-1} and 4 653 min^{-1}.

In an induction motor, the speed is inversely proportional to the load; however, when it is connected to the gearbox, there is certain speed fluctuation. So, it was noticed that with an increase in the rotational speed of the "rotor-shaft MGU" system from 3 000 min^{-1} to 4 653 min^{-1} at the control points, the vibration acceleration values increase by 1.32 mm/s and 3.74 mm/s, respectively.

The reason is that the vibration of the gearbox housing, both for the loaded state and in the case of determining its own vibration, is transmitted to the gearbox through a flexible rolling bearing. There is a very strong excitation of the gearbox due to various time-varying parameters such as the gearing stiffness of the tooth, frictional forces and self-torques, as well as the forces of the bearings; thereby causing speed fluctuations [118].

The vibration activity of the intermediate shaft of the gearbox can be most informative when detecting MGU defects at low loads and in case of its absence. All other components change arbitrarily depending on the load.

Figures 5.11 and 5.12 show the spectra of vibration signatures in the range 0–1000 Hz. The frequency range is very important for the study of a transmission gearbox. The level of vibration activity fixed on the Y-axis takes place, and therefore it is reasonable to assume the action of tangential forces arising in magnetic field of the motor (MGU). Excitation of the vibroactivity of the MGU can occur due to the ripple of the torque in closed circuit between the frequency converter and the MGU [119], [120].

Time harmonics are generated by the frequency converter by switching power semiconductors, which in turn can amplify torsional vibrations. On the Fig. 5.14 and Fig. 5.15 shows a general view of the location of the MGU on a platform with a spring suspension.
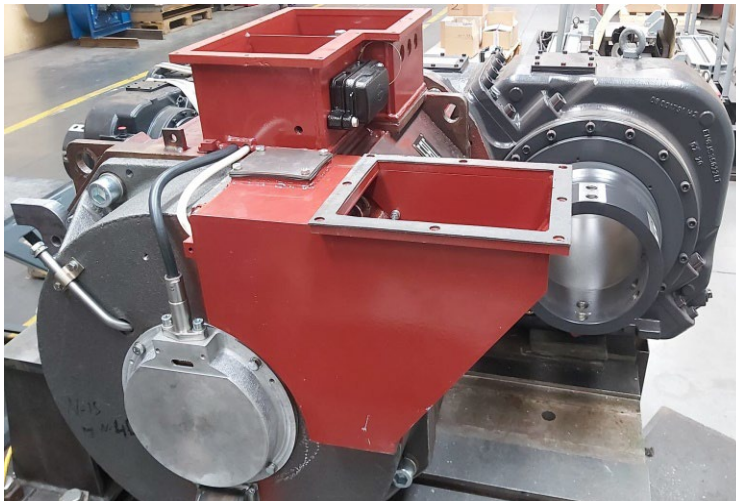

Fig. 5.14 View of MGU from motor side

Fig. 5.15 View of MGU from gearbox side

Comparing the results of the spectral analysis of the vibroactivity of the MGU and the control scheme, it can be assumed that the level of the vibrational activity of the MGU decreases when testing under load simultaneously for two MGUs.

Electromagnetic processes in machines are determined by magnetic field in the air gap created by currents flowing along the Y axis of the machine. The distribution of flux over the air gap of the machine and the change in time, ultimately effects the traction and energy characteristics of the traction motor as part of the MGU, as well as its controllability.

In addition, the changing air gap prevents air convection and therefore negatively affects the thermal processes in the winding, increasing the relative temperature difference between the frontal and slot parts of the stator winding.

5.2. Determination of the level of vibration activity of MGU in the mutual load mode

To implement a mathematical model of the power equipment of the experimental testbench for two MGU mutual load, their discretization was carried out. The subsystems shown in Fig. 5.5 are nodes and aggregates of the object under study. Inside the subsystems are the logical components of the model, grouped according to the principle of belonging. The variable composition of the input and output data of the motor model is determined by its traction and energy characteristics. The input variables of the model include control signals. For motor, this is the required torque or a value proportional to it. The power converter control controller provides for the implementation of a control system developed within the framework of a model for which a signal form is used and which is recognized by the motor control unit.

In the model, the characteristics of the speed of the electric motor are set, which link the "start-braking" signal with the torque as a function of the angular velocity of the shaft. The velocity ω for the vector control system is used by the feedback signal from the rotor position sensor. The traction and energy characteristics of tested motors are shown in Fig. 3.7. For feedback control, the speed sensor transmits information about the speed of the motor rotor to the speed controller, which is a PI controller with acceleration speed limits, and outputs a reference torque. The torque and magnetic flux are estimated by the observer in accordance with the measured currents and voltages based on equivalent q-d circuits.

The electrical and mechanical systems are connected by the motor rotor. The electrical subsystem generates an electromagnetic moment, which is the input to the mechanical

subsystem. The electromagnetic torque at the motor output is one of the inputs for the mechanical state space block (the other input is the torque of the mechanical load). Damping moments and stiffness moments occur along the shaft in couplings, shaft segments and bearings.

To determine the value of the vibration velocity of the MGU under load, two identical MGUs are assembled, the hollow shafts of which are connected by a coupling, and the assembly itself is mounted on a shock-absorbing platform as it is shown in Fig. 5.16. The parameters of the test modes of vibration activity of the MGU under load are the same as given in Table 5.5.

In the docked state, the middle position of both roller bearings of the traction motors in ensured.

<div align="right">Table 5.5</div>

<div align="center">Mutual Loaded MGU Speed Test Parameters</div>

No.	Speed test parameters			
	Part	Duration [min]	Position	Speed point [min^{-1}]
1	t_1, t_{11}	15	n_1, n_4	300
2	t_2, t_{10}	5	n_2, n_6	4 653
3	t_3, t_9	2	n_3, n_5	3 000
4	t_4, t_6, t_8	10	Speed direction	CW/CCW
5	t_5, t_7	10		
Total:		94		

Fig. 5.16. Physical testbench of MGU under the mutual load control.

The characteristics of the change in the auto-spectrum of vibration velocity with vector control of the PWM with constant frequency for rotation speeds of the coupled MGU shafts – 3 000 min^{-1} and 4 653 min^{-1} are shown in Fig. 5.17, 5.18, 5.19 and 5.20. The general level of vibration acceleration in the frequency range 0–1000Hz was 0,0990 g at 3 000 min^{-1} and 0,794 g at 4 653 min^{-1}, and the vibration velocity in the frequency range 0–1000Hz was 1.28 mm/s at 3 000 min^{-1} and 1.89 mm/s at 4 653 min^{-1}.

A spectrogram is needed in applications where the vibration frequency changes with time. A spectrogram works by breaking the time domain data from Fig. 5.17 and Fig. 5.18 into a series of chunks, as it is shown in Fig. 5.19 and Fig. 5.20 and taking the FFT of these time periods. These series of FFTs are then overlapped to visualize how both the amplitude and

frequency of the vibration signal change with time. Using a spectrogram allows gaining a much deeper understanding of the vibration profile and how it changes with time.
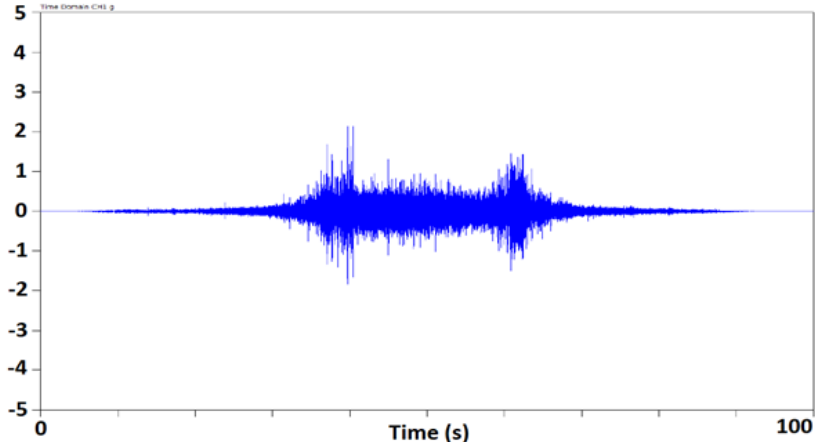

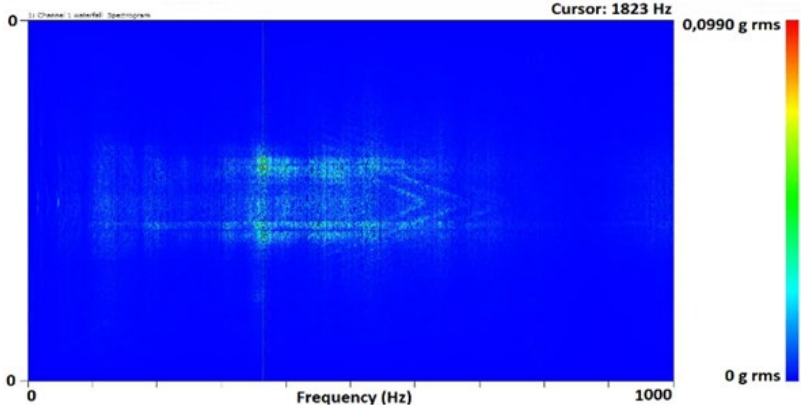Fig. 5.17. The waveform at the rotor speed of 3 000 min^{-1} in Y-axis direction.

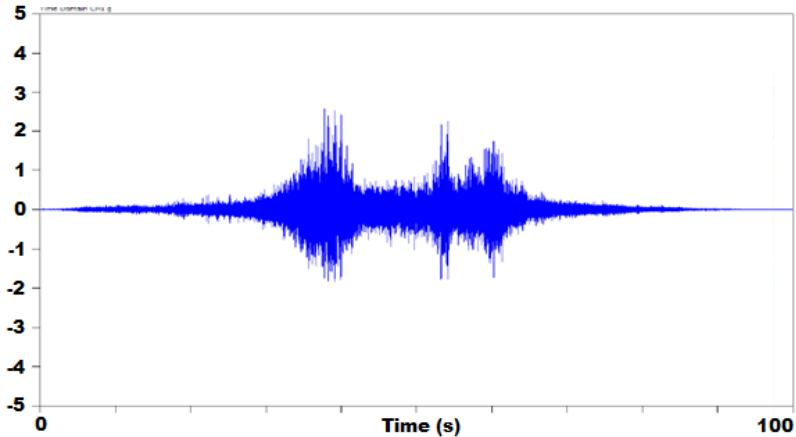Fig. 5.18. The wavefall spectrogram the rotor speed of 3 000 min^{-1} in Y-axis direction.

Fig. 5.19. The waveform at the rotor speed of 4 653 min^{-1} in Y-axis direction.
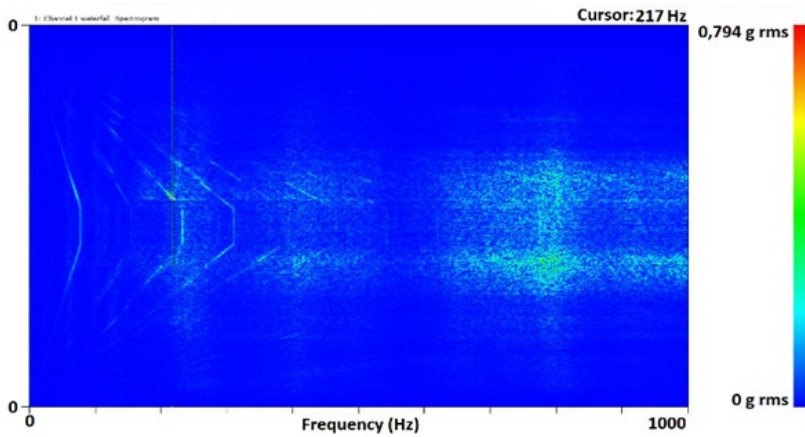
Fig. 5.20. The wavefall spectrogram the rotor speed of 4 653 min^{-1} in Y-axis direction.

It is recommended to carry out an autonomous check of traction single-support motors for mechanical strength, before their docking with the gearbox. The tests carried out relate to the MGU, in which the geometry of the flange and the gearbox housing ensure the middle position of the roller bearing of the motor, which is the most favorable from the point of view of reducing vibration activity. When the rollers are displaced relative to the middle position, the vibration activity indicators will deteriorate, while the bearing heating temperature will increase.

The presence of resonance of the rotating system "motor rotor - gearbox input shaft" in the range of rotation speeds close to the nominal leads to long-term sustained oscillating processes at the output shaft of the MGU and increased vibration. The main task in the design and manufacture of MGU is to exclude resonant frequencies from the range of nominal operating speeds.

The changing level of vibration velocity in the direction of the Y axis is the determining value when controlling the strength-vibration, noise and thermal parameters of MGU. The data obtained make it possible to identify the zone of dangerous resonance of the MGU design from the point of view of electromechanical resonances and suggest ways to control the state of the MGU nodes. It is recommended to determine the intrinsic vibration of the MGU with a mutual load.

RESULTS AND CONCLUSIONS

In the Doctoral Thesis, the dynamics, mechanical strength and technical condition evaluation possibilities of the traction geared motor block were investigated in industrial and continuous production conditions. A methodology was developed that increases the reliability of pre-commissioning tests, based on the integrated approach to the control and analysis of mechanical strength and vibration activity of traction equipment.

The developed methodology is based on real peculiarities of the technological process of production, as well as on real working conditions of the equipment, taking into account the mechanical loads of the tration drive.

In the course of the Thesis research, a strength calculation of the zones of maximal stress of the gearbox was performed under various loads, including shock loads. The analysis of the safety margin of the bearing structure of the traction gear was carried out. According to the results of the calculation, by means of a physical experiment, the level of vibration activity of the structure of the gearbox as part of the MGU and controlled by the original voltage and frequency converter was established. The experimentally determined indicators of the vibration activity of the gearbox in the loaded state make it possible to confirm the simulated strength and stability of the structure to the effects of external purely mechanical disturbances and mechanical disturbances caused by electromagnetic phenomena of the traction drive.

It is recommended to carry out an autonomous check of traction single-support motors for mechanical strength before their docking with the gearbox. The tests carried out relate to the MGU in which the geometry of the flange and the gearbox housing ensure the middle position of the roller bearing of the motor, which is the most favourable from the point of view of reducing vibration activity. When the rollers are displaced relative to the middle position, the vibration activity indicators will deteriorate, while the bearing heating temperature will increase.

The presence of resonance of the rotating system "motor rotor – gearbox input shaft" in the range of rotation speeds close to the nominal leads to long-term sustained oscillating processes at the output shaft of the MGU and increased vibration. The main task in the design and manufacture of MGU is to exclude resonant frequencies from the range of nominal operating speeds.

The changing level of vibration velocity in the direction of the Y-axis is the determining value when controlling the strength-vibration, noise and thermal parameters of MGU. The data obtained make it possible to identify the zone of dangerous resonance of the MGU design from the point of view of electromechanical resonances and suggest ways to control the state of the MGU nodes. It is recommended to determine the intrinsic vibration of the MGUH with a mutual load.

To calculate the strength data of MGU nodes, an experimental evaluation of the amplitude-frequency characteristics obtained on the MGU body was carried out. The limit values of the vibration frequency for MGU are 26–33 % of the maximum allowable value.

It is revealed that the vibration is continuous in time and corresponds to spectrum of the broadband region. In addition to vibration caused by external causes (from the upper structure of the track), vibrations that occur during the operation of the drive act on the wheel-motor unit

of the electric train, which under certain conditions causes shock vibrations, and this significantly increases the amplitude of vibrations of its local parts.

The results of vibration research during testing of the MGU of a suburban electric train in traction mode and with shock load removal are obtained and presented.

The experimental measurements carried out confirm the calculated strength of MGU and determine the frequency spectrum under shock loads.

The vibration of the gearbox housing, both for the loaded state and in the case of determining its own vibration, is transmitted to the gearbox through a flexible rolling bearing. There is a more powerful excitation of the gearbox due to time-varying parameters such as the gearing stiffness of the tooth, frictional forces and self-torques, as well as the forces of the bearings; thereby causing speed fluctuations.

For example, a vibration level fixed on the Y-axis may be due to shear forces generated in the motor magnetic field. Also, the existing vibration excitation of the MGU can occur due to the torque pulsation in a closed circuit between the frequency converter and the MGU twin. Temporal harmonics are generated by the frequency converter by switching power semiconductors, which in turn can amplify torsional vibrations.

Considered as an example, the design of MGU meets the requirements of design reliability in terms of critical parameters of mechanical rigidity and short-term shock loads. However, due to the presence of a large number of bolted connections in the design, each manufactured unit of the MGU must undergo acceptance tests to check the level of vibration activity and also be subjected to careful control during operation.

The cast-iron casing of the MGU with axial-support suspension and the fastening of the traction motor flange to the gearbox casing flange ensure the rigidity of the structure and meet the requirements of extremely high external mechanical influences. With a high level of vibration and single shocks, the operation of the MGU will be characterized by increased wear of the gears of the reducer and the thrust bearing of the traction motor.

LIST OF REFERENCES

1. Барков, А. В. Новое поколение систем мониторинга и диагностики машин // Виброакустические системы и технологии (ВАСТ). – 2002. – Saite: http://chemtech.ru/novoe-pokolenie-sistem-monitoringa-i-diagnostiki-rotornogo-oborudovanija/ (skatīts: 24.05.2022).

2. Tiboni, M.; Remino, C.; Bussola, R.; Amici, C. A Review on Vibration-Based Condition Monitoring of Rotating Machinery. Appl. Sci. 2022, 12, 972. https://doi.org/10.3390/app12030972

3. Malla, C.; Panigrahi, I. Review of Condition Monitoring of Rolling Element Bearing Using Vibration Analysis and Other Techniques. J. Vib. Eng. Technol. 2019, 7, 407–414.

4. Suresh, S.; Naidu, V. P.S . Gearbox Health Condition Monitoring Using DWT Features. In Proceedings of the 6th National Symposium on Rotor Dynamics; Rao, J. S., Arun Kumar, V., Jana, S., Eds.; Springer: Singapore, 2021; pp. 361–374.

5. Umbrajkaar, A. M.; Krishnamoorthy, A.; Dhumale, R. B. Vibration Analysis of Shaft Misalignment Using Machine Learning Approach under Variable Load Conditions. Shock Vib. 2020, 2020, 1–12. https://doi.org/10.1155/2020/1650270

6. Lee, S. B.; Stone, G. C.; Antonino-Daviu, J.; Gyftakis, K. N.; Strangas, E. G.; Maussion, P.; Platero, C. A. Condition Monitoring of Industrial Electric Machines: State of the Art and Future Challenges. IEEE Ind. Electron. Mag. 2020, 14, 158–167. https://doi.org/10.1109/MIE.2020.3016138

7. De Oliveira Neto, J. M.; Oliveira, A. G.; de Carvalho Firmino, J. V. L.; Rodrigues, M. C.; Silva, A. A.; de Carvalho, L. H. Development of a smart system for diagnosing the operating conditions of a helicopter prototype via vibrations analysis. Res. Soc. Dev. 2021, 10, e304101220546. https://doi.org/10.33448/rsd-v10i12.20546

8. Ehya, H.; Lyng Rødal, G.; Nysveen, A.; Nilssen, R. Condition Monitoring of Wound Field Synchronous Generator under Inter-turn Short Circuit Fault utilizing Vibration Signal. In Proceedings of the 2020 23rd International Conference on Electrical Machines and Systems (ICEMS), Hamamatsu, Japan, 24–27 November 2020; pp. 177–182. https://doi.org/10.23919/ICEMS50442.2020.9291088

9. Sharma, V. A Review on Vibration-Based Fault Diagnosis Techniques for Wind Turbine Gearboxes Operating Under Nonstationary Conditions. J. Inst. Eng. Ser. C 2021, 102, 507–523.

10. Суслов, А. Г. Качество машин : Справ. в 2т. Т1. / А.Г. Суслов, Э. Д. Браун, Н. А. Виткевич и др.– М.: «Машиностроение», 1995. – 256 с.

11. Абрамов, И. В. Надежность и организация ремонта больших механических систем / И. В. Абрамов, Ю. В. Турыгин. – Ижевск: Изд-во ИжГТУ, 1992. – 156 с.

12. Абрамов, И. В. Основы надежности и современные методы организации технического обслуживания и ремонта технических систем (техники) / И.В. Абрамов, Ю.В. Турыгин, С. А. Юрченко, Б. А. Якимович. – Ижевск: Изд-во ИжГТУ, 2002.–188 с.

13. Дайерд, Стюарт Р. Обнаружение повреждений подшипников качения путем статистического анализа вибраций: Пер. с англ. Конструирование и технология машиностроения / Стюарт Р. Дайерд. – М.: Мир, 1978. – т. 100, № 2. – С.23–31.

14. Горелик, А. Л. Методы распознавания / А.Л. Горелик, В.А. Скрипкин. – М.: Высшая школа, 1977. – 22 с.

15. Sendhil Kumar, S.; Senthil Kumar, M. Condition monitoring of rotating machinery through vibration analysis. J. Sci. Ind. Res. 2014, 73, 258–261.

16. Русов, В. А. Диагностика дефектов вращающегося оборудования по вибрационным сигналам / В. А. Русов. – Пермь: Изд-во «Вибро-Центр», 2012. – 244 с.

17. Hou, D.; Qi, H.; Luo, H.; Wang, C.; Yang, J. Comparative study on the use of acoustic emission and vibration analyses for the bearing fault diagnosis of high-speed trains. Struct. Health Monit. 2021, 14759217211036025. https://doi.org/10.1177/14759217211036025

18. ISO 17359:2018 Condition monitoring and diagnostics of machines – General guidelines, p. 29.

19. ISO 13380:2002 Condition monitoring and diagnostics of machines – General guidelines on using performance parameters, p. 19.

20. ISO 13379-1:2012 Condition monitoring and diagnostics of machines – Data interpretation and diagnostics techniques – Part 1: General guidelines, p. 33.

21. ISO 10816-8:2014 Mechanical vibration – Evaluation of machine vibration by measurements on non-rotating parts, p. 27.

22. ISO 13373-1:2002 Condition monitoring and diagnostics of machines – Vibration condition monitoring – Part 1: General procedures, rev. 2018, p. 51.

23. ISO 15242-1:2015 Rolling bearings – Measuring methods for vibration – Part 1: Fundamentals, rev. 2021, p. 16.

24. ISO 13374-3:2012 Condition monitoring and diagnostics of machines – Data processing, communication and presentation – Part 3: Communication, rev. 2017, p. 21.

25. Азовцев, Ю.А. Вибрационная диагностика роторных машин и оборудования целлюлозно-бумажных комбинатов: учебное пособие / Ю.А. Азовцев, Н.А. Баркова, А. А. Гаузе. – СПб.: СПбГУРП, 2014. – 127с.

26. Русов, В. А. Спектральная вибродиагностика / В. А. Русов. – Пермь: Изд-во «Вибро-Центр», 1996. – 176 с.

27. Тэттэр, В. Ю. Вибродиагностика подшипников качения и зубчатых передач подвижного состава комплексом «Прогноз-1» при переходе на ремонт по фактическому состоянию / В. Ю. Тэттэр, В. И. Щедрин // Разработка и исследование автоматизированных средств контроля и управления для предприятий железнодорожного транспорта: Межвуз. темат. сб. науч. тр. – ОмГУПС. – Омск, 1999. – С. 68–71.

28. Тэттэр, В. Ю. Прикладные вопросы диагностирования роторных узлов по вибрации / В. Ю. Тэттэр, А. Ю. Тэттэр // LAP LAMBERT Academic Publishing Saarbrucken. 2013. – 131 с.

29. Тэттэр, В. Ю. Определение технического состояния агрегатов железнодорожной техники в условиях нестационарных режимов работы / А. Ю. Тэттэр, В. Ю. Тэттэр // Омский научный вестник, 2017. № 6 (156). – С. 132–136.

30. Ibarra-Zarate, D.; Tamayo-Pazos, O.; Vallejo-Guevara, A. Bearing fault diagnosis in rotating machinery based on cepstrum pre-whitening of vibration and acoustic emission. Int. J. Adv. Manuf. Technol. 2019, 104, 4155–4168. https://doi.org/10.1007/s00170-019-04171-6

31. Othman, M. S.; Nuawi, M. Z.; Mohamed, R. Experimental comparison of vibration and acoustic emission signal analysis using kurtosis-based methods for induction motor bearing condition monitoring [Eksperymentalne porównanie i analizy sygnałów emisji akustycznej do

monitorowania stanu łozysk]. Przeglad Elektrotechniczny 2016, 92, 208–212. https://doi.org/10.15199/48.2016.11.51

32. Li, K.; Feng, Z.; Liang, X. Planetary Gearbox Fault Diagnosis via Torsional Vibration Signal Analysis in Resonance Region. Shock Vib. 2017, 2017, 1–18. https://doi.org/10.1155/ 2017/ 6565237

33. Харламов, В. В. Диагностирование межвитковой изоляции якорной обмоткитягового электродвигателя магистральных локомотивов / В. В. Харламов, П. К. Шкодун, А. Д. Галеев // Известия Транссиба. 2019. № 1 (37). – С. 44–54.

34. Харламов, В. В. Диагностика тяговых электродвигателей / В. В. Харламов, П. К. Шкодун, А. Д. Галеев // Железнодорожный транспорт. 2015. № 11. – С. 71–73.

35. Костюков, В. Н. Диагностирование электромашинного преобразователя электропоезда в условиях эксплуатации / В. Н. Костюков, А. Е. Цурпаль // Мир транспорта. 2014. Т. 12. № 4 (53). – С. 46–53.

36. Гаврин, С.В. Развитие систем диагностики оборудования / С. В. Гаврин, А. А. Козлов, Н. В. Яцюк, В. Н. Костюков, А. В. Костюков // Мир нефтепродуктов. Вестник нефтяных компаний. 2012. № 8. – С. 43–46.

37. Костюков, В. Н. Диагностика качества сборки электрических цепей электропоездов / В. Н. Костюков, А. В. Костюков, Д. В. Казарин // Сборка в машиностроении, приборостроении. 2009. № 12. – С. 25–34.

38. Моисеев, В. А. Опыт разработки и внедрения бортовой системы мониторинга технического состояния электропоезда / В.А. Моисеев, А.В. Костюков, Д.В. Казарин, А. В. Цургаль // Железнодорожный транспорт. 2016. № 8. – С. 58–61.

39. Костюков, В. Н. Совершенствование диагностического обеспечения подшипниковых узлов колесно-моторных блоков электропоездов / В. Н. Костюков, Д. В. Казарин, А. В. Костюков, А. В. Зайцев // Известия Транссиба. 2015. № 4 (24). – С. 33–39.

40. Костюков, В. Н. Формирование вектора диагностических признаков на основе характеристической функции виброакустического сигнала / В. Н. Костюков, А. П. Науменко, С. Н. Бойченко, И. С. Кудрявцева // Контроль. Диагностика. 2016. № 8. – С. 22–29.

41. Костюков, В. Н. Нормативно-методическое обеспечение диагностики и мониторинга поршневых компрессоров / В. Н. Костюков, А. П. Науменко // Безопасность труда в промышленности. 2013. № 5. – С. 66–70.

42. Feldman, J.; Hanrahan, B. M.; Misra, S.; Fan, X. Z.; Waits, C. M.; Mitcheson, P. D.; Ghodssi, R. Vibration-based diagnostics for rotary MEMS. J. Microelectromech. Syst. 2015, 24, 289–299. https://doi.org/10.1109/JMEMS.2014.2383171

43. Dos Santos Pedotti, L. A.; Zago, R. M.; Giesbrecht, M.; Fruett, F. Low-cost MEMS accelerometer network for rotating machine vibration diagnostics. IEEE Instrum. Meas. Mag. 2020, 23, 25–33. https://doi.org/10.1109/MIM.2020.9234762

44. Laval, X.; Mailhes, C.; Martin, N.; Bellemain, P.; Pachaud, C. Amplitude and phase interaction in Hilbert demodulation of vibration signals: Natural gear wear modeling and time tracking for condition monitoring. Mech. Syst. Signal Process. 2021, 150, 107321. https://doi.org/10.1016/j.ymssp.2020.107321

45. Sheen, Y.–T. A complex filter for vibration signal demodulation in bearing defect diagnosis. J. Sound Vib. 2004, 276, 105–119. https://doi.org/10.1016/j.jsv.2003.08.007

46. Сиротин, Д. В., Чернов А. В., Пугачева Е. А. Проявление торсионных вибраций электропривода в токовом сигнале асинхронного двигателя / Д. В. Сиротин, А. В. Чернов, Е. А. Пугачева // Известия высших учебных заведений. Северо-Кавказский регион. Технические науки, 2006. – С.40–42.

47. Чернов, А. В. Автоматизированная система технического диагностирования теплообменных аппаратов / А. В. Чернов, С. Э. Гоок, Д. В. Сиротин и др. // Материалы III международной научно-технической конференции «Новые технологии управления движением технических объектов». Секция «Теория, методы и средства измерений, контроля и диагностики». Том 3. – Новочеркасск, 2002. – С.26–29.

48. Сиротин, Д. В. Возможность применения преобразования Гильберта для определения основных параметров асинхронного двигателя / Д. В. Сиротин, С. В. Русинов, М. В. Письменский // Актуальные проблемы современной науки. Технические науки: тр. 5-й Междунар. конф. молодых ученых и студентов, 7–9 сент. 2004 г. – Самара, 2004. – Ч. 18 (от М до Я). – С.51–53.

49. Buzzoni, M.; Mucchi, E.; D'Elia, G.; Dalpiaz, G. Diagnosis of Localized Faults in Multistage Gearboxes: A Vibrational Approach by Means of Automatic EMD-Based Algorithm. Shock Vib. 2017, 2017, 1–22. https://doi.org/10.1155/2017/8345704

50. Gałka, T. A comparison of two symptom selection methods in vibration-based turbomachinery diagnostics. J. Vibroeng. 2015, 17, 3505–3514.

51. Chen, X.; Feng, Z. Time-frequency analysis of torsional vibration signals in resonance region for planetary gearbox fault diagnosis under variable speed conditions. IEEE Access 2017, 5, 21918–21926. https://doi.org/10.1109/ACCESS.2017.2763172

52. Шпрехер, Д. М. Контроль технического состояния электромеханических систем при помощи нейросетевых схем распознавания / Бабокин Г. И., Шпрехер Д. М. // Известия Тульского государственного университета. Сер. Технические науки. – 2010. – Вып.1. – С.109–114.

53. Шпрехер, Д. М. Нейросетевая технология диагностики электромеханических систем горных машин / Бабокин Г. И., Шпрехер Д. М. // Известия вузов Горный журнал. – 2011. – №3. – С.39–44.

54. Шпрехер Д. М. Применение нейронных сетей для прогнозирования технического состояния электромеханических систем / Шпрехер Д. М. // Известия Тульского государственного университета. Сер. Технические науки: в 2 ч. – 2011. – Вып. 6.– Ч.1. – С. 48–53.

55. Riaz, S.; Elahi, H.; Javaid, K.; Shahzad, T. Vibration Feature Extraction and Analysis for Fault Diagnosis of Rotating Machinery-A Literature Survey. Asia Pac. J. Multidiscip. Res. 2017, 5, 103–110.

56. Hong, L.; Dhupia, J. S. A time domain approach to diagnose gearbox fault based on measured vibration signals. J. Sound Vib. 2014, 333, 2164–2180. https://doi.org/10.1016/j.jsv.2013.11.033

57. Rzeszucinski, P. J.; Sinha, J. K.; Edwards, R.; Starr, A.; Allen, B. Amplitude of probability density function (APDF) of vibration response as a robust tool for gearbox diagnosis. Strain 2012, 48, 510–516. https://doi.org/10.1111/j.1475-1305.2012.00849.x

58. Устройство диагностирования технического состояния электромеханических систем : Пат. на полезную модель RU 144352 U1 Рос. Федерация: МПК G01R 31/34 / Шпрехер

Д. М., Степанов В. М., Бабокин Г. И. – № 2014114354/28; заявл. 11.04.2014; опубл. 20.08.2014, Бюл. №23. – 1 н.п.ф. 2 илл.

59. Устройство прогнозирования остаточного ресурса электромеханической системы : Пат. на полезную модель RU146951 U1 Рос. Федерация: МПК G01R 31/02 / Шпрехер Д. М., Степанов В. М. Колесников Е. Б. – № 20141181318/28; заявл. 07.05.2014; опубл. 20.10.2014, Бюл. №29.

60. Attoui, I.; Oudjani, B.; Boutasseta, N.; Fergani, N.; Bouakkaz, M.-S.; Bouraiou, A. Novel predictive features using a wrapper model for rolling bearing fault diagnosis based on vibration signal analysis. Int. J. Adv. Manuf. Technol. 2020, 106, 3409–3435. https://doi.org/10.1007/s00170-019-04255-3

61. Барков, А. В. Диагностика и прогнозирование технического состояния подшипников качения по их виброакустическим характеристикам / А. В. Барков // Судостроение. – 1985. – №3. – С.21–23.

62. Gelman, L.; Zimroz, R.; Birkel, J.; Leigh-Firbank, H.; Simms, D.; Waterland, B.; Whitehurst, G. Adaptive vibration condition monitoring technology for local tooth damage in gearboxes. Insight Non-Destr. Test. Cond. Monit. 2005, 47, 461–464. https://doi.org/10.1784/insi.2005.47.8.461

63. Баркова, Н. А. Неразрушающий контроль технического состояния горных машин и оборудования: учебное пособие / Н. А. Баркова, Ю. С. Дорошев. – Владивосток: Изд-во ДВГТУ, 2009. – 157 с.

64. Feng, K.; Wang, K.; Zhang, M.; Ni, Q.; Zuo, M. J. A diagnostic signal selection scheme for planetary gearbox vibration monitoring under non-stationary operational conditions. Meas. Sci. Technol. 2017.

65. Elbhbah, K.; Sinha, J. K. Vibration-based condition monitoring of rotating machines using a machine composite spectrum. J. Sound Vib. 2013, 332, 2831–2845. https://doi.org/10.1016/j.jsv.2012.12.024

66. Барков, А. В. Мониторинг и диагностика роторных машин по вибрации / А. В. Барков, Н. А. Баркова, А. Ю. Азовцев. – СПб.: Изд. центр СПб ГМТУ, 2000. – 169 с.

67. ГОСТ Р ИСО 13373-1-2009. Контроль состояния и диагностика машин. Вибрационный контроль состояния машин. Часть 1. Общие методы. – М.: Стандартинформ, 2010. – 43 с.

68. ГОСТ Р 52545.1-2006 Методы измерения вибрации. – М.: Стандартинформ, 2006. – 15 с.

69. ГОСТ 24346-80 Вибрация. Термины и определения. – М.: Стандартинформ, 2010. – 26 с.

70. ГОСТ ИСО 10816-3-2002. Вибрация. Контроль состояния машин по результатам измерений вибрации на невращающихся частях. Часть 3. – М.: Стандартинформ, 2007. – 16 с.

71. ГОСТ 32106-2013. Мониторинг состояния оборудования опасных производств. Вибрация центробежных насосных и компрессорных агрегатов. – М.: Стандартинформ, 2014. – 8 с.

72. ГОСТ ISO 20958-2015 Контроль состояния и диагностика машин. Сигнатурный анализ электрических сигналов трехфазного асинхронного двигателя URL: http://docs.cntd.ru/document/1200133099.

73. ГОСТ Р ИСО 13379-2-2016 Контроль состояния и диагностика машин. Методы интерпретации данных и диагностирования. Часть 2. Подход на основе данных / [Электронный ресурс]. – Режим доступа URL: http://docs.cntd.ru/document/1200141435 (дата обращения: 20.02.2019).

74. Сиротин, Д. В. Использование параметров токового сигнала электродвигателя для оценки технического состояния электромеханического оборудования / Д. В. Сиротин // Известия высших учебных заведений. Северо-Кавказский регион. Технические науки, 2006. – С.57–62.

75. Чернов, А. В. Обработка диагностической информации при оценке технического состояния электроприводной арматуры АЭС / А. В. Чернов, О. Ю. Пугачёва, Е. А. Абидова // ИВД, 2011. – №3. – С. 337–342.

76. Короновский, А. А. Непрерывный вейвлет-анализ и его приложения / А. А. Короновский, А. Е. Храмов. – М.: ФИЗМАТЛИТ, 2003. – 176 с.

77. Астафьева, Н.М. Вейвлет-анализ: основы теории и примеры применения / Н. М. Астафьева // Успехи физических наук. – 1996. – Т. 166, №11. – С. 1145–1170.

78. Мурманский, Б. Е. Концепция системы вибрационной диагностики паровых турбин / Б. Е. Мурманский, Е. В. Урьев, Ю. М. Бродов // Теплоэнергетика. – 1995. – № 4. – С. 36–39.

79. Ананьин, А. Д. Диагностика и техническое обслуживание машин / А. Д. Ананьин, В. М. Михлин, И. И. Габитов и др. – М.: Издательский центр «Академия», 2008. – 432 с. 80. Cardona-Morales, O.; Avendaño, L. D.; Castellanos-Domínguez, G. Nonlinear model for condition monitoring of non-stationary vibration signals in ship driveline application. Mech. Syst. Signal Process. 2014, 44, 134–148. https://doi.org/10.1016/j.ymssp.2013.08.029

81. Tse, P. W.; Wang, D. The automatic selection of an optimal wavelet filter and its enhancement by the new sparsogram for bearing fault detection. Part 2 of the two related manuscripts that have a joint title as "Two automatic vibration-based fault diagnostic methods using the novel sparsity measurement – Parts 1 and 2". Mech. Syst. Signal Process. 2013, 40, 520–544. https://doi.org/10.1016/j.ymssp.2013.05.018

82. Gelman, L.; Murray, B.; Patel, T.H.; Thomson, A. Novel wavelet technology for vibration condition monitoring of rolling element bearings. Insight Non-Destr. Test. Cond. Monit. 2015, 57, 40–47. https://doi.org/10.1784/insi.2015.57.1.40

83. Puchalski, A.; Komorska, I. Application of the wavelet multifractal analysis of vibration signal for rotating machinery diagnosis. Vib. Phys. Syst. 2019, 30, 1–8.

84. Gelman, L.; Kolbe, S.; Shaw, B.; Vaidhianathasamy, M. Novel adaptation of the spectral kurtosis for vibration diagnosis of gearboxes in non-stationary conditions. Insight Non-Destr. Test. Cond. Monit. 2017, 59, 434–439. https://doi.org/10.1784/insi.2017.59.8.434

85. Isham, M. F.; Leong, M. S.; Hee, L. M.; Ahmad, Z. A. B. Iterative variational mode decomposition and extreme learning machine for gearbox diagnosis based on vibration signals. J. Mech. Eng. Sci. 2019, 13, 4477–4492. https://doi.org/10.15282/jmes. 13.1.2019.10.0380

86. Mauricio, A.; Zhou, L.; Mba, D.; Gryllias, K. Vibration-Based Condition Monitoring of Helicopter Gearboxes Based on Cyclostationary Analysis. J. Eng. Gas Turbines Power 2020, 142, 031010. https://doi.org/10.1115/1.4044453

87. Барков, А. В. Идентификация состояния механизмов с узлами вращения по результатам вибрационного мониторинга и контроля температуры. Методика

МВ.03.7826741252./23.12.2011 / А.В. Барков, Н.А. Баркова, Д.В. Грищенко. – Санкт-Петербург, 2011. – 80 с.

88. All about Vibration Measuring Systems. Vibration Technical guide // el. resource: https://www.imv-tec.eu/pr/vibration_measuring/chapter03/ (last visit: 12.08.2022)

89. Huang, S.; Zheng, J.; Pan, H.; Tong, J. Order-statistic filtering Fourier decomposition and its application to rolling bearing fault diagnosis. JVC J. Vib. Control 2021, 0, 1–16. https://doi.org/10.1177/1077546321997598

90. Hartono, D.; Halim, D.; Roberts, G. W. Gear fault diagnosis using the general linear chirplet transform with vibration and acoustic measurements. J. Low Freq. Noise Vib. Act. Control 2019, 38, 36–52. https://doi.org/10.1177/1461348418811717

91. Guoji, S.; McLaughlin, S.; Yongcheng, X.; White, P. Theoretical and experimental analysis of bispectrum of vibration signals for fault diagnosis of gears. Mech. Syst. Signal Process. 2014, 43, 76–89. https://doi.org/10.1016/j.ymssp.2013.08.023

92. Kawada, M.; Yamada, K.; Yamashita, K. Fundamental Study on Vibration Diagnosis for High Speed Rotational Machine using Wavelet Transform. IEEJ Trans. Power Energy 2003, 123, 1229–1241. https://doi.org/10.1541/ieejpes.123.1229

93. Stander, C.J.; Heyns, P. S.; Schoombie, W. Using vibration monitoring for local fault detection on gears operating under fluctuating load conditions. Mech. Syst. Signal Process. 2002, 16, 1005–1024. https://doi.org/10.1006/mssp.2002.1479

94. Ocak, H.; Loparo, K. A. A new bearing fault detection and diagnosis scheme based on hidden Markov modeling of vibration signals. In Proceedings of the ICASSP, IEEE International Conference on Acoustics, Speech and Signal Processing-Proceedings, Salt Lake City, UT, USA, 7–11 May 2001; Volume 5, pp. 3141–3144. https://doi.org/ 10.1109/ICASSP.2001.940324

95. Betta, G.; Liguori, C.; Paolillo, A.; Pietrosanto, A. A DSP-based FFT-analyzer for the fault diagnosis of rotating machine based on vibration analysis. IEEE Trans. Instrum. Meas. 2002, 51, 1316–1321. https://doi.org/10.1109/TIM.2002.807987

96. Оппенгейм, А. Цифровая обработка сигналов / А. Оппенгейм, Р. Шафер; пер. с англ. С. А. Кулешова // под ред. А. С. Ненашева. – М.: Техносфера, 2006. – 856 с.

97. Гиоев, З. Г. Основы виброакустической диагностики тяговых приводов локомотивов.: Дис. докт. тех. наук. – Ростов-на-Дону, 1998. –261с.

98. Труханов, В. М. Надёжность изделий машиностроения. Теория и практика: учебник. Рек. ГК РФ по высшему образованию / В. М. Труханов. - М.: Машиностроение, 1996. - 336 с.

99. Барков, А. В. Вибрационная диагностика колесо-редукторных блоков на железнодорожном транспорте. / А. В. Барков, Н. А Баркова, В. В. Федорищев. – СПб.: Изд. центр СПбМТУ, 2002. – 103 с.

100. Генкин, М. Д. Виброакустическая диагностика машин и механизмов/ М. Д. Генкин , А.Г. Соколова. – М.: Машиностроение, 1987. – 288 с.

101. Taylor, J. I. The Vibration Analysis Handbook / J. I. Taylor.VCI, 2003. – 375 p.
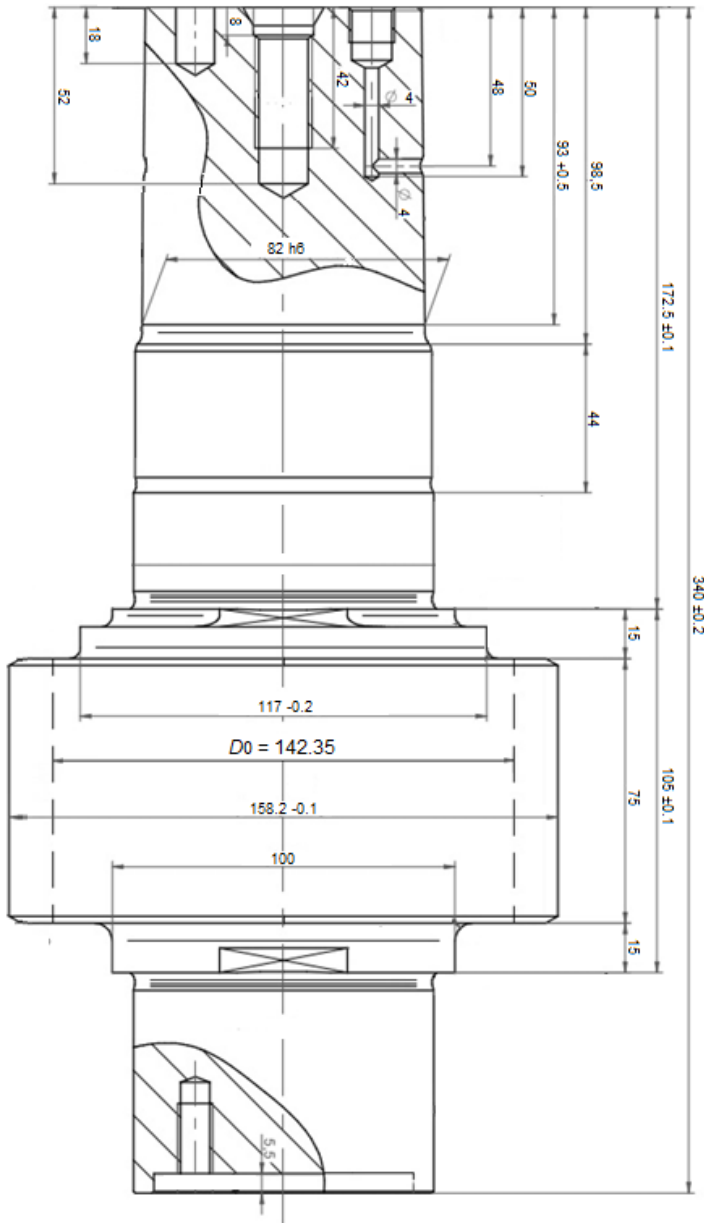
102. Mitchell, J. S. An Introduction to Machinery Analysis and Monitoring. PennWell, 1993

103. Артоболевский, И. И. Введение в акустическую динамику машин / И.И. Артоболевский, Ю. И. Бобровницкий, М. Д. Генкин. - Москва: Наука, 1979. – 296 с.

104. Randall, R. B. Vibration - based condition monitoring: industrial, aerospace and automotive applications // John Wiley & Sons. March 2011. 289 p.

105. Wowk, V. Machinery Vibration: Measurement and Analysis. McGraw – Hill Professional, 1991, 358 p.

106. Костюков, В. Н. Основы виброакустической диагностики и мониторинга машин: учеб. пособие / В. Н. Костюков, А. П. Науменко; М-во образования и науки РФ, ГОУ ВПО «Омский гос. тех. ун-т»; НПЦ «Динамика». – 2-е изд., с уточн. – Новосибирск: Издательство СО РАН, 2014. – 378 с.

107. Костюков, В. Н. Мониторинг безопасности производства / В. Н. Костюков. – М. : Машиностроение, 2002. – 224 с.

108. Костюков, А. В. Автоматическая система оценки состояния узлов электроподвижного состава. В том числе колесно-моторных блоков и колесных пар / А. В. Костюков, А. А. Лагаев, А. В. Зайцев // Мир транспорта. – 2010. – №10. – С. 70–74.

109. Зайцев, А. В. Определение возможности уменьшения числа датчиков вибрации при диагностировании колесно-моторных блоков электропоезда / А. В. Зайцев, А. А. Лагаев, В. Н. Костюков //Наука, образование, бизнес: регион. науч. – практ. конф. – Омск, 2009. – С.154–157.

110. Леоненко А. С. Моделирование динамики машин и механизмов, методическое пособие. - Иркутск: Изд-во ИрГТУ, 2003. – 39 с.

111. Радкевич Я. М. Методология оценки качества и управления состоянием горных машин с использованием вибрационных характеристик./ М.С. Островский, Я.М. Радкевич.//Горные машины и автоматика. – 2008 № 10. – С. 8–12.

112. Gierlak, P.; Burghardt, A.; Szybicki, D.; Szuster, M.; Muszynska, M. On-line manipulator tool condition monitoring based on vibration analysis. Mech. Syst. Signal Process. 2017, 89, 14–26.

113. Dvorņikovs, Iļja. Virtual-Physical Tests of Vehicles with Combined Traction Electrical Drive. PhD Thesis. Rīga: [RTU], 2021. 111 p.

114. Dvornikov, I., Marinbahs, M., Sliskis, O., Ketners, K. "Investigation of autonomous traction motor dynamic using method of mutual loading and computer simulation" in *2018 IEEE 59th International Scientific Conference on Power and Electrical Engineering of Riga Technical University (RTUCON)*, Riga, Latvia, 2018

115. Kobenkins, G.,Marinbahs, M., Burenin, V., Zarembo, J., Sliskis, O. "Carrying Out of Strenght Tests of Geared Motor Box as Part of a Frequency-Controlled Traction Electric Drive" in *2021 17th Conference on Electrical Machines, Drives and Power Systems (ELMA)*, Sofia, Bulgaria, 2021

116. Dvornikov, I., Marinbahs, M., Kobenkins, G., Sliskis, O., Ketners, K. "Carrying Out of Tests for the Functionality of the Traction Autonomous Drives in the Conditions of Industry and Serial Production" in *2021 17th Conference on Electrical Machines, Drives and Power Systems (ELMA)*, Sofia, Bulgaria, 2021

117. Kobenkins, G., Marinbahs, M., Burenin, V., Zarembo, J., Bizans, A., Sliskis, O. "Determination of the Level of Own Vibration of Geared Motor Boxes in Industrial Conditions" in *2021 IEEE 62nd International Scientific Conference on Power and Electrical Engineering of Riga Technical University (RTUCON)*, Riga, Latvia, 2021

118. Kobenkins, G., Marinbahs, M., Bizans, A., Rilevs, N., Burenin, V., Sliskis, O. "Carrying Out of Strength Control of Mutual Loaded Traction Geared Motor Boxes as a Part of Industrial Tests" in *2022 9th International Conference on Electrical and Electronics Engineering (ICEEE)*, Alanya, Turkey, 2022

119. WIKOV MGI // Technical report, Hronov 2020, p. 57.

120. Marinbahs, M., Kobenkins, G., Pavelko, V. Bizans, A., Rilevs, N., Sliskis, O. "Determination of the Strength Characteristics of Traction Gears Under Shock Loads" in the *8th International Youth Conference on Energy (IYCE-2022)* 6-9 July 2022, Eger, Hungary

121. Kobenkins G., Marinbahs M., Bizans A., Rilevs N., Burenin V., Sliskis O. "Evaluation of the Strength of Traction Geared Motor Units by Permissible Stresses and the Level of Vibration Activity" in *Proc. of the International Conference on Electrical, Computer and Energy Technologies (ICECET 2022)* 20-22 July 2022, Prague, Czech Republic

122. M. Bruha, Z. Peroutka, "Torsional Vibration in Large Variable Speed Drive Systems: Origin and Mitigation Methods", *17th European Conference on Power Electronics and Applications (EPE'15 ECCE-Europe)*, 8–10 Sept. 2015, Geneva, Switzerland.

Pitch circle diameter D_0